Energy & Environmental Science

Flexible Metal-gas Batteries: A Potential Option for the Next-generation Power Accessories of Wearable Electronics

Journal:	*Energy & Environmental Science*
Manuscript ID	EE-REV-01-2020-000039.R1
Article Type:	Review Article
Date Submitted by the Author:	23-Feb-2020
Complete List of Authors:	Zhou, Jingwen; New Materials R&D Center, Institute of Chemical Materials, Academy of Engineering Physics, Chengdu, Sichuan 621900, China Cheng, Jianli; Institute of Chemical Materials, China Academy of Engineering Physics, Wang, Bin; New Materials R&D Center, Institute of Chemical Materials, Academy of Engineering Physics, Chengdu, Sichuan 621900, China, Peng, Huisheng; Fudan University, Lu, Jun; Argonne National Laboratory, Chemical Science and Engineering Division

REVIEW

Flexible Metal-gas Batteries: A Potential Option for the Next-generation Power Accessories of Wearable Electronics

Received 00th January 20xx,
Accepted 00th January 20xx

DOI: 10.1039/x0xx00000x

Jingwen Zhou,[a] Jianli Cheng,[a,*] Bin Wang,[a,*] Huisheng Peng [b,] and Jun Lu [c]

Flexible metal-gas batteries are becoming more and more attractive to wearable electronics in recent years due to their large theoretical energy density and superior adaptability to irregular geometric surfaces, like human body. As the continuous improvement of design strategies and assembly technologies, various advanced flexible metal-gas batteries have been attempted to fabricate. Despite of these efforts, how to synchronously integrate high-flexibility, safety, comfortability and high-performance into flexible metal-gas batteries with specifically-functionalized configurations still remains a big challenge. To solve these dilemmas, re-design on cathode catalysts, gel polymer electrolyte, and battery configuration/components have been focused. In this paper, we make an overview on recent technical advances together with major dilemmas facing current flexible metal-gas batteries, highlighting how flexible cathodes and gel polymer electrolyte with various structures and components affect the electrochemical performance and functionality of flexible metal-gas batteries. Flexible Zn-air, Li-O_2/air and Li-CO_2 batteries are mainly exemplified to elucidate their great potential. Finally, based on our consideration, unsolved technical hurdles and future research perspectives of flexible metal-gas batteries for wearable electronics are given.

1. Introduction

Over the past decades, global economy has been greatly improved at the sacrifice of rapid natural resources consumption, which is far beyond human's imagination.[1-4] This is particularly the case when fossil fuels, the dominant resources that are utilized to produce electricity and serve as power for vehicles, is taken into consideration. It predicts that fossil fuels will be totally exhausted at year 2050 based on current consumption rate.[1, 5, 6] Therefore, numerous efforts have been devoted into exploiting alternative resources to ensure the sustainable development of earth, including solar power, geothermy, wind, tide and so on.

Among them, lithium ion batteries (LIBs) emerged as one of the most representative applications of clean electrochemical energy techniques in the beginning of 1970s.[7-10] With the gradual development of commercial technology, LIBs do provide much convenience for human's daily life and even stimulate the revolution of electronic devices toward portability and miniaturization. Nowadays, the application of LIBs has been even extended to electric vehicles (EVs). A long driving range (≥ 500 km) requires power batteries with energy density in excess of 500 Wh kg^{-1}, provided that the battery pack system including indispensable ancillaries weighs no more than 300 kg per vehicle.[11, 12] Whereas, conventional LIBs based on $LiCoO_2$/graphite cannot satisfy this requirement due to their theoretical limitation of 350 Wh kg^{-1}. It is generally accepted that 30% improvement on energy density is the upper limit by optimizing current technology, which means that endurance mileage is difficult to increase significantly when driving a conventional LIBs powered EV.[13-16] Hence, developing next-generation high-performance energy storage systems with new electrochemistry seems to be an inevitable choice if we want to break through the intrinsic obstacles of current batteries, accessing to our targeted energy density of above 500 Wh kg^{-1} and a fabrication cost of less than $100 kW h^{-1}.[17-19]

Metal-gas batteries have attracted significant interests in recent years considering their much higher energy density.[33] For example, Li-O_2 batteries possess a theoretical energy density of approximately 3500 Wh kg^{-1} based on discharge product Li_2O_2, which is nearly ten times as much as that of LIBs.[17, 34] Through a long development history of over 100 years, numerous categories of metal/gas couples have already been attempted to realize effective electrochemical energy transformation. According to the different nature of metals and electrolytes employed, metal-gas batteries can be divided into two main kinds: aqueous and nonaqueous. Theoretical energy densities together with equilibrium potentials of previously known metal-gas batteries are presented in Fig. 1 for a general comparison.[20-32] Averagely, the energy storage capability of nonaqueous metal-gas batteries is higher than that of their aqueous counterparts. The exceptionally high gravimetric energy density originates from the great free energy release of metal ions-gas molecules reactions happening on cathode catalyst surface.[18, 34] The gases acting as energy resources are commonly available from outside atmosphere instead of being stored within the battery, which is also beneficial for achieving high energy density. In fairness, although the energy density of metal-gas batteries is closely approaching that of ideal power systems, their viability to replace LIBs for future EVs still remains unclear at the present stage, if given

[a] Institute of Chemical Materials, China Academy of Engineering Physics, Mianyang, Sichuan, 621900, P.R. China.
[b] Department of Macromolecular Science and Laboratory of Advanced Materials, Fudan University, Shanghai, 200438, China.
[c] Chemical Sciences and Engineering Division, Argonne National Laboratory, Argonne, IL, 60439, USA
* Corresponding authors: (J. Cheng)Jianlicheng@caep.cn;
B. Wang (binwang@caep.cn),

the problems on sluggish gas reduction reaction rate and rapid catalysis decay, which might not meet the power/longevity criteria for high-power and frequently-used applications.[35, 36] Meanwhile, quick charging (corresponding to gas evolution at high rates) is more difficult to realize by present metal-gas batteries with relatively large overpotential,[17, 34, 37] leading to a long period of waiting for re-use. It also should be pointed out that gas storage tanks or gas depuration/ transportation systems are indispensable on board to stabilize the energy supply, which may encounter challenges on safety, weight, space, reliability and replacement as well. However, what inspires us is, in spite of the above dilemmas, metal-gas batteries have revealed great potential of becoming advanced novel energy storage systems for consumer electronic products, especially proper for wearable electronics with the characteristics of long-term and low-power operation, on basis of current research findings,[38-40] which are rapidly accumulating within the last five years (Fig. 2a). Firstly, their outstanding energy storage capability enables the functional components more durable after a recharge process, compared with conventional LIB devices in the same size or weight. It is a pronounced advantage that is urgent for consumer markets. Secondly, the reversible capacity delivered by metal-gas batteries is originated from electrocatalytic gas reduction/oxidation reactions in open system so that a relatively small quantity of cathode catalysts together with easier encapsulation is required, which significantly lowers the fabrication cost of batteries, thereby making them widely affordable to customers. Thirdly, based on discharge capacity and cycling behavior of current lab-scale metal-gas batteries, their service life allows them to keep the pace with the generational change (about every 2-3 years) of portable and wearable electronics. The moderate total energy storage of lab-scale devices indicates that the way to promoting their electrochemical performance toward industrial products for consumer electronics is quite promising.[41-43]

Nevertheless, the aforementioned favorable viewpoints do not mean that there are no bottlenecks for metal-gas batteries to become the next-generation power accessories of wearable electronics. On one hand, a metal-gas battery also consists of metal anode, separator/electrolyte and air cathode, similar to the configuration of a half-cell LIB.[7, 18, 33] The main structure difference between the two kinds of batteries lies in the cathode, namely, active materials are coated on aluminum foil for LIBs, while for metal-gas batteries, catalysts need to be sprayed onto a well inter-connected and porous current collector to permit sufficient gas diffusion from outside environment to cathode, such as carbon paper, nickel foam, stainless steel mesh. Owing to the introduction of gas diffusion layers, most metal-gas batteries are produced in rigid bulk structure. Lack of flexibility means that electronic devices require extra space to place the power accessories so that the volume and weight of the devices will be enlarged unnecessarily. Simultaneously, it has reached an agreement that batteries in rigid structure are detrimental to construct flexible devices, especially for those wearable electronics which are designed to directly contact with human's body (Fig. 2b). Many high-tech smart electronic devices have to compromise on operational performance due to the non-deformability of batteries, like Huawei Mate X-5G with foldable screen, Apple Watch and Google glasses.[38, 43-45] It is recognized that flexibility should be an indispensable factor of metal-gas batteries that are adaptable for wearable electronics. Of course, while solving the problem of flexibility, other factors like comfortability, water/fire-resistance, stretchability, mechanical strength and so on, should also be taken into consideration in real service conditions.[38, 41, 42, 46-48]

On the other hand, apart from device functionality, current researches about metal-gas batteries also concentrate on optimizing the electrochemical performance of catalysts. Irreversible discharge products will gradually accumulate on cathodes as discharge/charge cycle proceeds owing to the limited catalysis of traditional carbon nanophases-based catalysts, which induces the continuous catalytic activity decay and remarkable decrease on reaction kinetics, thereby making the overpotential aggrandize and even resulting in unexpected electrolyte decomposition. That is the dominated reason why most of current metal-gas batteries show unsatisfying long-term cycling stability at high rates.[18, 34, 37, 49] Furthermore, it is equally important that all used gases (*e.g.*, O_2, CO_2, and N_2) which can diffuse through separator/liquid electrolyte would result in obvious corrosion to alkali metal anodes and meanwhile, inhomogeneous solid electrolyte interphase (SEI) with low ionic conductivity and poor interfacial compatibility also enables the growth of dendrite and "dead" metal aggregation that may puncture separator and cause short circuit. These two detrimental factors suppress the electrochemical performance and even become a potential threat to battery safety.[29, 50] Additionally, it also should be taken into account that liquid electrolyte takes a high risk of leakage if used in metal-gas batteries with open holes on cathode encapsulation. This is another inevitable problem that needs to be addressed urgently before discussing the possibility of applying metal-gas batteries as practical power accessories for wearable electronics. Otherwise, health and safety problems caused by electrolyte leakage will not be tolerated and accepted by industrial council or customers.[18, 37, 42, 51]

Aimed at the above issues, quite a few efforts have been made, among which three main strategies have been employed, including cathode catalyst microstructure/component design, metal anode modification and novel electrolyte synthesis.[22, 29, 52-54] Of course, it is a fact that compared with the long history of metal-gas electrochemistry, the concept of flexibility for metal-gas batteries emerged within the recent ten years as the increasing demand on flexible electronic devices and relevant explorations are still at a premature stage.[34, 55-58] Whereas, these efforts do push forward the development of flexible metal-gas batteries toward large-scale industrial deployment, especially in the field of wearable electronics. For convenience, a brief chronology illustrating the development of new families of flexible metal-gas batteries is presented in Fig. 2c, to the best of our knowledge.[21, 29, 55, 59-70]

In this paper, we do not intend to have a comprehensive overview of previously reported metal-gas battery catalysts or electrolytes. Instead, we will focus on recent technical advances together with major dilemmas facing current flexible metal-gas battery devices, highlighting how flexible cathodes with various catalyst microstructures and components affect the electrochemical performance of different categories of metal-gas batteries. Meanwhile, some impressive works related to flexible metal anodes and (quasi-) solid-state gel polymer electrolyte (GPE) have also been introduced for better directing the construction of solid-state flexible metal-gas batteries. Flexible Zn-air and Li-O_2/air batteries are mainly discussed. Besides, an emerging new type of flexible Li-CO_2 battery has been briefly overviewed to elucidate the great potential of novel metal-gas batteries. In the end, critical technical hurdles and future

research directions are discussed regarding rechargeable and flexible metal-gas batteries for wearable applications.

2. Flexible metal-air batteries

2.1 Working principles and development history

Of many available options for metal-gas couples, gaseous O_2 was primarily utilized to explore metal-O_2 electrochemistry because of its high activity and abundance in ambient atmosphere.[18, 56, 71] The final target of metal-O_2 couples is to fabricate batteries which can directly work in air so that metal-O_2 batteries are also known as metal-air batteries. In these battery systems, metal anodes have a wide selection range including alkali metals (Li, Na and K), alkaline earth metals (e.g., Mg and Al) and first-row transition metals (e.g., Fe and Zn).[34, 72] According to the different properties of metal anodes, present metal-air batteries can be divided into two categories: aqueous and nonaqueous, as can be seen in Fig. 3. The former which relies on air-stable metals (such as Zn, Fe, Mg and so on), commonly use OH^- based aqueous electrolyte, while the latter employing alkali metals (Li^+, Na^+ and K^+) choose to use aprotic organic ether-based electrolyte owing to the high chemical activity to moisture.[34, 73] On basis of the above features, the metal-O_2 couples using air-stable metals/aqueous electrolyte and operating in ambient atmosphere can be called "real metal-air batteries" (represented by Zn-air batteries), but the ones using alkali metals/organic electrolyte and operating in dry and pure O_2 gas in most cases if without other special structural protection should be called metal-O_2 batteries (represented by Li-O_2 batteries), more precisely. Of course, the electrochemical mechanisms for aqueous and nonaqueous systems differ considerably. For aqueous metal-air batteries, metal anode can be firstly passivated in alkaline circumstance, forming a corresponding oxide or hydroxide protective layer which only permits the migration of metal ions, thereby enabling a compatible interface with aqueous electrolyte. In discharge process, metal is oxidized into metal ions, while gaseous O_2 is reduced into hydroxy radicals with the assistance of catalysts on porous air cathode. The general mechanism can be illustrated by the following equations:[73, 74]

Anode: $M \rightleftharpoons M^+ + e^-$

Cathode: $O_2 + 2H_2O + ne^- \rightleftharpoons 4OH^-$

Where M presents the different kinds of metals and n is the stable oxidation number of metal ions. The aforementioned electrochemistry is reversible during charge, with metal depositing on anode as well as O_2 evolving from cathode.

Notably, the situation is much different in nonaqueous metal-air batteries. Upon discharge, the highly-sensitive alkali metal anode (Li, Na and K) is oxidized into metal ions similarly, followed by forming solvation clusters with organic electrolyte molecules and diffusing into the cathode. Meanwhile, cathode reactions involve an initial one-electron reduction of O_2 to form superoxide radical O_2^-. Desolvated metal cations are able to react with them to generate M_mO_2 accumulating on cathode. According to the hard-soft acid-base theory,[17, 18, 34] larger-sized Na^+ and K^+ can effectively help stabilize superoxide metal species (NaO_2 and KO_2), while in the case of Li^+, intermediate LiO_2 is not able to exist steadily. Its disproportionation leads to the formation of Li_2O_2 as the discharge product in Li-O_2 batteries, particularly. The oxygen reduction reaction (ORR) and oxygen evolution reaction (OER) mechanisms for nonaqueous metal-gas batteries can be explained as follows:[75-77]

Anode: $M \rightleftharpoons M^+ + e^-$

Cathode: $mM + O_2 + me^- \rightleftharpoons M_mO_2$ (*m=1 or 2*)

Because of the low solubility in organic electrolyte, superoxides or peroxides will accumulate on the surface of air cathode, gradually blocking the gas diffusion and ion transportation channels toward interior catalyst and eventually shutting off the battery. Hence, aimed at promoting the storage capacity, most developed catalysts for nonaqueous metal-gas batteries are highly porous to provide more space to accommodate discharge products.[78-80] Despite of these efforts, attempts on nonaqueous metal-gas batteries are still in their infancy. In fact, the origin of aqueous metal-gas batteries is much earlier than their nonaqueous counterparts. In 1878, the primary zinc-air battery was designed by Maiche and the corresponding commercial products started to enter the market about 50 years later.[81] In the following, Fe-air, Al-air and Mg-air batteries were successively developed from 1960.[82-84] However, until 1996, a rechargeable nonaqueous Li-air battery using carbonate-based electrolyte was initially introduced by Abraham et., al.[85] More recently, Na-O_2 together with K-O_2 begins to attract research interests from scientists, due to the abundance of Na and K metals in earth as well as their lower overpotential.[26, 77]

Based on different mechanisms, recent progress and challenges on flexible metal-air batteries will be mainly exemplified using zinc-air and lithium-O_2/air batteries as the representatives for aqueous and nonaqueous systems in the following discussions, respectively.

2.2 Flexible Zn-air batteries

Due to the inexpensive, earth-abundant, highly-safe, and bio-friendly features, zinc-air batteries (ZABs) have been utilized for hearing aids, which is the only commercialized metal-gas battery among their families until now.[17, 18, 56] ZABs can work in ambient atmosphere because other air components, like N_2 and CO_2, are much more difficult to be reduced on cathode in aqueous system, compared to O_2 with high activity.[72, 86] The basic working principle of ZABs can be specified as follows. During discharging, zinc metal firstly loses two electrons and is oxidized to Zn^{2+} gathering at anode while atmospheric O_2 molecules are catalytically reduced to OH^- at the triple-phase boundaries among air cathode, gas and electrolyte. The generated OH^- on cathode dissolve in electrolyte, migrate to the surface of zinc anode, and react with Zn^{2+} to form $Zn(OH)_4^{2-}$ which is further decomposed to insoluble ZnO. The accumulation of ZnO and shuttle effect of Zn^{2+} finally block the migration channels of Zn^{2+} and degrade the active catalytic sites for ORR, thus giving rise to polarization increment and even the collapse of battery. The overall reactions can be illustrated as the following equations, where the theoretical energy density and equilibrium potential are calculated to be 1084 Wh kg^{-1} and 1.65 V, respectively.[87-89]

Cathode: $O_2 + 4H_2O + 4e^- \rightleftharpoons 4OH^-$

Anode: $Zn + 4OH^- \rightleftharpoons Zn(OH)_4^{2-} + 2e^-$

$Zn(OH)_4^{2-} \rightleftharpoons ZnO + H_2O + 2OH^-$

Overall: $2Zn + O_2 \rightleftharpoons 2ZnO \quad (E^{\theta} = 1.65\ \mathrm{V})$

When Zn-air battery is charged, zinc is reversibly deposited at metal anode and O_2 is released from air cathode through OER process. Notably, ORR active sites are vulnerable compared with OER sites. Their low tolerance against reduplicative reductive-oxidative operations leads to the poor cycling stability of Zn-air batteries.[90-92] Meanwhile, despite the cost-effective zinc metal together with aqueous alkaline electrolyte enables ZABs to reach the entrance of commercial applications, they are still produced in a conventionally rigid stack-type structure. Hence, employing ZABs as power supply for wearable electronic devices still remains a challenge.

2.2.1 Flexible air cathodes

The first obstacle for flexible ZABs is to realize the flexibility of air cathodes. In this regard, a bendable and tough substrate (e.g. carbon nanotube (CNT) paper, carbon nanofiber (CNF) cloth, porous graphene (G) film, nickel foam) is necessary for catalyst loading.[56, 93-96] Generally speaking, current flexible air cathodes have been prepared *via* two main strategies: spraying catalyst ink into flexible porous current collectors (spraying technique) and *in-situ* constructing catalyst/current collector integrated free-standing electrodes (*in-situ* construction).

Also, it is noteworthy to reconsider the bottleneck on sluggish ORR/OER kinetics and electrocatalytic durability of cathode catalysts, resulting in quite limited energy conversion efficiency, low output power efficiency and unsatisfactory cycling performance.[92, 97] Although Platinum (Pt) and its alloys are currently regarded as the best electrocatalyst for aqueous ORR, the high cost and remarkably declined activity do hinder their large utilization.[17, 34] To solve this dilemma, substantial efforts have been made on exploiting flexible cathodes anchoring catalysts with high efficiency and long durability, such as carbon nanophases, non-noble metals and their derivatives, rare metal-based hybrids. They are expected to achieve a satisfying electrochemistry even when the ZABs were tolerating complex and repetitive deformations. Some typical works related to flexible ZAB cathodes are selected here and presented in Fig. 4, where it compares the potential difference (Fig. 4a) between the half-wave potential of ORR and overpotential at 10 mA cm^{-2} of OER (tested in aqueous alkaline solution using three-electrode system) and the electrochemical properties of corresponding flexible ZABs (Fig. 4b).[22, 59, 93, 94, 98-108]

2.2.1.1 Flexible cathodes prepared by spraying technique

The spraying technique is almost a universal strategy to fabricate flexible cathodes loaded with target catalysts as long as the catalyst powder can be synthesized. There are quite a few impressive works related to this.

Firstly, cost-effective and durable carbon nanophases have been widely used to fabricate flexible cathodes by spraying themselves onto porous current collectors. For example, Xia et., al synthesized a N-doped CNT/reduced graphene oxide (rGO) hybrid through pyrolyzing metal-organic frameworks grown on rGO nanosheets (Fig. 5a,b).[109] This composite demonstrated the higher onset voltage of 0.92 V and half-wave potential of 0.85 V, which are comparable to those of commercial Pt/C catalysts. After being loaded on carbon cloth, this N-CNT/rGO hybrid could be utilized to fabricate an excellent bifunctional flexible air electrode for flexible ZABs.

Despite that the catalysis of carbon materials is relatively stable and durable, their electrocatalytic activity is far from satisfaction. To reduce the discharge/charge overpotential, metal-based composites were introduced into the design and preparation of flexible cathodes for ZABs. Peng et., al used cross-stacked aligned CNT sheets dipped with RuO_2-based catalyst ink to prepare a flexible and porous air cathode for ZABs.[103] The air cathode consisting of 30 layers of CNT sheets and a cross-stacking angle of 90° demonstrated the best rate performance due to the sufficient O_2 diffusion and lower resistance. The cathode could maintain the discharge voltage at around 1.0 V for 30 cycles at 1 A g^{-1}. Besides rare-metal oxides, some transition metals and their derivatives have also been studied as efficient catalysts for flexible ZAB cathodes. Cathode catalysts comprising atomically dispersed metals in carbon matrices have attracted numerous insights in recent years on account of their superior catalytic efficiency. Peng et., al prepared Co atoms well-dispersed in coordination polymers (2,3,6,7,10,11-hexaiminotriphenylene) by varying the ratio of employed metal and polymer precursors.[110] The unpaired 3d electrons of as-obtained samples were able to enhance the ORR activity and selectivity of cathodes owing to the less coplanarity but more radical character. Chen et., al utilized $ZnCl_2$ crystals to create abundant defects in three-dimensional (3D) interconnected carbon networks, allowing more $C\text{-}N_4$ sites to accommodate Fe single atoms.[111] The formed FeN_4 active sites significantly promoted the ORR activity, thus boosting the electrochemical performance of corresponding flexible air cathodes. Wang et., al prepared single Co atoms anchored in porous N-doped carbon through the pyrolysis of 2D ZIF-67 formed in a solution with water as the solvent (Fig. 5c).[112] After acid pickling, single Co atoms were highly dispersed in the N-doped carbon nanosheets and tightly pinned at those N-C sites, as represented in Fig. 5d,e. This single atoms-based catalyst demonstrated an obviously larger saturation current of 10.38 mA cm^{-2} at 0.60 V in contrast to those of Co nanoparticles loaded carbon nanosheets and commercial Pt/C catalyst. Meanwhile, the lower overpotential for OER process elucidate that single Co atoms also facilitated kinetics of OH^- decomposition. As a result, the assembled flexible ZABs using single Co atoms-based cathodes delivered lower discharge/charge overpotential and more stable cycling behavior.

Apart from metal single atoms, metal and their derivatives clusters have also received equal attention due to the more facile preparation. Simultaneously, compared with metal single atoms which have the much higher utilization efficiency of materials, metal and their derivatives clusters commonly possess a stronger tolerability to structural damage during the repetitive ORR and OER processes, at the sacrifice of the decline of specific capacity. The easier preparation conditions enable this kind of catalysts to have more choices on materials design. Wu et., al synthesized 1 nm-scale ultrathin cobalt oxide layers highly-dispersed on Co/N co-doped reduced graphene oxide through a solution adsorption and subsequent high-temperature calcination process, as shown in Fig. 5f.[98] The CoO_x layers not only facilitated the electron transfer but also provided more active sites. Simultaneously, Schottky barrier formed between CoO_x layer and metallic Co sites doped in graphene was beneficial for charge separation, thus promoting both the ORR and

OER kinetics (Fig. 5g). The air cathode was prepared by coating hydrophobic carbon cloth with CoO_x/Co-N-graphene catalyst ink. It exhibited a certain flexibility and decent electrochemical performance, namely, a relatively stable discharge/charge profiles were recorded even when the cathode was bent from 0° to 180°. Additionally, after recovery from bendable state, the cathode showed negligible voltage change during the subsequent cycling behavior for 10 h. In the following optimizations, Deng et., al reported a modified cobalt oxide-based hybrid which comprised atomically thin mesoporous Co_3O_4 layers strongly coupled with N-doped reduced graphene oxide (N-rGO) nanosheets as a highly-active and durable bifunctional catalyst for ORR and OER, showing low Tafel scopes of 54 and 101 mV decade^{-1}, respectively.[93] Interestingly, they constructed a continuous production line to spray catalysts ink to a bundle of carbon fibers to fabricate a length-controllable fiber-shaped air electrode, which were then directly wrapped on the rest configuration of battery. The as-obtained battery revealed a high discharge potential of 1.2 V and a low charge potential of 2.0 V. Apart from cobalt based materials, other earth-abundant and low-cost metals, like Fe, Mn, have already been introduced into the family of ORR and OER catalysts.[59, 101, 107] Cho et., al prepared a Fe_3C/Fe/N-doped carbon catalyst derived from the pyrolysis of iron acetylacetonate and commercial silk fibroin.[59] The flexible cathode was obtained by casting Fe_3C/Fe/N-doped carbon catalyst suspension on a tailor-made gas diffusion layer composed of activated charcoal and poly-tetrafluoroethylene (PTFE) binder. Notably, this Fe-based catalyst loaded air electrode delivered a flat discharge voltage plateau at nearly 0.90 V for 10 h at 0.1 mA cm^{-2}. Furthermore, bimetallic catalysts were also employed as catalysts for ZABs. For example, a bimetal-carbon hybrid catalyst was developed by Ma et., al,[107] where alloyed FeCo nanoparticles embedded in bamboo-like structured N-doped graphitic carbon nanotubes (N-GCNT/FeCo) was synthesized by a pyrolysis and catalytic growth method at 500~800 ℃. After a similar spraying process, the N-GCNT/FeCo based flexible cathode was obtained. It demonstrated an outstanding long-term cycling stability of 240 cycles for 40 h and the discharge/charge potential gas was only 0.26 V. The corresponding energy density and peak power density could reach 653.2 Wh kg^{-1} and 89.3 mW cm^{-2}, respectively, based on the weight of catalysts. Some other categories of catalyst powders like metal phosphides, metal chalcogenides have been also used for fabricating flexible air cathodes for ZABs.

In general, catalytic sites from metal-based species showed better electrocatalytic activity than those from their carbon-based counterparts, and catalysts with smaller size (*e.g.* single atoms, few layers or defects) and homogeneous distribution are more likely to possess the faster reaction kinetics but more vulnerable structures, enabling the lower overpotential but weaker cycling stability during discharge/charge processes in contrast to large-sized nanoparticles, nanotubes or nanosheets. On the other hand, the flexibility of air cathodes prepared by spraying techniques highly depends on the flexibility of original substrates. Commonly, CNT and G clothes are capable of advantageous deformability compared with CNF clothes and nickel foams because the former has thinner thickness and larger crosslinked microstructures. It also should point out that despite of the high feasibility to fabricate flexible cathodes loaded with any target catalysts, spraying method is difficult to ensure intimate interfacial bonding between active catalyst and current collector which is critical to further promote the cycling stability as well as rate capability. Also, it enlarges the total weight and reduces the energy density of battery, unnecessarily.

2.2.1.2 Flexible cathodes prepared by *in-situ* construction

How to find another preparation strategy to simultaneously keep enough interfacial bonding and flexibility has hindered the advance of flexible ZABs. Under such a circumstance, *in-situ* synthesis of free-standing catalyst cathodes has been proposed to address the above problems exposed by spraying methods. Comparatively speaking, the synthesis process for integrated free-standing catalysts cathodes commonly requires meticulous design and relatively tedious post treatment. At current technology status, a certain of free-standing catalysts with specific microstructure and component can be prepared mainly through three ways: hydrothermal/solvothermal growth, electrostatic spinning, floating catalyst chemical vapor deposition (FCCVD) or their combinations.[22, 94, 102, 106, 108] These as-obtained integrated free-standing catalyst cathodes were highly flexible and demonstrated better electrochemical performance even at various deformation conditions.

Flexible carbon substrates themselves could demonstrate a certain electrocatalytic activity after suitable surface modifications. For examples, a flexible carbon cloth cathode with abundant oxygen-rich functional groups and nanoporous surface was manufactured by Zhao et., al *via* an acid oxidation treatment followed by air calcination.[99] The facile oxidation steps activated commercial carbon cloth to produce an efficient flexible metal-free cathode for ZABs, of which the oxygen electrocatalytic performance outperformed the oxygen-doped carbon materials reported to date. Only a low overpotential of 360 mV at 10 mA cm^{-2} for OER was realized by this cathode, which was among the best performances of previous metal-free catalysts. When used in ZABs, the cathode showed an excellent cycling stability during the initial 1000 min test. Choi et., al reported a composite consisting of graphene hydrogel/B-doped graphene quantum dots which was prepared *via* the self-assembly of rGO during hydrothermal process.[114] The obtained composite showed a 3D interconnected architecture with high porosity and large specific surface area. B-doped graphene quantum dots were highly dispersed in the skeleton of rGO, allowing abundant and stable active sites for long-term cycling (94% of initial current density after 25 h of operation). Chen et., al reported an ordered multidimensional array assembled by 1D CNTs and 2D carbon nanoridges on nickel foam which avoided the internal blockage of electrode in ORR process (Fig. 6a).[113] Numerous CNTs were grown on the outer walls of ordered carbon nanoridges so that enough voids were remained between adjacent CNTs/nanoridges sheets, providing abundant gas diffusion channels for interior active sites (Fig. 6b-d). Consequently, this flexible air cathode showed a current density of 0.8 V for ORR and a potential of 300 mV at 10 mA cm^{-1} for OER, as shown in Fig. 6e. The assembled flexible ZABs using this cathode demonstrated an impressive energy density of 946 Wh kg^{-1}.

Whereas, the issues on limited electrocatalytic activity also occur in integrated free-standing air electrodes. Hence, metal-based components have been similarly introduced into the free-standing composites, as what are focused in the section of spraying method. Deng et., al designed an integrated free-standing electrode based on

$NiCo_2S_4$/graphic carbon nitride/CNT hybrid ($NiCo_2S_4$@g-C_3N_4-CNT, Fig. 6f).[102] They took advantage of the self-assembly effect of C_3N_4 nanosheets to interconnect all components together during the *in-situ* hydrothermal growth, as proved by TEM images in Fig. 6g,h. The synergistic effect of bimetallic Ni/Co sites and pyridinic-N site in g-C_3N_4 greatly facilitated the electron transfer and reaction kinetics while the entangled CNTs ensured the high electronic conductivity of the whole electrode. Benefit from these favorable features, $NiCo_2S_4$@g-C_3N_4-CNT manifested a great potential as the flexible cathode for ZABs. It exhibited a higher onset potential of 0.87 V and larger limited current density of 4.8 mA cm^{-2}. Simultaneously, the Tafel slope of $NiCo_2S_4$@g-C_3N_4-CNT was measured to be 74 mV $decade^{-1}$, closely approaching 69 mV $decade^{-1}$ of Pt/C, the best ORR catalyst. The LSV curves presented in Fig. 6i indicated its much improved OER activity compared to the control samples. Further modification to $NiCo_2S_4$ catalysts was implemented by Chen et., al.[115] They adopted electrophoretic deposition to anchor defect-enriched N-doped graphene quantum dots (N-QDGs) on needle-like $NiCo_2S_4$ arrays grown on carbon cloth. Bifunctional active sites and synergistic coupling enabled this N-QGDs/$NiCo_2S_4$ catalyst to deliver enhanced OER and ORR capabilities and excellent cycling stability of 200 h. Meanwhile, its mechanical bendability was well maintained.

Several modifications on cobalt oxide-based integrated free-standing catalysts have been attempted by Lu et., al through *in-situ* hydrothermal growth of Co(OH)F nanowire arrays on carbon cloth and the subsequent N-dopant reaction.[22] These as-synthesized flexible air cathodes of N-doped Co_3O_4 mesoporous nanowire arrays anchoring on carbon cloth exhibited a high ORR kinetics, namely, it achieved a high open-circuiting voltage of 0.94 V and maintained at this level during the discharge process for 10 h. What is more impressive is its outstanding volumetric capacity of 98.1 mAh cm^{-3} at 2.5 mA cm^{-3} and 84 mAh cm^{-3} at 25 mA cm^{-3}, indicating its decent high-rate capability. It is also noteworthy that the peak power density could reach 32.0 mW cm^{-3} at 90 mA cm^{-3}, opening the gate for practical applications. Another impressive work of constructing Co_3O_4-based nano-micro arrays on carbon cloth was reported by Li et., al.[116] ZIF-67 nano-polyhedrons were formed on the surface of ZIF-67 micro-sheets through two-step growth in water and methanol, successively. After calcination, the unique nano-micro arrays were well maintained on carbon cloth. This hierarchical structure guaranteed enough catalyst loading, abundant active sites and fast reaction kinetics. The Lower overpotential of 310 mV at 10 mA cm^{-2} and Tafel slope of 58 mV dec^{-1} were recorded, illustrating their superior electrocatalytic capabilities toward ideal ORR and OER. The excellent electrochemical performance of corresponding flexible ZABs under different deformation conditions further evidenced the great potential of this Co_3O_4-based cathode.

Apart from individual preparation strategy (e.g. hydrothermal growth/assembly, high-temperature calcination), combination of various technologies endows the integrated free-standing catalyst design with more choices on complex microstructure and species range. Here, three typical cases related to Co-based free-standing catalysts are exemplified to better elucidate the above statement. As expected, optimization on cobalt-based catalyst's microstructure has been further implemented by Lu et., al.[105] They employed atomic layer deposition (ALD) technique to generate Al_2O_3 as both confinement and protective nanolayers to grasp volatile carbon and alleviate the aggregation of metal oxides during the pyrolysis of zeolitic imidazolate framework, fabricating an electrode comprising Al_2O_3 nanolayer coated Co_3O_4/N-doped carbon hollow microcubes (Co-NC@Al_2O_3) on carbon cloth as bifunctional catalysts for ZABs (Fig. 7a-d). The electrode demonstrated a half-wave potential of 0.86 V for ORR and a low Tafel slope of 47.8 mV $decade^{-1}$ for OER, displaying decent durability with no remarkable activity degradation after running oxygen electrocatalytic reactions for 10 h. A potential difference of 787 mV between the half-wave potential of ORR and the overpotential at 10 mA cm^{-2} of OER (an indicator for the bifunctionality of catalysts) was achieved by this cathode. Notably, the excellent flexibility of this air cathode has been identified by the similar galvanostatic discharge/charge profiles under different deformation conditions. Zhang et., al utilized electrospinning technique to root 3D intertwined polypyrrole (PPY) nanofibers network on carbon cloth, followed by in-situ growing pearl-like ZIF-67 strung on these nanofibers through solvothermal method, as illustrated in Fig. 7e.[94] After calcination in inert atmosphere, porous N-doped carbon species anchoring noble-metal-free Co_4N nanoparticles and Co-N-C active sites were formed on the interconnected N-doped carbon nanofibers, shown in Fig. 6f-h. The superior OER activity of Co_4N coupled with the high ORR activity of Co-N-C coordination sites enabled this specially designed free-standing electrode to be bifunctional electrocatalysts for ZABs. Meanwhile, benefit from the enhanced structural stability of intertwined N-doped CNF networks, this cathode not only revealed a low overpotential of 310 mV at 10 mA cm^{-2} for OER and a high half-wave potential of 0.8 V for ORR but steadily run for over 20 h. When evaluated as ZAB cathode, it displayed a low discharge/charge difference of 1.09 V at 50 mA cm^{-2} and a superior longevity up to 408 cycles. Li et., al used a mixed solution of ethyl alcohol, ferrocene and thiophene as the carbon resource and catalyst to generate CNT film via a FCCVD method, followed by CV activation and hydrothermal reaction to create N/O-dopants in CNT walls and electrodeposition of $NiCo_2O_4$ nanosheets on CNT surface.[108] The obtained flexible cathode demonstrated excellent oxygen electrocatalytic activities with low Tafel slopes of 50 and 92 mV $decade^{-1}$ for ORR and OER, respectively. As the ZAB cathode, it revealed a low discharge overpotential of ~0.7 V as well as a relatively stable cycling behavior. More attractively, this N/O-co-dodped CNT/$NiCo_2O_4$ film could serve as an "all-in-one" air electrode for flexible ZABs without any additional binder, current collector and gas diffusion layer, ensuring the high conductivity of the whole electrode as well as reducing the unnecessary components used for interconnecting active materials.

It needs to point out that due to the advance of preparation technologies and equipment, other integrated free-standing catalysts with certain unique microstructures and complex components, like Fe/N/C-S-Fe_xC/Fe active sites embedded in microporous carbon fibers,[101] $CuCo_2S_4$ nanosheets anchored on N-doped carbon nanofibers,[104] Co nano-islands rooted on Co/N-doped carbon nanosheets supported by carbon felts,[106] porous Co-FeCo/N-C needle-like arrays anchored on carbon cloth[117] and so on, have also been explored as ZAB cathodes, showing comparable or better electrochemical performances and enough mechanical flexibility. Whereas, according to previous

reports, air cathodes prepared by *in-situ* construction seem to reveal weaker mechanical strength when compared with their counterparts prepared by spraying techniques. This is possibly because the interactional surface radicals and crosslinked microstructure of soft carbon substrates would be partially damaged in the *in-situ* construction process, thus leading to a lower resistance to external strain or stress. Although there are still some obstacles, recent development of flexible air cathodes does help flexible ZABs put forward a big step toward practical applications.

2.2.2 Flexible Zn metal anodes

As an indispensable component of flexible Zn-air batteries, Zn metal anodes are less concerned yet compared with the wide researches on catalytic cathodes at the present stage. In fact, Zn anodes are responsible for the reversible storage of Zn^{2+}, which is also a critical factor to determine the final rate capability and cycling stability of assembled Zn-air batteries.

In most cases, commercial zinc foil or zinc wire are used directly as flexible metal anodes.[98-108] This is possibly based on the following considerations. First of all, for the majority of reported works related to flexible ZABs, they commonly focused on cathode design to highlight the significance of the newly-proposed catalysts to facilitated ORR and OER kinetics. Hence, flexible battery devices were fabricated as a proof-of-concept application for cathodes through using commercial Zn products to simplify the procedure and lower the cost. Secondly, air-insensitive zinc foils and wires have both good mechanical strength, flexibility and processability so that they can be easily handled into target objects in ambient environment. Thirdly, currently-used commercial products are absolutely excessive when acting as a ZAB anode, compared to the real amount of Zn that is needed for reactions. Simultaneously, almost all previous ZABs were tested under a short-time discharging/charging roundtrip (commonly <30 min/cycle) to evaluate their cycling performance, during which a very small quantity of Zn had participated in the deposition/extraction reactions on anodes. As a result, local collapse of Zn seems to make negligible impact on electrochemical performances of the entire batteries under current evaluation methods. However, the low utilization of anode will obviously reduce the energy density of device and pure Zn metal is easily damaged or even broken during repeated deformations on account of inherent metal fatigue. Furthermore, when working time per cycle is enlarged, SEI fracture and dendritic or "dead" crystals caused by pure Zn anode will lead to serious battery performance decay. The above issues deserve heavy attention when it comes to practical products for consumer market.

It is believed that existing anode modification strategies in Zn-ion batteries (ZIBs) may be also effective for ZABs, considering the similar functions of their anodes. In ZIBs, four modification means are mainly adopted to achieve better zinc deposition on anodes, including: regulating crystal orientation, adjusting SEI components, coating nucleation-inductive layers and constructing nanostructures confined by carbon substrates.[118-126] For examples, Archer et., al. took use of graphene to drive the epitaxial deposition of Zn with a locked crystallographic orientation relation, which delivered superior reversibility over thousands of cycles even at moderate and high rates.[119] Cui et., al. designed a ZnF_2-rich, ionically permeable SEI film on Zn anode surface via regulating solvation structure.[118] These artificial SEI-decorated Zn anodes showed small voltage hysteresis as well as stable cycling performance in galvanostatic Zn plating/stripping test. Lu et., al. constructed a 3D flexible CNT/CNF hierarchical framework as the robust scaffold for uniform Zn plating and stripping.[122] The obtained Zn/CNT/CNF anodes not only lowered Zn nucleation overpotential but promoted the homogenous distribution of electric field thus achieving highly reversible Zn deposition without dendrites or other byproducts.

In fact, because of the higher handleability than another three modification ways, constructing Zn nanostructures confined by carbon substrates was adopted to fabricate novel flexible Zn anodes for ZABs, as reported by Wang et., al,[69] Yang et., al[22] and Zhi et., al.[100] They synthesized various Zn nanoarrays on N-doped carbon foam, carbon cloth and plicated CNT film via electrodeposition, respectively. Nevertheless, attention was only paid to the mechanical functions of anodes (e.g. compressibility, flexibility and stretchability) while the structure designs induced improvement on electrochemical performance were not involved or ignored in their literatures.[69, 111] To approach industrialization, more concerns on metal anode modification (like dendrite-free deposition, SEI design, gas corrosion protection) should be made in this important part of flexible ZABs.

2.2.3 Optimization on aqueous gel polymer electrolyte (GPE)

At present, it is a fact that the ORR and OER activities of cathode catalysts are usually measured in O_2-saturated alkaline or acidic aqueous solution. Liquid electrolyte is obviously detrimental to construct flexible ZABs for wearable electronics, considering the safety and health problem caused by the potential leakage of electrolyte.[40, 73, 127, 128] Therefore, several efforts have been made to develop quasi- or solid-state electrolyte, among which gel polymer electrolyte (GPE) received the most eyesight and has been widely used in flexible ZABs, owing to their features of good interfacial compatibility, relatively high chemical stability and facile preparation. Of course, continuous optimization has been further conducted to synthesize some multifunctional GPE with higher ionic conductivity as the "blood" of flexible ZABs. A comparison on different kinds of GPE for solid-state flexible ZABs has been summarized in Tab. 1,[12, 54, 100, 113, 116, 117, 129-137] including indexes like matrices, components, ionic conductivity, merits and weaknesses.

In brief, polyvinyl alcohol (PVA), polyethylene oxide (PEO), polyacrylonitrile (PAN), polyacrylic acid (PAA) and polyacrylamide (PAM) are commonly selected as the host polymer substrates for current GPE used in ZABs and numerous additives are introduced into polymer matrices to enhance their mechanical and electrochemical performances.[138, 139] Several recent impressive works will be simply introduced in this section. In most cases, PVA was employed. for examples, Hu et., al reported a porous PVA-based GPE composite which was synthesized through mixing PVA and PEG solution, followed by adding 5%$_{wt}$ SiO_2 nanoparticles as ceramic fillers to improve electrolyte retention and ion diffusion, shown in Fig. 8a.[129] After cross-linking and imbibing 6 M KOH solution, the GPE membrane was obtained. It exhibited a good ionic conductivity of 57.3 mS cm^{-1} (Fig. 8b) and ensured the assembled ZABs to work steadily for over 48 h. Chen et., al fabricated a PVA-gelled electrolyte membrane by utilizing glutaraldehyde (GA) and HCl to cross-link freeze-dried PVA membrane.[133] After being soaked in KOH/PVA

solution sufficiently, the GPE membrane with an ionic conductivity of 15 mS cm^{-1} was able to serve for ZABs. The GPE could support the assembled flexible ZABs to work normally under bendable state with the bending angle up to 180°. Benefit from the simple preparation process, this membrane could be produced on large scale, which lay the foundation for industrial-scale ZABs.

Next, the structure and components of this kind of membrane has been optimized by Qiao et., al.[130] Similarly, they also employed PVA as the matrix to accommodate guar hydroxypropyltrimonium chloride (GG) but via a binary cross-linking strategy using glutaraldehyde and pyrrole-2-carboxaldehyde (PCL) as cross-linking agents. It is noteworthy that this membrane demonstrated an interconnected porous structure originated from the trapped GG chains in PVA network, providing abundant channels for ion migration. As a result, the resultant membrane showed superior OH^- ionic conductivity of 123 mS cm^{-1} at room temperature. Besides, the fabricated hybrid membrane exhibited excellent tensile strength of 90 MPa and high thermal degradation onset temperature up to 230 ℃, much better than those of commercial counterpart (A201) and most previous polymer electrolyte membranes. Hence, the ZABs with this hybrid GPE membrane represented enhanced capacity, cycling stability and stable electrochemical performance within the temperature range from 0 to 120 ℃. Moreover, biomass like bacterial cellulose (BC), has been brought into PVA substrate to increase the mechanical strength of GPE. Chen et., al prepared a flexible PVA/BC/KOH/$Zn(CH_3COO)_2$ composite hydrogel electrolyte through mixed solution combined with freeze-drying methods.[132] The GPE was composed of the dual networks of PVA and BC, showing an intertwined and microporous structure. Thanks to the unique load-bearing dual networks, this composite membrane exhibited a high tensile strength of 0.951 MPa while the ionic conductivity could still reach 80.8 mS cm^{-1}. The ZABs using this kind of GPE delivered better rechargeability as well.

Some other kinds of GPE based on dimethyloctadecyl [3-(trimethoxysilyl) propyl] ammonium chloride (DMOAP),[131] polyacrylamide (PAM)[54] or cellulose[132] were also obtained by UV irradiation or temperature induced chemical cross-linking. In Fig. 8c-f, Chen et., al reported a nanoporous DMOAP-functionalized cellulose nanofiber film as solid-state electrolyte for ZABs by a simple mixed solution and vacuum filtration method.[131] The as-obtained electrolyte film is transparent, highly flexible and processable, with an ionic conductivity of 21.2 mS cm^{-1}. Noteworthily, a special work reported by Zhi et., al. is worth emphasizing here.[100] To date, PVA-based GPEs have to face a big challenge of poor stretchability and quite limited ion-transport capability. By contrast, although hydrogels, such as polyacrylic acid (PAA) and polyacrylamide (PAM), possess stronger water-retention capability, while they will lose their mechanical robustness when alkaline KOH electrolyte is incorporated. Aimed at the absence of GPE with both high stretchability and ionic transport capability, Zhi et., al developed a super-stretchable dual-network hydrogel electrolyte where sodium polyacrylate (PANa) chains played the role of soft domains and the carboxyl/hydroxyl groups coupled with cellulose served as the KOH stabilizer (Fig. 8g-i). The GPE showed an ionic conductivity of 280 mS cm^{-1} and could be easily stretched to 1200%. The flat ZABs using this GPE maintained normal function (with stable discharge voltage of ~1.2 V and charge voltage of ~2.1 V) even after being stretched up to 800 %. Chains' physical entanglements and chemical cross-linking as well as hydrogen bonds in polymer networks should take responsibility for the enhanced mechanical property. The dynamical recombination of broken inter-molecular hydrogen bonds during the deformation process also contributed to the superior stretchability.

2.2.4 Different battery configurations

Until now, planar and fiber-shaped configurations dominate flexible ZABs. Comparatively speaking, present technology is relatively mature to fabricate batteries in two-dimensional (2D) stack-type structure and a few attempts have been further devoted to achieving multi-functions while maintaining the flexibility of ZABs.

Noteworthily, before discussing the details of representative works, a confusing evaluation situation was firstly proposed here for readers to consider while they are going through the following discussion. Currently, there is lack of widely-accepted criteria to evaluate the flexibility of batteries. Researchers commonly made a judgment based on their own subjective consciousness instead of objective indexes so that almost all reported works spoke highly of the device flexibility themselves no matter what kinds of deformation the batteries tolerated. In addition, the flexibility is indeed closely related to the size of devices and test standards. It is unfair to judge which battery has a better flexibility if they are not under the same test conditions. For example, when conducting bending test, after fixing the length/thickness of devices and the curvature radius/applied stress, the max bending angle is reasonable and convincing index to evaluate their flexibility. Therefore, it is hoped that more attention will be paid to this research direction and relevant test criteria can be established as soon as possible.

2.2.4.1 Flexible planar configurations

All the procedure for assembling planar flexible ZABs is similar to that for coin-type ZABs but through using flexible electrodes, quasi- or solid-state electrolyte and flexible encapsulating materials for protection (e.g., polydimethylsiloxane (PDMS), polyethylene terephthalate (PET), Al-plastic film, shrinkable tube). Typically, Han et, al fabricated such a planar flexible ZABs employing free-standing bimetallic Ni/Co catalyst as cathode, Zn foil as metal anode, PVA/KOH-based GPE as electrolyte and separator and Al-plastic film with through holes as encapsulation, respectively (Fig. 9a-c).[102] This solid-state ZAB exhibited a high specific capacity of 480.7 mAh g^{-1} based the weight of consumed Zn, corresponding to an energy density of 530.5 Wh kg^{-1} which rivaled that of liquid ZABs. Meanwhile, this battery also revealed superior rechargeability as it could last for more than 42 cycles (14 h) without recognizable discharge/charge voltage change. The similar discharge voltage platforms at different bending angles of 0°, 90° and 180° with various applied current density proved the considerable flexibility of the battery. Notably, the assembled solid-state flexible ZABs could work as the wristband and provide electricity for a watch with light-emitting diode (LED) screen, further giving an evidence of their great potential for flexible and wearable electronics.

2.2.4.2 Flexible fiber-shaped configurations

Compared with 2D planar counterparts, one-dimensional (1D) flexible fiber-shaped energy storage devices have significantly

advantageous geometrical conformability to irregular surface (e.g. human body), which enables them more attractive to wearable electronics.[15, 41, 45, 48, 140, 141] Therefore, attempts to make 1D flexible fiber-shaped Zn-air batteries have risen in recent years.[59, 93, 94, 103] It is recognized that 1D flexible batteries proposes higher requirements on battery configuration design as well as flexibility and catalytic activity of cathode.

Based on the flexible degree of cathodes, whether Zn spring/spiral Zn foil or Zn wire would be determined as fiber-shaped anode to adjust the curvature of wrapping cathode. As displayed in Fig. 9d,e, Park et., al. used spiral zinc foil and carbon cloth loading catalysts to fabricate an all-solid-state cable-type ZABs,[59] which showed almost unchanged discharge voltages at different bending angles. Meng et., al. adopted a similar strategy to design another cable-type ZAB using zinc spring as anode.[94] After encapsulating by shrinkable tubes with through holes, the ZAB could be bended, twisted or even knotted without electrochemical function collapse. However, the diameter of 1D ZABs prepared by this method was relatively large, thus leading to the fact that the flexibility of battery was not as good as expected. Employing highly flexible carbon fiber bundles or CNT paper as cathode substrate could effectively avoid this problem. Zeng et., al. directly wrapped CNT paper band on GPE coated Zn wire, preparing an ultralong fiber-shaped ZABs with the length of above 50 cm,[108] which exhibited great flexibility that it could tolerate pattern-like deformations like cotton wire. Li et., al. obtained a high aspect ratio fiber-shaped ZABs with coaxial structure through wrapping catalysts-containing carbon fiber bundles on GPE coated Zn wire.[93] This fiber-shaped ZAB with the volumetric energy density of 36.1 mWh cm^{-3} could be easily woven into fabric to produce a self-powering textile which was capable of driving electronic watch, LED screen and smart phones (Fig. 9f-h), revealing the promising applications of this flexible ZABs in a wide variety of wearable electronics.

2.2.4.3 Flexible configurations with multi-functions

In the process of pursuing ideal flexible ZABs, stretchable function has been further achieved by strain-accommodating engineering of device structure. For example, Zhong et., al connected four flexible anode/GPE/cathode units by serpentine-shaped Cu conductors to constitute a planar ZAB prototype.[70] The whole active components were encapsulated in highly elastic Ecoflex substrates. Benefit from the elastic properties of serpentine-shaped conductors and encapsulation materials, this 2D ZAB prototype achieved flexibility and stretchability at the same time. The electrochemical performance could be retained at an acceptable level even if the flexible device was stretched up to 125% strain. As a proof-of-concept, this flexible and stretchable ZAB prototype was attached onto a fabric worn at human elbow. It could facilely bend, stretch and shrink along with the body movement. Similarly, Xu et., al took use of zinc spring as metal anode and spinnable aligned CNT arrays as flexible cathode to prepare such a fiber-shaped ZAB, but the recoverable distortion was only less than 10 %.[103]

Stretchability could also be incorporated into flexible ZABs as an intrinsic feature by fabricating both stretchable electrodes and GPE. Ma et., al reported an 800% stretchable flat-shaped ZABs by assembling plicated catalyst-loading CNT paper, Zn-deposited CNT paper and 1200% stretchable GPE.[100] Unexpectedly, the electrochemical performance even became better after the battery was stretched up to 800%. Simultaneously, this kind of flexible ZABs presented a certain water-proof capability owing to the hydrophobicity of cathode, demonstrating an excellent environmental adaptability of the batteries (Fig. 10a-d). In addition, compressible property can also be realized by electrode design. Particularly, a planar squeezable ZAB was reported by Wang et., al very recently.[69] Melamine sponges were utilized to fabricate 3D nitrogen-doped carbon foams (NCFs). The corresponding anodes and cathodes were obtained by electroplating Zn nanosheets and Fe-Co_3O_4 nanowires in highly porous NCFs skeleton. After the impregnation of GPE into electrode sponges, they were assembled together with a separator set in the middle. The assembled ZABs delivered negligible changes on discharge/charge voltage during the compressing (up to 60% strain) and releasing processes and their power density could retain ~95% after 500 deformation cycles.

Nevertheless, in spite of these remarkable progress made by current researches, flexible ZABs are still facing numerous questions need to be solved on the road to practical power accessories for flexible devices, including cathode catalysts with high efficiency and low cost, metal anodes with superior Zn^{2+} plating/stripping and durable flexibility, GPE with high safety and ionic conductivity, interfacial bonding between GPE and electrodes, encapsulating materials, packaging technique, integration processes, eligibility criteria and reliability.

2.3 Flexible Li-O_2/air batteries

Compared with aqueous ZABs, nonaqueous Li-O_2/air (Li-O_2 operates in pure O_2 and Li-air operates in ambient air) batteries have a much higher theoretical energy density of ~3500 Wh kg^{-1} based on ORR process.[75, 76, 142] Due to this merit, Li-O_2/air batteries have been attracting tremendous eyesight over the past decade. For example, in 2009, IBM first proposed the “Battery 500” project, followed by active correspondence or participance from plenty of famous research organizations all over the world. They held a great ambition that develop practical Li-air battery packages to ensure a 500 mile (800 km) driving range for EVs.[17, 18] However, the progress of Li-air batteries is proven to be distinctly more complicated than initially thought so that no Li-air battery technologies are able to satisfy the above target to date. Comparatively speaking, the ORR process of Li-O_2/air batteries proceeds in aprotic organic ether-based electrolyte through a mechanism drastically different from that in aqueous alkaline solution for ZABs. (It needs to mention that there are also some explorations on constructing aqueous Li-O_2/air batteries, but the corresponding energy density is absolutely not comparable to that of nonaqueous counterparts.[33, 35, 36] Hence, they do not belong to the discussion scope of this paper). Unlike common electrocatalytic reactions in aqueous solution, Li^+ should play a certain role in ORR and OER of Li-O_2 batteries, which in term, puts forward stricter requirements on ionic conductivity, ion transport number, chemical stability and volatility of electrolyte. The general reaction steps of nonaqueous Li-O_2 batteries can be understood by the following illustrations.[76, 78, 143]

Cathode: $O_2 + e^- \rightarrow O_2^-$

$$O_2^- + Li^+ \rightarrow LiO_2$$

$$LiO_2 + Li^+ + e^- \rightarrow Li_2O_2$$

$$2LiO_2 \rightarrow Li_2O_2 + O_2$$

Anode: $Li \rightarrow Li^+ + e^-$

Overall: $2Li + O_2 \leftrightarrow Li_2O_2 \quad (E^\theta = 2.96\ \mathrm{V})$

During the discharge process (ORR), O_2 is firstly reduced to super oxide radicals and then combines with desolvated Li^+, generating intermediate LiO_2 on cathode. Due to the inherent thermodynamical instability of LiO_2, it will spontaneously convert into Li_2O_2 through further lithiation or disproportionation. As the final discharge product, Li_2O_2 has strong oxidability, which is easy to render structural damage to air electrodes and electrolyte, thereby resulting in performance decay of batteries. Upon charging, Li_2O_2 is decomposed into Li^+ and O_2 under the assistance of OER sites.

Notably, on account of the high sensitivity of Li metal to air, moisture and organic electrolyte, the fabrication processes of Li-O_2 batteries are more complicated and rigorous. All the assembling processes should be operated in Ar-protected glove box with strict requirements on H_2O and O_2 content (commonly < 1 ppm). Furthermore, considering the formation of lithium superoxides or lithium peroxides, most Li-O_2 batteries have to be evaluated under dry and pure O_2 atmosphere.[142, 144] Otherwise, CO_2, NO_2, H_2O and other air components would easily react with discharge products, leading to a fast decay on cycling performance or even shutting down the battery suddenly.[145] Despite of these harsher preparations and working conditions, Li-O_2 batteries are still captivating enough to academia and industry because of their unique electrochemistry and convenient O_2 harvest from ambient environment. That is the reason why explorations on flexible Li-O_2 batteries have been increasingly devoted in recent years, although Li-O_2 batteries need to face more complex scientific and industrial problems. More encouragingly, through coupling multifunctional catalyst components as well as designing gas protective layer, Li-O_2 batteries has embarked on the way to real Li-air batteries recently.[76, 78]

2.3.1 Flexible gas cathodes for different battery configurations

Through constructing specially-structured catalysts, preparing novel electrolyte and re-designing battery configurations, multifunctional flexible Li-O_2 batteries with better electrochemical performances have been developed gradually. Nevertheless, there are something that should be extra specified. On one hand, the performance of cathode catalysts for Li-O_2 batteries cannot be measured by conventional electrocatalysis evaluation methods (e.g. LSV and Tafel slopes) because Li^+ really involves in the cathode redox reactions in organic electrolytes.[146, 147] Although the role of Li^+ is not very clear to date, it is still much different from the common electrocatalytic processes in aqueous alkaline or acidic solutions for ZABs (Zn^{2+} does not participate in ORR and OER on cathodes). Hence, the ORR and OER activities of cathode catalysts are directly reflected by the electrochemical performances of assembled full Li-O_2 batteries, instead of using three-electrode system in aqueous solution to evaluate these two indexes separately ($E_{(ORR)1/2}$ and $E_{(OER)j=10}$, like that in ZABs related researches). On the other hand, compared with flexible ZABs, researches about flexible Li-O_2/air batteries began much later so that they are still in infancy. But fortunately, the existing design strategies and knowledge accumulated for flexible ZABs can be transplanted to the researches of flexible Li-O_2 batteries. As a result, most current flexible Li-O_2 cathodes are integrated free-standing catalysts and they are carefully designed to accommodate the special configurations of proposed flexible batteries.

Hence, for a better and more comprehensive understanding, typical battery configurations together with their specially-designed flexible cathodes will be synchronously introduced in the following discussion. First of all, representative works were compared in Fig. 11,[50, 53, 55, 60-62, 64, 148-160] in terms of their discharge/charge voltage, discharge capacity and cycling behaviors. Obviously, different microstructures and components of cathode catalysts result in significant disparity on electrochemical properties of Li-O_2/air batteries. On average, flexible cathodes with active components of metals and their derivatives outperform those with pure carbon nanophases in reaction kinetics, but it is hard to find a general regulation between rare metals, metal carbides/oxides/sulfides on basis of currently limited experimental results[60-62, 64, 148-160] This is possibly because microstructure and configuration design could effectively promote the ORR and OER capabilities of different kinds of catalysts.

2.3.1.1 Flexible planar configurations

After systematical investigation, it is found that planar configurations based on 2D flexible electrodes still dominate in current flexible Li-O_2/air batteries. Representatively, Zhang et., al have implemented some impressive works in this field.

For example, a flexible, free-standing and recoverable cathode was successfully fabricated by growing hierarchical rutile TiO_2 nanowire arrays onto carbon textiles (TiO_2 NAs/CT) (Fig. 12a).[60] This hybrid cathode showed better catalytic activities than pristine carbon textiles. The cell with TiO_2 NAs/CT cathode delivered a larger discharge capacity of 3000 mAh g^{-1} (vs. 770 mAh g^{-1} for carbon textiles) (Fig. 12b) and could last for over 356 cycles which is nearly 30 times longer than the one with untreated carbon textiles. More Importantly, the TiO_2 NAs/CT cathode exhibited decent mechanical rechargeability. After being washed, the collapsed cathode would come back to the normal status and keep cycling again (up to 1000 cycles). Besides, the good performance retention in harsh bending and twisting tests illustrated its potential on advanced flexible Li-O_2 batteries (Fig. 12c). Also conducted by them was an integrated self-package flexible Li-O_2 battery with thin thickness and high deformability, which is presented in Fig. 12d.[161] On one hand, in flexible cathode, ultrathin RuO_2 nanoparticles were electrodeposited on TiO_2 arrays grown on carbon cloth to further reduce the energy barriers of ORR and OER (Fig. 12e,f). Not only the discharge/charge voltage difference was reduced from 1.56 V (pure carbon cloth) to 0.7 V (Fig. 12g) but also the full discharge capacity (~9000 mAh g^{-1}), rate capability and lifespan (210 cycles) were significantly improved. On the other hand, because a specially designed elastic PDMS sheet with interconnected open pores acted as both gas diffusion layer and encapsulation material, the whole configuration of this Li-O_2 battery was closely compacted. This intimate and thin structure enabled the battery with high flexibility, which was easy to be largely bended,

folded, rolled or even twisted without obvious capacity decay (Fig. 12h,i). Such high deformability is quite eye-catching among reported 2D flexible Li-O_2 batteries until now. Besides, motivated by the special shape and structure of golden-toad eggs, Zhang et. al synthesized a self-standing, light-weight N-doped carbon nanofiber cloth with hierarchical macropores *via* a hard-template-assisted electrospinning method.[153] After the precursor was subjected to pre-oxidation, carbonization and de-templating, the obtained CNF cloth was decorated with homogenously distributed ultrafine RuO_2 nanoparticles by solution impregnation. This RuO_2-N-doped carbon hybrid flexible cathode reached a high full discharge specific capacity of 13290 mAh g^{-1} even at the large current density of 1 A g^{-1}. Simultaneously, it also exhibited an excellent rate performance and cycling behavior of above 150 cycles.

Of course, there are still some other special free-standing catalysts with various microstructures and components that have been successfully synthesized to fabricate traditional 2D flexible Li-O_2 batteries, such as brush-like CoN_4 anchored carbon nanofiber membrane,[162] free-standing 3D $CuCo_2S_4$ nanosheet arrays grown on nickel foam,[163] hierarchical porous $NiCo_2O_4$ nanoneedle arrays on carbon cloth[155] and so on. They all demonstrated obviously enhanced electrochemical performances while maintaining flexibility, compared with the pristine flexible substrates.

Designing ion/gas diffusion pathways in flexible cathodes is another research hot point in this field, which is quite meaningful for enhancing the electrode structure and electrochemical performance of flexible Li-O_2/air batteries toward industrial levels. Hu et., al have pioneered the design and preparation of gas cathodes possessing high-speed pathways for gas diffusion and ion migration.[149, 150] They proposed two kinds of cathodes with decoupled ion transport and gas diffusion channels for high-performance flexible Li-O_2 batteries. The former was cotton fibers knitted textile coated with single carbon nanotubes and Pd nanoparticles, in which the hierarchical structure of conductive textile networks provided separate pathways for ion/gas diffusion.[149] Electrolyte could diffuse along the cotton fiber bundles while O_2 gas could permeate through the woven gaps. Benefit from the non-competitive transportation channels, the cathode revealed a high area specific capacity of 8.6 mAh cm^{-1}, a low discharge-charge voltage difference of 1.15 V and a good cycling duration of 50 cycles at an optimized amount of electrolyte. In contrast, the later came from a nature-inspired wood structure which had abundant hierarchical channels for multiphase transport (gas diffusion, ion migration and discharge product deposition). Similar to the artificial textile-based multichannel cathode described above, natural wood could retain these favorable features after the delignification treatment.[150] Cellulose nanofibers had enough nanopores to allow fast Li^+ ion transportation, while unperturbed wood lumina played a role of diffusion channel for gas permeation (Fig. 13a-f). After loaded with carbon nanotube/Ru catalysts, the cathode showed a record areal capacity of 67.2 mAh cm^{-2}, a low overpotential of 0.85 V and a decent life duration of 220 cycles, as the consequence of non-competitive triple pathways design. These electrochemical indexes are much better than those of the cathodes with densified or flooded structures (Fig. 13g). It also should be pointed out that the assembled Li-O_2 battery based on wood-derived cathode had both high mechanical strength and superior flexibility.

2.3.1.2 Flexible fiber-shaped configurations

As specified in the part of "flexible Zn-air batteries", 1D flexible devices have advantageous adaptability to irregular geometric surface. This is also very effective for flexible Li-O_2 batteries.

Especially, Peng et., al have pioneered 1D energy storage devices based on cable-type structure. In 2016, a new family of flexible Li-air batteries was reported by them, namely, a fiber-shaped flexible Li-air battery with a coaxial-fiber architecture.[62] They produced this battery by wrapping aligned CNT sheets on GPE coated lithium wire, followed by encapsulating the whole device inside a shrinkable tube with numerous ventholes. The aligned CNT arrays endowed the cathode with a certain elastic property, thereby ensuring enough electro-conductivity and avoiding mechanical failure in the bending operation. The battery exhibited a discharge capacity of 12470 mAh g^{-1} and could be normally discharged/charged for 100 cycles even in ambient air instead of pure O_2 atmosphere. Notably, the obtained fiber-shaped batteries were easily woven into fabric and the self-powered textile prototype could be used for powering a commercial LED display screen, suggesting the great potential of this fiber-shaped Li-air battery on wearable consumer electronics. To alleviate the negative effect of moisture and greenhouse gases from ambient air on electrochemical performance, they further improved the configuration and active components of the fiber-shaped "real" Li-air batteries (Fig. 14a-c).[154] A low-density polyethylene (LDPE) film was inset between aligned CNT array cathode and porous shrinkable tube as the protective layer to suppress the permeation of H_2O into cathode while retaining a high O_2 permeability. After optimizing the battery configuration, the fabricated fiber-shaped Li-air battery could really operate at ambient atmosphere instead of dry and pure O_2 gas, and the cycling life of the battery was extended to surprising 610 cycles. Additionally, because of the flexible components and moisture-resistant LDPE protective layer, this fiber-shaped Li-air battery could not only be woven into fabric to constitute wearable self-powered textiles as the power supply for portable electronics, but also retain normal functions even in water, extending the adaptability of Li-air batteries to practical working conditions.

To extend the usage scenario, Yan et., al further re-designed the structure of common fiber-shaped Li-O_2 batteries, as illustrated in Fig. 14d.[148] This unique "trans-structure" enabled that O_2 gas could be provided from the inner channels while the outer walls of device were protected by complete shrinkable tubes without pores. Benefit from the combination of the advantages of trans-structure and fire/water-resistibility of GPE, this special Li-O_2 battery could still work even though the whole device was immersed under water completely (Fig. 14e,f), and it was not easy to catch fire compared to common fiber-shaped Li-O_2 batteries with holes on encapsulations to allow gas diffusion from outside atmosphere. This work provided new design thoughts for future flexible fiber-shaped Li-O_2/air batteries.

Undoubtedly, several other researchers have also carried out impressive works on 1D flexible Li-O_2 batteries. For examples, Liu et., al sprayed commercial carbon material Super P and polymer binders onto flexible carbon textiles, fabricating a simple carbon-based cathode for Li-O_2 batteries in a cost-effective strategy.[158] The fabricated flexible fiber-shaped Li-O_2 battery delivered a good life duration of more than 90 cycles at the discharge terminal voltage above 2.0 V. Unexpectedly, the battery also demonstrated a certain

water-survivable capability, which could still light up a red LED even though part of the battery was immersed in water. Yang et., al synthesized a blood-capillary-like structured free-standing, flexible and low-cost cathode where super-hydrophobic N-doped carbon nanotubes forests *in-situ* grew on stainless steel mesh (N-CNT@SS) through a facile and scalable FCCVD method.[160] The N-CNT@SS cathode exhibited a high discharge capacity of 9299 mAh g^{-1} and a stable cycling behavior up to 232 cycles. As for the fiber-shaped devices, strong mechanical properties and superior moisture resistibility were simultaneously achieved.

2.3.1.3 Unique configurations with multi-functions

On the way to constructing practical flexible Li-O_2/air batteries, several unique configurations have also been proposed to achieve multi-functions besides flexibility, which are worth emphasizing here.

Zhang et., al exploited a large-scale flexible cathode fabrication method by employing brush to coat catalysts ink on commonly used paper in various patterns.[61] The low cost of paper and ink together with the facile and effective electrode synthesis approach seems to be quite attractive to industrial production. More interestingly, inspired by the unique characteristics of paper-ink cathode, a foldable Li-O_2 battery pack was prepared for the first time. The unique foldable structure of the battery played a critical role of power switch, which enabled this Li-air battery to provide electricity at a compression state and automatically stop after releasing external force (Fig. 15a-c). It also should note that the light weight (~1.93 g) of the device was beneficial for improving its whole gravimetric/volume energy density. Similarly, to achieve light weight, robust and wearable features, Zhang et., al designed a novel segmented Li-O_2 battery pack where overall air electrode was broken up into an array of disks without the necessity of gas diffusion layers (Fig. 15d).[55] The active catalytic component in cathode was RuO_2 nanoparticles dispersed carbon nanotubes (RuO_2@CNTs). Thanks to the light weight (0.637 g) and ultrathin configuration (0.474 mm), this fabricated wearable Li-O_2 battery delivered a quite high gravimetric energy density of 294.68 Wh kg^{-1} (based on the total weight of device) and reached a large volumetric energy density of 274.06 Wh L^{-1}. The two values were obviously higher than those of conventional coin-type, cable-type and soft-package type Li-O_2 batteries. Impressively, even after 10000 cycles of folding or stretching processes, the discharge/charge profiles still overlapped, further elucidating that the specially designed battery configuration was highly flexible.

Not limited to this, other efforts on novel cathode catalysts and practical assembly configurations for high-performance and flexible Li-O_2 batteries have been carried out. Typically, a distinct flexible Li-O_2 battery configuration was reported by Liu et., al, which seemed to be inspired by Chinese ancient bamboo slips (Fig. 15e).[157] A commonly used conductive additives, super P, was coated on the surface of carbon wire to constitute air electrode, without remarkable negative influence on flexibility. After being matched with GPE-coated lithium metal anode, the bamboo slips-like structured Li-O_2 battery was obtained. It could be easily attached onto the cloth worn on human body and tolerate intricate deformations. Moreover, Peng at., al succeeded in fabricating a flexible and stretchable Li-air battery for the first time through combining rippled CNT sheets and Cu springs connected lithium metal sheets, as demonstrated in Fig. 15f.[64] Even if the battery had experienced 1000 stretching cycles at the strain of 100 %, the electrical resistance was only increased by less than 4 %. What is more, the discharge voltage plateau of this as-prepared battery could be well maintained at a stretched state (Fig. 15g,h). This work presented a new and general function of flexible Li-O_2 batteries that should be taken into consideration in future researches.

Combining flexible Li-O_2/air batteries with other energy systems to construct flexible integrated devices with multi-functions is also a very meaningful research direction deserving our attention, although relevant reports are few up to now. An illumination-assisted flexible self-powered energy system based on a Li–O_2 battery reported by Zhang et., al is noteworthy here.[164] They grew porous TiN/TiO_2 nanowires on carbon cloth as bifunctional cathodes for flexible Li-O_2 batteries. Due to the photocatalytic activity of TiN/TiO_2 composites, the overpotential of the battery could be reduced to 0.19 V with the aid of solar energy (Fig. 16a,b). Inspired by this particular physico-chemical property, a flexible self-powered energy system was constructed *via* attaching a 2D flexible solar cell onto the anode side of Li-O_2 battery, presented in Fig. 16c. Through rational circuit design, the Li-O_2 battery could utilize the electricity provided by solar cell to recharge itself under a low overpotential when there was enough illumination, while powering other electronics in external circuit when the environment became dark (Fig. 16d,e). Simultaneously, due to the integrated configuration, this self-powered energy system was capable of enough deformability, suggesting its great potential as ideal uninterruptible power supply for wearable electronics.

Generally speaking, these attempts on designing or optimizing electrode structure and battery configuration have made a positive effect on promoting the development of "real" flexible Li-air batteries toward ideal power suppliers in practical service conditions. Enhancing total energy storage capability of battery packs while maintaining enough flexibility and multifunctionality is one of the most focused concerns at the present stage.

2.3.2 Flexible Li metal anodes

Similar to the situation of flexible ZABs, lithium foils or lithium sticks/wires were widely utilized in current flexible Li-O_2/air batteries to better highlight the advantages of newly-proposed cathode catalysts or electrolytes.[148-160] But fortunately, lithium anode modification has obtained much more researches in contrast to their Zn counterparts under the academic prosperity of lithium-ion-based energy storage systems. The air-/moisture-sensitive properties and easier dendrite growth make lithium anode a rapid performance response to structure/component modifications no matter whether it is used in secondary ion batteries or metal-gas batteries.[165-169]

How to solve the dendrite issues is the first priority for Li anode researches, which underlies the foundation of battery safety. In the preliminary studies, porous metal frameworks were employed as host scaffolds to accommodate Li through melting-impregnation or electrodeposition methods on account of the good wettability between different metals.[166] Nickel foam, porous Cu, Cu nanotube arrays and so on have usually been selected as the soft substrates for Li deposition. 3D highly-conductive pathways provided by metal substrates are beneficial for electric field distribution, inducing the

first deposition of Li^+ along the surface of metal scaffolds until all voids are filled instead of the formation of dendrite. However, Li anodes prepared by this strategy are of poor flexibility due to the limited flexibility of original metal substrates and intrinsic metal fatigue. As a result, most of them can only tolerate a small bending angle (<90°) at a large curvature radius. In addition, their volume mass has been remarkably enlarged, which will decline the energy density of device. Aimed at the above problem, carbon nanophases have been utilized as Li host materials, including free-standing GO film,[168] CNF clothes,[165] CNT arrays/films[167] and bio-derived porous carbon.[169] Similarly, large specific surface area and abundant defects of carbon nanophases offer uniform nucleation sites and action channels for Li^+ plating/stripping so that dendritic and "dead" Li were largely supressed in these Li/C hybrid anodes even at high rates. Whereas, the decline on flexibility was not thoroughly avoided because of the existence of Li-C interfaces and LiC_x phases. Although ideal flexible anodes for Li-O_2/air batteries have not been developed, a recent research outcome may provide some inspiration for future design. Li et., al fabricated a Li anode by infusing a suitable amount of molten Li into the CNT fibers modified with ZnO nanowire arrays.[170] Because ZnO is lithiophilic, Li prefers to deposit on their surface as a film coating rather than combine with CNT fibers. Hence, the obtained hybrid Li anode inherited the superior flexibility of pristine CNT fiber and it even can be wrapped on an elastic wire to achieve stretchability. It is hoped that these modified Li anodes can be early attempted and evaluated, accelerating the advance of Li anodes toward particularly appropriate ones for flexible Li-O_2/air batteries.

Besides, we also consider that constructing artificial SEI on Li anodes may be another promising solution, considering that pretreated SEI can effectively alleviate dendrite growth and gas corrosion in some rigid Li-O_2 cells reported previously,[171-174] but how to enhance the integrity and prevent the breakage of SEI during deformation seems to be a Gordian knot.

2.3.3 Optimization on aprotic GPE

In comparison to electrode design and modification, it deserves noting as well that electrolyte which is adaptable for flexible Li-O_2 batteries has already become another focused research point. It needs to admit that health and safe problem are rather the first important factor for possible commercial applications of flexible Li-O_2 batteries (especially those purposed at wearable electronics which requires to be directly contacted with human skin) when taking into account the poisonousness and dangerousness of used organic electrolyte, so that problems like leakage of electrolyte, flammable property, dendrite, atmosphere's sensitivity and mechanical failure, should be avoided as much as possible. It is considered that GPE advance is the critical step to address the aforementioned dilemmas and underlies the development of flexible Li-O_2/air batteries toward commercialization.

Some efforts related to this have been made recently. In contrast to ZABs, the polymer host of GPE for flexible Li-O_2/air batteries is relatively fixed because those well-known polymer frameworks can hardly satisfy the comprehensive requirements of Li-O_2/air batteries.[172, 182] For examples, PEO-based GPE exhibited a narrow potential window and poor room-temperature ionic conductivity. PAN-based GPE only showed an unsatisfactory interfacial compatibility with Li metal anode, while polymethyl methacrylate (PMMA)-based GPE suffered from weak mechanical property and flexibility. Among them, poly(vinylidene fluoride-co-hexafluoropropylene) (PVDF-HFP) was commonly chosen as the primary polymer matrix for GPE of Li-O_2/air batteries due to its low crystallinity, abundant ionic migration channels, stable chemical property, good processability and fire-resistance. Besides PVDF-HFP, a few other polymers, like polyimide (PI), poly(methyl methacrylate-styrene) (PMS), ethylenediamine (EDA), polyethylene glycol dimethyl ether (PEGDME) and thermoplastic polyurethane (TPU), have also been attempted, which demonstrated advantageous features in some aspects. Typical previous works about GPE for flexible Li-O_2/air batteries are presented in Tab. 2,[50, 53, 148, 154, 156, 175-181] illustrating their basic structural and electrochemical features as well as unique merits and weaknesses.

We selected several typical works among them to discuss in detail here. Wang et., al prepared an integrated quasi-solid-state electrolyte by infusing PVDF-HFP/super hydrophobic nanofumed silica (SH-SiO_2) ceramic homogeneous solution into cellulose paper (denoted as PS-QSE),[53] which took advantage of component interaction to realize high ionic conductivity (0.93 mS cm^{-1}), chemical stability (a stable voltage range of up to 3.63 V), mechanical strength and flexibility. This synthesized PS-QSE could effectively prohibit the growth of dendrite during cycling and suppress the lithium metal anode corrosion caused by O_2 and H_2O in air. Therefore, the overpotential of Li-air battery based on PS-QSE was much lower than that of the one based on conventional liquid electrolyte under ambient air. Benefit from the high safety and flexibility of PS-QSE, the assembled flexible Li-air battery was deformable and tailorable according to desired shapes. Aimed at the issue of high charge overpotential of traditional Li^+/TEGDME-based electrolyte, Peng et., al added a redox mediator LiI into TEGDME/lithium difluorosulfimide (LiSFI)/PVDF-based GPE prepared by UV radiation to the mixed precursor solution.[154] LiI could effectively play a role of ferry to boost the electron transport between discharge product and electrolyte/electrode, thus facilitating the reversible formation and decompose of Li_2O_2. As a result, the modified GPE with LiI reduced the charge potential to around 3.5 V, which was distinctly lower than that of the original GPE. At the same time, the cycling stability was enhanced because of the less decomposition of electrolyte during the low-voltage charge processes. Attractively, Yan et., al designed a PVDF-HFP/polyimide (PI) membrane as a composite multifunctional separator (PIPV) with high electrolyte uptake, as elucidated in Fig. 17a-d.[148] Although the obtained PIPV film revealed abundant pores in their framework, it still inherited strong mechanical strength coupled with high flexibility from PI. Owing to the hydrophobicity of both two components, this composite film could largely prevent Li anode from moisture corrosion. However, it only showed a quite limited ionic conductivity of 0.025 mS cm^{-1}.

Besides PVDF-HFP, a few other polymers have also been attempted as novel host polymers. Two examples are briefly introduced here. Ding et., al reported that a TEGDME (also known as G4) induced GPE was *in-situ* formed *via* the cross-linking reaction between liquid G4 and lithium ethylenediamine (LiEDA) on the surface of Li anode (Fig. 17e-g).[180] This G4 GPE showed a surprising voltage window of up to 5.5V, which was among the highest group in all reported GPEs for Li-O_2 batteries up to now. The Li-air batteries

employing G4 GPE also showed a significantly enhanced cycling stability. Nevertheless, such a preparation strategy exposed a shortcoming that the G4 GPE film was absolutely not processible and it was easily damaged during deformation on account of the small thickness of *in-situ* reaction layer. Shao et., al employed a similar strategy to fabricate a highly crosslinked quasi-solid electrolyte (FST-GPE) consisting of thermoplastic polyurethane (TPU), aerogel SiO_2 and nonwoven cotton fabric which were plasticized by conventional lithium bis(trifluoromethylsulfonimide) (LiTFSI)/tetraglyme (TEGDME) liquid electrolyte.[156] The resulting flexible Li-O_2/air battery could reach up to 250 discharge/charge cycles with operation time over 1000 h in O_2 gas and kept normal working for over 20 days under extreme bending conditions in ambient air.

Furthermore, ionic liquid gel electrolyte, as an emerging GPE for Li-O_2 batteries, starts to receive interests from researchers recently. For example, Sun et., al developed a novel category of ionic liquid gel electrolyte on account of the fact that it could offer wider electrochemical window and lower volatility.[50] The ionic liquid gel electrolyte was prepared by mixing ionic liquid of 1-n-butyl-1-methylpyrrolidinium bis(trifluoromethylsulfonyl)imide (BMPy-TFSI), LiTFSI and PVDF-HFP (Fig. 17h). Consequently, the obtained fiber-shaped Li-air battery realized stable working over a large arrange of temperature from 25 to 140 ℃. Particularly, it could demonstrate a high full discharge capacity of ~12000 mAh g^{-1} at 100 ℃ and an excellent long-term cycling stability of 380 cycles at the high rate of 10 A g^{-1} at 140 ℃ (Fig. 17i,j). On account of the inevitable heat accumulation when battery is working or recharging, this work promoted the high-temperature performance and safety protection of flexible Li-O_2/air batteries into a higher research level.

Although several progress on flexible Li-O_2/air batteries have been achieved *via* continuous electrode/electrolyte/configuration optimization until now,[183, 184] three main components including efficient catalytic cathodes, stable and highly ion-conductive (quasi)/solid-state electrolyte and dendrite-free flexible lithium metal anodes (few attention currently) still need more special explorations for flexible systems.

2.4 Other advanced metal-O_2/air batteries

Apart from Zn-air and Li-O_2/air batteries, their alkaline counterparts, such as Na, K, Mg, Fe, Al, Si and so on,[20, 21, 23, 26, 27, 63, 65, 77, 84, 185-187] have also been attempted to construct metal-O_2/air batteries. Their general working principles coupled with other electrochemical indexes are included in Tab. 3 for reading conveniently. Among them, some novel kinds of metal-O_2/air batteries have already achieved flexible devices or flexible components successfully so forth, while the remaining still needs tremendous efforts to overcome this challenge.

Herein, it has a brief introduction to some representative works on these potential novel flexible metal-gas batteries. Zhang et., al prepared a binder-free N-doped carbon nanofibers embedded and coated with homogeneously dispersed Co nanoparticles by a scalable electrospinning strategy for Na-O_2 battery cathodes[188]. This electrospun and carbonated core-shell nanofibers cathode performed an enhanced discharge capacity of 6102 mAh g^{-1}, a lower charge voltage plateau (3.4 V) and a longer cycling life up to 112 cycles, compared with N-doped carbon nanofibers. Zhou et., al directly used benzene/ferrocene-catalyzed CNT paper as the flexible cathodes for Na-O_2 batteries,[185] which exhibited the full discharge and charge capacity of 7530 and 3300 mAh g^{-1}, respectively, and a small overpotential gap of 0.2 V during cycles. Wu et., al reported a K-O_2 battery of which the discharge product was stable KO_2 instead of hyperoxide species for Li-O_2 batteries.[27] KO_2 could be reversibly formed and decomposed during discharge/charge processes in 0.5 M KPF_6/dimethoxyethane (DME) electrolyte without the utilization of catalysts, resulting in a quite low discharge/charge potential difference of less than 0.05 V. It was the lowest overpotential value in ever reported metal-O_2 batteries. Du et., al synthesized a PdSn/CNTs nanocomposite catalysts for Mg-air batteries by a facile chemical reduction method.[20] This hybrid catalyst revealed remarkable ORR activity in alkaline solution, enabling the assembled Mg-air battery to have a flat discharge voltage plateau at around 1.25 V within 13 h as well as the highest power density of 112.4 mW cm^{-2}. Fascinatingly, Peng et., al created two new kinds of all-solid-state fiber-shaped metal-O_2 batteries (Al-O_2 and Si-O_2 batteries) for the first time.[63, 65] The former fiber-shaped Al-O_2 battery not only demonstrated a specific capacity of 935 mAh g^{-1} and an energy density of 1168 Wh kg^{-1}, but also could be integrated into fabric-based wristbands and provide electricity for a LED watch.[63] The later Si-O_2 battery was designed with a highly flexible coaxial architecture, which ensured its effective operation after bending for 20000 cycles.[65] Also, the battery produced in a continuous scale demonstrated the capability of being woven with textile fibers to constitute a real self-powering fabric, suggesting great potential for commercial applications. Generally, despite all these novel metal-gas batteries are in the initial stage, they do provide alternative choices for future power accessories of wearable electronics.

3. Flexible metal-CO_2 batteries

Once proposed, metal-CO_2 batteries have been considered as a very ideal candidate for next-generation high-performance energy storage and conversion system for portable electronics and even (hybrid) electric vehicles. They not only demonstrate a high theoretical energy density but also provide a novel and facile strategy to achieve CO_2 capture without the necessity of extra energy consumption which is inevitably demanded in traditional CO_2 fixation methods. Consequently, this environmentally-friendly property is beneficial for alleviating greenhouse effect and endowing metal-CO_2 batteries with a promising significance in the progress of sustainable development.

3.1 Working principles

So forth, the feasibility of Li-CO_2,[189] Na-CO_2,[191] K-CO_2,[190] Al-CO_2[30] and Zn-CO_2[24] systems has been successfully verified through coupling various groups of electrodes and electrolytes. Li/Na-CO_2 batteries which possess relatively higher theoretical energy densities take use of ether-based organic electrolyte while Al-CO_2 battery employs ionic liquid as electrolyte. In contrast, two different kinds of Zn-CO_2 batteries are constructed in the mode of two cells using aqueous solution. The general information of the above four metal-CO_2 batteries is concluded in Tab. 4.

Among various kinds of metal-CO_2 batteries, Li-CO_2 battery is one of the most attractive representatives because it possesses a high

working voltage (~2.8 V) and energy density (~1875 Wh kg^{-1}) by 4-electrons transfer reaction. Its theoretical energy density is the largest among all known metal-CO_2 batteries, which is comparable to that of Li-O_2 batteries.[192, 193] Hence, literatures related to Li-CO_2 batteries are more reported, compared with their counterparts. Despite some efforts have been made to explore the detailed energy storage mechanism of Li-CO_2 batteries, it cannot reach an agreement at current stage. One possible reaction procedure is presented here for reference.[37, 194-196]

Cathode: $2CO_2 + 2e^- \rightarrow C_2O_4^{2-}$

$$C_2O_4^{2-} \rightarrow CO_2^{2-} + 2CO_2$$

$$CO_2^{2-} + C_2O_4^{2-} \rightarrow 2CO_3^{2-} + C$$

$$2Li^+ + CO_3^{2-} \rightarrow 2Li_2CO_3$$

Anode: $Li \rightarrow Li^+ + e^-$

Overall: $4Li + 3CO_2 \leftrightarrow 2Li_2CO_3 + C \quad (E^\theta = 2.80\ \mathrm{V})$

On basis of this mechanism, oxalate species are the intermediate discharge product of CO_2 reduction reaction (CO_2RR) which will then disproportionate to carbonate and amorphous carbon. During the charge process, active sites for CO_2 evolution reaction (CO_2ER) help facilitate Li_2CO_3 to decompose and release Li^+ and gaseous CO_2. According to the overall reaction, it offers a hopeful perspective that the future commercialized flexible Li-CO_2 batteries can provide a renewable energy for wearable, portable or flexible electronics and even (hybrid) electronic vehicles. Meanwhile, a large amount of CO_2 has been fixed into these batteries, greatly alleviating the greenhouse effect on earth. More oxygen can be remained for biology's survival. The environmentally-friendly property enables Li-CO_2 batteries to help reduce CO_2 emission and contribute to the sustainable development of human society. Additionally, compared with the discharge product Li_2O_2 in Li-O_2 batteries, lithium carbonate species in Li-CO_2 batteries are more chemically stable and safer, making it especially suitable for wearable consumer electronics.

3.2 Development of Li-O_2/CO_2 batteries toward Li-CO_2 batteries

The primary studies on Li-O_2/CO_2 batteries were originated from the purpose of understanding what happened in ORR and OER electrochemistry of Li-O_2 batteries if ambient air which contained contamination gases like CO_2, instead of pure O_2 gas, was utilized as the gas resources.[193, 197, 198] It is recognized that this is a crucial step for enabling current Li-O_2 batteries to become real Li-air batteries.

The first exploration was conducted by Takechi et., al,[197] where Li-O_2/CO_2 batteries demonstrated enhanced discharge capacities in the mixed gases with a wide range of CO_2 ratio from 10% to 80%. Nevertheless, only Li_2CO_3 was detectable in the discharged cathode and the morphology of discharge products was quite different from that of Li_2O_2 in Li-O_2 battery. The discharge voltage plateau of Li-O_2/CO_2 batteries was observed at 2.7 V, identical to that of Li-O_2 batteries. They considered that the enhanced performance should be attributed to the rapid capture of CO_2 to $O_2^{\cdot-}$, forming Li_2CO_3 which was slowly deposited. Later, McCloskey et., al. studied the electrochemical behaviors of rechargeable Li-O_2 batteries when CO_2, as the contamination gas (10% volume concentration), participated in the chemical reactions.[199] It was found that besides larger capacity, the overpotential saw an obvious upward trend in subsequent cycles. Based on the results of isotopic labeling measurements of $^{18}O_2$ and $C^{18}O_2$, it was deduced that the formation of Li_2CO_3 was originated from the chemical reactions between Li_2O_2 and CO_2. No CO_2 was involved in real electrochemical reduction or oxidation processes. Gradually, the content of CO_2 in the mixed O_2/CO_2 gas was increased to 50 % by Kang et., al.[193] They found that reactions between O_2^- radical and CO_2 were favorable when using high dielectric dimethyl sulfoxide (DMSO), while these reactions were supressed in low dielectric DME. Consequently, the Li-O_2/(50%)CO_2 battery using DMSO-based electrolyte could last for 20 cycles. Whereas, sulfoxide was vulnerable by nucleophilic attacks from reduced oxygen species. In addition, Li et., al achieved a rechargeable Li-O_2/CO_2 battery (O_2/CO_2=1:2, in volume) using tetraethyleneglycol dimethyl ether (TEGDME)-based electrolyte but with rapid increment of overpotential during the discharge/charge cycles.[198] Most researchers agreed that CO_2 did not attend redox reactions in Li-O_2/CO_2 batteries.

In the following process of pursuing full CO_2 as the gas resource for Li-gas batteries, A. Archer and co-workers firstly reported a primary high-temperature Li-CO_2 battery with conductive carbon particles as the cathode.[189] By employing ionic liquid electrolyte, the battery delivered increasing capacities and discharge voltages as the environment temperature rose from 25 to 100 ℃. Next, Li et., al found that Super P-based cathode could be reversibly discharged and charged in O_2/CO_2 atmosphere and even lasted for 7 cycles in pure CO_2 gas with the electrolyte of 1 M $LiCF_3SO_3$ in TEGDME.[198] Inspired by the possible CO_2 electrochemically catalytic utilization in the case of transition metal carbonates as anode materials for LIBs, Zhou et., al exploited practical rechargeable Li-CO_2 batteries with moderate electrochemical performances using CNTs or graphene as air cathodes in TEGDME-based electrolyte at room temperature.[28, 200] Starting from this milestone, the research gate of Li-CO_2 batteries has been opened.

3.3 Present flexible Li-CO_2 batteries

At present, the research interests in this field mainly focus on developing novel catalysts or redox mediators for Li-CO_2 batteries. Very few works related to flexibility have been reported so far. The dominated challenges of preparing high-performance flexible Li-CO_2 batteries lie in the following aspects:

(i) Conventional carbon nanophase catalysts induce the formation of thermodynamically stable Li_2CO_3, blocking active catalytic sites and resulting in sluggish kinetics of CO_2 reduction (O=C=O cleavage) and evolution reactions (CO_2 release). The dramatically increased charge overpotential (4.2-4.5 V) leads to the rapid failure of batteries.

(ii) The majority of current catalysts are in powder state. They need to be sprayed onto rigid current collectors to constitute air electrodes, which is obviously not beneficial for fabricating flexible Li-CO_2 batteries.

(iii) Traditional liquid organic electrolyte is not appropriate to construct flexible Li-CO_2 batteries, due to the risk of electrolyte leakage and flammable property. Several attempts have been made to solve part of the above problems through exploring novel catalysts and (quasi-) solid-state electrolyte.

Similarly, like Li-O_2 batteries, Li-CO_2 batteries also need to operate in pure and dry CO_2 gas and their electrochemical performance can be only evaluated in assembled full batteries with organic electrolyte containing solvated Li^+. Therefore, we will also introduce several impressive works on gas cathodes by categories according to the different geometrical shapes or functions of their corresponding flexible Li-CO_2 batteries in the following discussion.

3.3.1 Flexible air cathodes for planar batteries

As expected, the origin of flexible Li-CO_2 batteries traditionally focuses on constructing 2D planar flexible configuration as well. Considering that known carbon nanophase powders (e.g. super P, CNT, graphene)[28, 198, 200-202] exhibited relatively limited catalytic activity in reported rigid Li-CO_2 cells, the cathode catalysts for flexible Li-CO_2 batteries start the researches from transition/rare metals and their derivatives which have higher electrochemical activity.[194, 203-213] Also, the preparation methods for 2D flexible cathodes mainly lie in spraying and *in-situ* integrating. The former is to spray catalyst powders onto flexible current collectors like nickel foam, carbon cloth and so on, while the latter is to directly generate active catalyst hybrids as a free-standing film *via* hydrothermal growth, electrospinning, etc.

For examples, Wang et., al synthesized N-doped worm-like carbon embedded with MoFeNi and MoC nanocomposites on nickel foam as a binder-free cathode.[216] Because of the high catalytic activity of transition metals, the cathode delivered an obviously lower charge potential of around 3.8 V. This Li-CO_2 battery could also run for 90 cycles with relatively stable discharge/charge plateaus. However, the flexibility of the cathode was barely satisfactory, based on our observation to the deformation test. A wood-derived flexible Ru/C-based cathode was reported by Hu et., al.[217] This cathode not only provided decoupled transportation channels for ions and gas but also achieved efficient catalysis by ultrafine Ru nanoparticles decorated CNT networks. Benefit from the synergistic effect of structure and component design, this cathode exhibited outstanding cycling stability of up to 200 cycles without any obvious catalytic activity decay. As a proof-of-concept, a flexible Li-CO_2 punch cell was fabricated employing this wood-derived cathode, which showed decent tolerance to bending deflection like foldable and rollable states. They also expected this kind of battery could be applied on Mars spacesuits, powering aerospace electronic equipment.

Zhou et., al fabricated free-standing Ir/C nanofiber networks by electrospinning and calcination method.[218] The porous structure together with the high activity of ultrafine Ir nanoparticles endowed the free-standing cathode with excellent CO_2RR and CO_2ER electrochemistry. Specifically, it exhibited a high areal discharge capacity of 11.54 mAh cm^{-2} with a flat discharge platform of 2.8 V at 40 μA, as well as an excellent cycling performance for more than 120 cycles. Similarly, Guo et., al synthesized a rare metal Ir-based catalyst,[214] where high-density wrinkled Ir nanosheets were fully anchored on the surface of highly porous, N-doped carbon nanofibers (denoted as Ir NSs-CNFs). These ultrathin Ir nanosheets exposed enough accessible active sites for CO_2RR and CO_2ER (Fig. 18a-d). The Li-CO_2 batteries with Ir NSs-CNFs cathode exhibited outstanding long-term cycling stability, namely, it delivered at least 400 deep discharge/charge cycles with a curtailing capacity of 1000 mAh g^{-1} at 500 mA g^{-1} (Fig. 18e), which was among the best cycling performances of all reported Li-CO_2 batteries. The operation time of this battery also could last for surprising 3000 h. In majority of common works, electrolyte had already been entirely volatilized at all before that time and the battery invalided within initial dozens of cycles. Li et., al prepared conjugated cobalt polyphthalocyanine (CoPPc) powders via a facile microwave heating method.[215] Due to its solubility and intrinsic crosslinked elasticity, the as-obtained catalyst powder was reprocessable and could be easily casted on elastic and flexible PET substrates (Fig. 18f-h). Impressively, this cathode achieved excellent cycling behaviors of more than 50 cycles even though the curtailing capacity was set to 1.0 mAh cm^{-2}, much larger than that of usual test conditions (approximately 0.05~0.2 mAh cm^{-2}, conversed from gravimetric unit). To verify the possibility of practical applications, a large-sized 2D pouch cell assembled by CoPPc-loaded carbon cloth and Li foil was attached to the watchband and utilized for powering the electronic device in CO_2 atmosphere under different bending status, as revealed in Fig. 18i,j.

3.3.2 Flexible air cathodes for fiber-shaped batteries

Owing to geometrical factors, traditional preparation methods would take high risk of electrolyte leakage in fiber-shaped metal-gas batteries with holes on encapsulation materials. It even might lead to potential comfortability, health and safety issues. Meanwhile, considering the high aspect ratio of battery, it imposes much higher requirement on electrode conductivity. Special design strategies need to be developed for 1D configuration and electrode materials, which will make fiber-shaped devices easier, safer and more efficient to be fabricated and utilized.

Inspired by the previously reported 1 D devices, Wang et., al reported some progress on fiber-shaped flexible Li-CO_2 batteries, considering their unique structural advantages as described in the section of Li-O_2/air batteries.[219] They firstly fabricated a flexible hybrid fiber compromising highly surface-wrinkled and N-doped CNTs networks anchored on Ti wire as a flexible fiber-shaped cathode (N-CNTs@Ti) integrated with high performance and high flexibility by a modified FCCVD method. Compared with traditional CNT powder-based planar non-deformable cathode, this specially designed flexible fiber-shaped N-CNTs@Ti cathode not only achieved a significantly enhanced full discharge capacity (9292. 3 mAh g^{-1}) but also lowered voltage polarizations at various current densities. It was considered that the highly-wrinkled surfaces and N-6/N-Q dopants brought in more efficient sites for catalytic reactions. As a proof of concept, a quasi-solid-sate fiber-shaped flexible Li-CO_2 battery was fabricated to power a PDMS/CNTs-based strain sensor which was attached onto human's palm. Next, after optimizing the FCCVD process, bamboo-like N-doped CNT arrays were successfully grown on Ti wire (B-NCNT@Ti) with a larger linear mass loading density (Fig. 19a-e).[220] As expected, this modified B-NCNTs@Ti electrode exhibited an outstanding long-term cycling stability of 360 cycles at 1 A g^{-1} (Fig. 19f). Besides, it was employed to fabricate a trans-structured fiber-shaped flexible Li-CO_2 battery where N-CNTs@Ti was placed in the center as cathode while Li foil was wrapped outside as anode and protected by an intact shrinkable tube without gas diffusion holes. This unique configuration enabled the battery to avoid any negative influence by environmental moisture and electrolyte leakage. To illustrate a potential application, the battery was incorporated with a fiber-shaped dye-sensitized solar cell using

B-NCNT@Ti as counter electrode to prepare an integrated self-powered energy system, achieving a total photochemical-electric energy conversion efficiency of 4.6 %. This self-powered was further used to drive a wearable breath sensor, which sufficiently elucidated its wide adaptability to wearable electronics (Fig. 19g-i).

In the following, to solve the issue of low energy efficiency caused by high charge voltage of carbon nanophase catalysts, they synthesized ultrafine Mo_2C nanoparticles anchored on CNT cloth hybrid films as free-standing and binder-free cathodes for quasi-solid-state flexible Li-CO_2 batteries with a coaxial-fiber architecture (Fig. 20a-h).[67] Because of the synergistic effects of CNT substrate and Mo_2C catalyst, it delivered a low charge potential of around 3.4 V, a high energy efficiency of 80% and could run for 40 cycles. The intermediate discharge product $Li_2C_2O_4$ stabilized by Mo_2C *via* coordinate electrons transfer should be responsible for the reduction of overpotential. Although component mass was not controlled purposely, it still revealed a decent energy density of 117 Wh kg^{-1} based on the total weight of device. Besides the excellent adaptability to irregular geometric surfaces, the fabricated Li-CO_2 battery was also not easy to catch fire (Fig. 20i-l), owing to the fire-resistance of GPE used. Accordingly, this Li-CO_2 battery was considered to have possessed several factors of ideal energy accessories for wearable electronics.

Apart from Li-CO_2 batteries, other typical alkaline metals have been explored to fabricate metal-CO_2 batteries, including Na-CO_2 battery,[29, 221] K-CO_2 battery,[190] Al-CO_2 battery,[30] aqueous Zn-CO_2 battery.[24, 44] Some of them have already achieved flexibility while some of them are still at the primary stage for principle investigation. These explorations on metal-CO_2 batteries are also very attractive to aerospace exploration, for example, it may be a possible energy system to provide electricity on Mars where the atmosphere consists of 96% CO_2 gas. More importantly, the further understanding of reversible Li-CO_2 reaction mechanism will facilitate to address the predicaments facing present Li-air batteries where CO_2 in ambient atmosphere results in the formation of thermodynamically-stable lithium carbonate in discharge products, decreasing the cycling performance rapidly. Of course, it is believed that by persistent efforts, more advanced flexible metal-CO_2 batteries with high safety and high performance will be constructed in the near future, facilitating energy storage systems for portable and wearable electronics to step forward to the next revolution.

3.3.3 GPE development and optimization

To avoid possible leakage of liquid electrolyte and improve safety, exploiting adaptable GPE is quite meaningful for preparing high-safe and comfortable (quasi-) solid-state flexible Li-CO_2 batteries, especially for those which are designed for wearable electronics. Whereas, researches on GPE began a little later than gas cathodes. They are at the very beginning of initial stage.[222, 223] At present, few GPE for Li-CO_2 batteries are reported and they are usually originated from the inheritance and modification of electrolyte or membranes for Li-air batteries, solar cells and fuel cells.[66, 224, 225]

Typically, Li et., al synthesized a novel kind of GPE which was composed of a PVDF matrix filled with TEGDME-based liquid electrolyte for Li-CO_2 batteries.[225] Compared with individual LiTFSI/TEGDME liquid electrolyte, the battery cells with GPE demonstrated enhanced discharge capacity, rate performance and cycling stability (up to 60 cycles. The discharge products of GPE-based Li-CO_2 showed an amorphous film-like morphology, which was quite different from the nanoparticles-like morphology of the battery using liquid electrolyte. Importantly, the synthesized GPE also demonstrated a certain flexibility, laying the foundation for constructing flexible solid-state Li-CO_2 batteries. Wang et., al added binuclear cobalt phthalocyanine (Bi-CoPc) into the above GPE as a redox mediator to boost the decomposition of discharge products at lower charge overpotential.[224] Expectedly, the discharge and charge voltage difference of the cells with Bi-CoPc based GPE was decreased to 1.14 V, which was distinctly lower than 1.90 V of the cells with pristine GPE. Moreover, the cycling life was also extended to 120 cycles and the flexibility was well-maintained. Chen et., al created another new family of composite polymer electrolyte (CPE) which consisted of poly(methacrylate) (PMA)/poly(ethylene glycol) (PEG)-$LiClO_4$-3wt% SiO_2 ceramic fillers for Li-CO_2 batteries.[66] The CPE had a high ionic conductivity of 7.14 x 10^{-2} mS cm^{-1} at 55 ℃. Multiwall CNTs were coated on the thin CPE to constitute an incorporated CPE@CNTs cathode. More importantly, a light-weight, flexible, all-solid-state planar Li-CO_2 battery was fabricated using the CPE@CNTs integrated cathode, nickel foam (air diffusion layer) and lithium foil anode. It could be reversibly discharged and charged for 100 cycles with a curtailing capacity of 1000 mAh g^{-1} at 55 ℃. Furthermore, the flexible liquid-free pouch-type battery demonstrated a lab-scale large full discharge capacity of 993 mAh, corresponding to high energy density of 521 Wh kg^{-1} based on the total weight of the battery. This study provided fundamental and technological progress on flexible Li-CO_2 batteries with practical-scale energy density and satisfactory flexibility.

4. Novel flexible metal-gas battery candidates

Besides metal-O_2/air and metal-CO_2 batteries, there are still a few innovation explorations on possible metal-gas batteries, including Li-N_2,[31, 226] Li-O_2/H_2O,[227] Li-O_2/HCl,[228] and Li-SO_2[32] batteries. All of them employed nonaqueous electrolyte. For convenient reading, the general reaction mechanisms coupled with theoretical electrochemical indexes corresponding to every novel metal-gas battery are summarized in Tab. 5.

Herein, it will make a brief introduction to these cutting-edge metal-gas batteries which might become the potential advanced flexible metal-gas candidates for commercialization. Zhang et., al proposed a new concept of reversible nitrogen fixation based on a rechargeable Li-N_2 battery.[226] By employing common carbon cloth as cathode and $LiCF_3SO_3$/TEGDME as electrolyte, the Li-N_2 cell prototype realized reversible N_2/Li_3N electrochemical cycles for 40 times. The N_2 fixation faradic efficiency of this Li-N_2 battery was 59%, without extra energy support from external environment. Since carbon cloth was chosen as the cathode, the first challenge to construct flexible Li-N_2 batteries (namely, flexible electrodes) has already been conquered. Hybrid and aqueous Li-air batteries have also been primarily studied. Andrei et., al reported a Li-O_2-H_2O hybrid energy system where organic electrolyte was used at the anode and aqueous electrolyte at the cathode.[227] The energy density coupled with specific capacity was positively affected by the increased solubility and the diffusion rate of O_2 in the cathode. The power density of the system was relatively low, due to the limited O_2

diffusion and large interface resistance. Whereas, it is noteworthy that such hybrid Li-O_2-H_2O battery possessed an ultrahigh energy density of 3804 Wh kg^{-1} as well as a stable working voltage of 3.4 V. Similarly, the electrochemistry of a hybrid Li-O_2-HCl battery has also been investigated.[228] Based on the reaction $4Li+O_2+4HCl \rightleftharpoons 4LiCl+2H_2O$, this hybrid energy system demonstrated the highest discharge voltage of 4.3 V among all reported metal-gas batteries, thus resulting in a high energy density of 2242 Wh kg^{-1}. It should admit that the detailed principles of the above hybrid Li-O_2 batteries are still not very clear. Moreover, a novel rechargeable system based on Li-SO_2 batteries was demonstrated by Kang and co-workers for the first time.[32] The Li-SO_2 battery stored and released electricity by the reversible formation and decomposition of discharge product $Li_2S_2O_4$. The rechargeable Li-SO_2 battery demonstrated a moderate discharge capacity of 5400 mAh g^{-1} at around 3.1 V, of which the performance is even slightly higher than that of Li-O_2 battery. Importantly, with the assistance of redox mediators, the Li-SO_2 battery only showed a small discharge/charge voltage polarization of less than 0.3 V, which is one of the highest energy efficiencies recorded by Li-gas batteries.

5. Summary and prospective

Metal-gas batteries, which employ gases as energy resources to generate electricity, have practical significance in exploiting next-generation high-performance energy storage systems for portable and wearable electronics, considering their ultrahigh theoretical energy density and convenient gas harvest from environment. Recent progress of flexible metal-gas batteries has been summarized in this review. Encouragingly, flexible and rechargeable Zn-air batteries, Li-O_2/air batteries, Li-CO_2 batteries and so on are generally achieved in ambient temperature. However, there are still tremendous obstacles hindering flexible metal-gas batteries toward commercial reality. These difficulties mainly lie in the sluggish electrochemical reactions in air cathode, the low ionic conductivity, instability and leakage risk of electrolyte and metal anodic corrosion together with dendrite growth, which result in limited discharge capacity, weak rate capability and poor cycling stability of these batteries. To conquer these challenges, numerous efforts have been devoted into the aspects of cathode catalyst, electrolyte and metal anode, as discussed in this article. It needs to admit that although these efforts have made a certain positive effect, there are still considerable scientific and technological difficulties to overcome. To look for new opportunities and technologies to break through the bottleneck dilemmas of current flexible metal-gas batteries, the subsequent research directions may deserve more academic attentions from a prospective of practical applications:

(i) Perform more *in-situ* characterizations and theoretical computations to better understand the detailed reaction mechanisms of metal-gas batteries. Different from electrocatalysis, what kind of roles the metal ions play in the gas/solid redox reactions are still unclear, especially for metal-CO_2 or N_2 batteries.

(ii) Develop new types of quasi- or solid-state electrolytes with high ionic conductivity, low volatility, stable chemical stability and fire-resistant property. The desirable electrolyte for flexible metal-gas batteries should firstly avoid the risk of electrolyte leakage and any potential health and safe problems, then pursue the ideal ion conductivity and ion migration number approaching those of liquid electrolyte. In addition, easy encapsulation is another necessary factor which deserves heavy consideration for GPE in engineering production.

(iii) The fabrication technologies of flexible cathodes need more investigations, focusing on exploiting novel cost-effective, eco-friendly and efficient free-standing catalysts at an acceptable level of practical energy storage. The cycling stability of cathodes under half or even full discharge/charge status (instead of 500 or 1000 mAh g^{-1} as the curtailing capacity) is urgent to overcome. This is the main bottleneck to enable flexible metal-gas batteries to become practicable and rechargeable next-generation energy storage devices with much higher energy density. Besides, how to keep a good balance between mechanical strength and structural voids of cathodes also deserves heavy attention. It decides whether the assembled flexible batteries can maintain their electrochemical performance and flexibility during long-term deformation.

(iv) Considering that current metal-gas batteries are commonly operated in a pure gas atmosphere (especially Li-O_2 battery), developing multifunctional catalysts and finding effective battery management systems to allow metal-gas battery to work in mixed gas atmosphere containing O_2, CO_2, N_2, et., al. are quite meaningful to promote metal-gas batteries toward "real" metal-air batteries which can directly harvest gas resources from ambient atmosphere conveniently.

(v) Devote more efforts into the exploitation of flexible metal anodes. Flexible metal anodes can be avoided to use in other flexible energy storage systems like supercapacitors and secondary metal-ion batteries, but they are an indispensable part of metal-gas batteries. Less concerns are focusing on anodes at current lab-scale devices. However, dendritic or "dead" crystals caused performance decay cannot be ignored especially when curtailing capacity or working time is enlarged in practical products for consumer market. In addition, durable deformability, gas corrosion protection and utilization efficiency are also noteworthy in future design.

(vi) Simplify and standardize the assembly processes together with test procedures of flexible metal-gas batteries. The configurations coupled with encapsulation problems are both noteworthy in engineering approaches. Meanwhile, the suitable measurement criteria for electrochemical performance, flexibility, mechanical strength and other comfortability/safe-related features should reach an agreement as soon as possible. Especially, it is more appropriate to evaluate the electrochemical performance of flexible cathodes in assembled flexible devices instead of in coin-type cells.

(vii) Explore other advanced metal-gas batteries. Employing earth-abundant, air-stable and high safe metals, such as Mg, Al, Zn and so on, to fabricate metal-CO_2/N_2 batteries will also be very eye-catching, due to their hopeful prospective of energy utilization and environmental conservation.

It is believed that after general understanding and addressing the inherent scientific issues existing in present flexible metal-gas batteries, more practical and appropriate flexible devices will be constructed, which in term, promote the integral development of flexible metal-gas batteries to become a cost-effective, safe, environmentally-friendly and advanced energy storage systems for portable and wearable consumer electronics in the future.

Conflicts of interest

There are no conflicts to declare.

Acknowledgements

The authors acknowledge the financial support from the National Natural Science Foundation of China (Grant No. 21875226), the Science Foundation for Distinguished Young Scholars of Sichuan Province (Grant Nos. 2017JQ0036 and 2016JQ0025), the Chengdu Rongpiao Talent Plan, the "QianYingBaiTuan" Plan of China Science City, the Tianfu Wanren Plan, and the "Global Experts" program. J. L. gratefully acknowledge support from the U.S. Department of Energy (DOE), Office of Energy Efficiency and Renewable Energy, Vehicle Technologies Office. Argonne National Laboratory was operated for DOE Office of Science by UChicago Argonne, LLC, under Contract No. DE-AC02-06CH11357.

Notes and references

1. M. Li, J. Lu, Z. Chen and K. Amine, *Adv. Mater.*, 2018, **30**, 1800561.
2. B. Kang and G. Ceder, *Nature*, 2009, **458**, 190.
3. Y. Xue, Q. Zhang, W. Wang, H. Cao, Q. Yang and L. Fu, *Adv. Energy Mater.*, 2017, **7**, 1602684.
4. Z. Wang, J. Cheng, Q. Guan, H. Huang, Y. Li, J. Zhou, W. Ni, B. Wang, S. He and H. Peng, *Nano Energy*, 2018, **45**, 210.
5. A. Mauger, H. Xie and C. M. Julien, *AIMS Mater. Sci.*, 2016, **3**, 1054.
6. Y. Lu, L. Yu and X. W. Lou, *Chem*, 2018, **4**, 972.
7. F. Cheng, J. Liang, Z. Tao and J. Chen, *Adv. Mater.*, 2011, **23**, 1695.
8. G. Zubi, R. Dufo-López, M. Carvalho and G. Pasaoglu, *Renew. Sust. Energy Rev.*, 2018, **89**, 292.
9. L. Zhou, K. Zhang, Z. Hu, Z. Tao, L. Mai, Y.-M. Kang, S.-L. Chou and J. Chen, *Adv. Energy Mater.*, 2018, **8**, 1701415.
10. X. Li, X. Li, J. Cheng, D. Yuan, W. Ni, Q. Guan, L. Gao and B. Wang, *Nano Energy*, 2016, **21**, 228.
11. J. Zhou, J. Qin, N. Zhao, C. Shi, E.-Z. Liu, F. He, J. Li and C. He, *J. Mater. Chem. A*, 2016, **4**, 8734.
12. C. Yang and S.-J. Lin, *J. Power Sources*, 2002, **112**, 497.
13. C. He, S. Wu, N. Zhao, C. Shi, E. Liu and J. Li, *ACS Nano*, 2013, **7**, 4459.
14. J. Qin, C. He, N. Zhao, Z. Wang, C. Shi, E. Z. Liu and J. Li, *ACS Nano*, 2014, **8**, 1728.
15. G. Qu, J. Cheng, X. Li, D. Yuan, P. Chen, X. Chen, B. Wang and H. Peng, *Adv. Mater.*, 2016, **28**, 3646.
16. J. Lu, Z. Chen, Z. Ma, F. Pan, L. A. Curtiss and K. Amine, *Nat. Nanotech.*, 2016, **11**, 1031.
17. Y. Li and J. Lu, *ACS Energy Lett.*, 2017, **2**, 1370.
18. Q. Liu, Z. Chang, Z. Li and X. Zhang, *Small Methods*, 2018, **2**, 1700231.
19. X. Xiao, H. Song, S. Lin, Y. Zhou, X. Zhan, Z. Hu, Q. Zhang, J. Sun, B. Yang, T. Li, L. Jiao, J. Zhou, J. Tang and Y. Gogotsi, *Nat. Commun.*, 2016, **7**, 11296.
20. C. Zhao, Y. Jin, W. Du, C. Ji and X. Du, *J. Electroanal. Chem.*, 2018, **826**, 217.
21. Y. Ma, A. Sumboja, W. Zang, S. Yin, S. Wang, S. J. Pennycook, Z. Kou, Z. Liu, X. Li and J. Wang, *ACS Appl. Mater. Inter.*, 2019, **11**, 1988.
22. M. Yu, Z. Wang, C. Hou, Z. Wang, C. Liang, C. Zhao, Y. Tong, X. Lu and S. Yang, *Adv. Mater.*, 2017, **29**, 1602868.
23. R. D. McKerracher, Carlos Ponce de Leon, R. G. A. Wills, A. A. Shah and F. C. Walsh, *ChemPlusChem*, 2015, **80**, 323.
24. J. Xie, X. Wang, J. Lv, Y. Huang, M. Wu, Y. Wang and J. Yao, *Angew. Chem. Int. Ed.*, 2018, **57**, 16996.
25. B. J. Bergner, A. Schurmann, K. Peppler, A. Garsuch and J. Janek, *J. Am. Chem. Soc.*, 2014, **136**, 15054.
26. B. Sun, K. Kretschmer, X. Xie, P. Munroe, Z. Peng and G. Wang, *Adv. Mater.*, 2017, **29**, 1606816.
27. N. Xiao, G. Gourdin and Y. Wu, *Angew. Chem. Int. Ed.*, 2018, **57**, 10864.
28. X. Zhang, Q. Zhang, Z. Zhang, Y. Chen, Z. Xie, J. Wei and Z. Zhou, *Chem. Commun.*, 2015, **51**, 14636.
29. X. Hu, Z. Li, Y. Zhao, J. Sun, Q. Zhao, J. Wang, Z. Tao and J. Chen, *Sci. Adv.*, 2017, **3**, 1602396.
30. W. Ma, X. Liu, C. Li, H. Yin, W. Xi, R. Liu, G. He, X. Zhao, J. Luo and Y. Ding, *Adv. Mater.*, 2018, **30**, 1801152.
31. X.-G. Wang, Q. Zhang, X. Zhang, C. Wang, Z. Xie and Z. Zhou, *Small Methods*, 2019, **3**, 1800334.
32. H. D. Lim, H. Park, H. Kim, J. Kim, B. Lee, Y. Bae, H. Gwon and K. Kang, *Angew. Chem. Int. Ed.*, 2015, **54**, 9663.
33. J. Lu, L. Li, J. B. Park, Y. K. Sun, F. Wu and K. Amine, *Chem. Rev.*, 2014, **114**, 5611.
34. P. Tan, B. Chen, H. Xu, H. Zhang, W. Cai, M. Ni, M. Liu and Z. Shao, *Energy Environ. Sci.*, 2017, **10**, 2056.
35. A. Manthiram and L. Li, *Adv. Energy Mater.*, 2015, **5**, 1401302.
36. N. Imanishi and O. Yamamoto, *Mater. Today*, 2014, **17**, 24.
37. Z. Xie, X. Zhang, Z. Zhang and Z. Zhou, *Adv. Mater.*, 2017, **29**, 1605891.
38. H. Sun, Y. Zhang, J. Zhang, X. Sun and H. Peng, *Nat. Rev. Mater.*, 2017, **2**, 17023.
39. X. Wang, G. Sun, P. Routh, D.-H. Kim, W. Huang and P. Chen, *Chem. Soc. Rev.*, 2014, **43**, 7067.
40. L. Ma, S. Chen, Z. Pei, H. Li, Z. Wang, Z. Liu, Z. Tang, J. A. Zapien and C. Zhi, *ACS Nano*, 2018, **12**, 8597.
41. Y. Zhang, Y. Zhao, J. Ren, W. Weng and H. Peng, *Adv. Mater.*, 2016, **28**, 4524.
42. W. Weng, P. Chen, S. He, X. Sun and H. Peng, *Angew. Chem. Int. Ed.*, 2016, **55**, 6140.
43. S. Pan, J. Ren, X. Fang and H. Peng, *Adv. Energy Mater.*, 2016, **6**, 1501867.
44. X. Wang, J. Xie, M. A. Ghausi, J. Lv, Y. Huang, M. Wu, Y. Wang and J. Yao, *Adv. Mater.*, 2019, **31**, 1807807.
45. Y. Zhao, Y. Zhang, H. Sun, X. Dong, J. Cao, L. Wang, Y. Xu, J. Ren, Y. Hwang, I. H. Son, X. Huang, Y. Wang and H. Peng, *Angew. Chem. Int. Ed.*, 2016, **55**, 14384.
46. Y. H. Zhu, S. Yuan, D. Bao, Y. B. Yin, H. X. Zhong, X. B. Zhang, J. M. Yan and Q. Jiang, *Adv. Mater.*, 2017, **29**, 1603719.
47. J. Ni, S. Fu, Y. Yuan, L. Ma, Y. Jiang, L. Li and J. Lu, *Adv. Mater.*, 2018, **30**, 1704337.
48. J. Ren, Y. Zhang, W. Bai, X. Chen, Z. Zhang, X. Fang, W. Weng, Y. Wang and H. Peng, *Angew. Chem. Int. Ed.*, 2014, **53**, 7864.
49. Y. Jing and Z. Zhou, *ACS Catal.*, 2015, **5**, 4309.
50. J. Pan, H. Li, H. Sun, Y. Zhang, L. Wang, M. Liao, X. Sun and H. Peng, *Small*, 2018, **14**, 1703454.
51. X. Cheng, J. Pan, Y. Zhao, M. Liao and H. Peng, *Adv. Energy Mater.*, 2018, **8**, 1702184.
52. D. Kundu, R. Black, B. Adams, K. Harrison, K. Zavadil and L. F. Nazar, *J. Phys. Chem. Lett.*, 2015, **6**, 2252.
53. C. Shu, J. Long, S. X. Dou and J. Wang, *Small*, 2019, **15**, 1804701.
54. M. J. Tan, B. Li, P. Chee, X. Ge, Z. Liu, Y. Zong and X. J. Loh, *J. Power Sources*, 2018, **400**, 566.
55. T. Liu, J. J. Xu, Q. C. Liu, Z. W. Chang, Y. B. Yin, X. Y. Yang and X. B. Zhang, *Small*, 2017, **13**, 1602952.
56. J. Fu, Z. P. Cano, M. G. Park, A. Yu, M. Fowler and Z. Chen, *Adv. Mater.*, 2017, **29**, 1604685.
57. L. Wang, X. Fu, J. He, X. Shi, T. Chen, P. Chen, B. Wang and H. Peng, *Adv. Mater.*, 2019, **31**, 1901971.
58. X. Xu, S. Xie, Y. Zhang and H. Peng, *Angew. Chem. Int. Ed.*, 2019, **58**, 1902425.
59. J. Park, M. Park, G. Nam, J. S. Lee and J. Cho, *Adv. Mater.*, 2015, **27**, 1396.

60. Q. C. Liu, J. J. Xu, D. Xu and X. B. Zhang, *Nat. Commun.*, 2015, **6**, 7892.
61. Q. C. Liu, L. Li, J. J. Xu, Z. W. Chang, D. Xu, Y. B. Yin, X. Y. Yang, T. Liu, Y. S. Jiang, J. M. Yan and X. B. Zhang, *Adv. Mater.*, 2015, **27**, 8095.
62. Y. Zhang, L. Wang, Z. Guo, Y. Xu, Y. Wang and H. Peng, *Angew. Chem. Int. Ed.*, 2016, **55**, 4487.
63. Y. Xu, Y. Zhao, J. Ren, Y. Zhang and H. Peng, *Angew. Chem. Int. Ed.*, 2016, **55**, 7979.
64. L. Wang, Y. Zhang, J. Pan and H. Peng, *J. Mater. Chem. A*, 2016, **4**, 13419.
65. Y. Zhang, Y. Jiao, L. Lu, L. Wang, T. Chen and H. Peng, *Angew. Chem. Int. Ed.*, 2017, **56**, 13741.
66. Xiaofei Hu, Zifan Li and J. Chen, *Angew. Chem. Int. Ed.*, 2017, **56**, 5785.
67. J. Zhou, X. Li, C. Yang, Y. Li, K. Guo, J. Cheng, D. Yuan, C. Song, J. Lu and B. Wang, *Adv. Mater.*, 2018, **30**, 1804439.
68. M. Hilder, B. Winther-Jensen and N. B. Clark, *J. Power Sources*, 2009, **194**, 1135.
69. Z. Pan, J. Yang, W. Zang, Z. Kou, C. Wang, X. Ding, C. Guan, T. Xiong, H. Chen, Q. Zhang, Y. Zhong, M. Liu, L. Xing, Y. Qiu, W. Li, C. Yan, Y. Zhang and J. Wang, *Energy Storage Mater.*, 2019, **23**, 375.
70. S. Qu, Z. Song, J. Liu, Y. Li, Y. Kou, C. Ma, X. Han, Y. Deng, N. Zhao, W. Hu and C. Zhong, *Nano Energy*, 2017, **39**, 101.
71. X. Bi, R. Wang, K. Amine and J. Lu, *Small Methods*, 2018, **3**, 1800247.
72. P. Gu, M. Zheng, Q. Zhao, X. Xiao, H. Xue and H. Pang, *J. Mater. Chem. A*, 2017, **5**, 7651.
73. J. Fu, R. Liang, G. Liu, A. Yu, Z. Bai, L. Yang and Z. Chen, *Adv. Mater.*, 2019, **31**, 1805230.
74. J. Pan, Y. Y. Xu, H. Yang, Z. Dong, H. Liu and B. Y. Xia, *Adv. Sci.*, 2018, **5**, 1700691.
75. L. Grande, E. Paillard, J. Hassoun, J. B. Park, Y. J. Lee, Y. K. Sun, S. Passerini and B. Scrosati, *Adv. Mater.*, 2015, **27**, 784.
76. A. C. Luntz and B. D. McCloskey, *Chem. Rev.*, 2014, **114**, 11721.
77. X. Ren and Y. Wu, *J. Am. Chem. Soc.*, 2013, **135**, 2923.
78. Z. Ma, X. Yuan, L. Li, Z.-F. Ma, D. P. Wilkinson, L. Zhang and J. Zhang, *Energy Environ. Sci.*, 2015, **8**, 2144.
79. Z. Guo, D. Zhou, X. Dong, Z. Qiu, Y. Wang and Y. Xia, *Adv. Mater.*, 2013, **25**, 5668.
80. J. Lu, Y. Lei, K. C. Lau, X. Luo, P. Du, J. Wen, R. S. Assary, U. Das, D. J. Miller, J. W. Elam, H. M. Albishri, D. A. El-Hady, Y. K. Sun, L. A. Curtiss and K. Amine, *Nat. Commun.*, 2013, **4**, 2383.
81. Z. Geng, Y. Liu, X. Kong, P. Li, K. Li, Z. Liu, J. Du, M. Shu, R. Si and J. Zeng, *Adv. Mater.*, 2018, **30**, 1803498.
82. L. Zhang, X. Ren, Y. Luo, X. Shi, A. M. Asiri, T. Li and X. Sun, *Chem. Commun.*, 2018, **54**, 12966.
83. S. Zaromb, *J. Electroanal. Chem.*, 1962, **109**, 1125.
84. J. Ma, C. Qin, Y. Li, F. Ren, Y. Liu and G. Wang, *Mater. Res. Express*, 2019, **6**, 085528.
85. K. M. Abraham and Z. Jiang, *J. Electroanal. Chem.*, 1996, **143**, 1.
86. Q. Xu, H. Jiang, Y. Li, D. Liang, Y. Hu and C. Li, *Appl. Catal. B: Environ.*, 2019, **256**, 117893.
87. L. Ma, S. Chen, Z. Pei, Y. Huang, G. Liang, F. Mo, Q. Yang, J. Su, Y. Gao, J. A. Zapien and C. Zhi, *ACS Nano*, 2018, **12**, 1949.
88. Q. Wang, Y. Ji, Y. Lei, Y. Wang, Y. Wang, Y. Li and S. Wang, *ACS Energy Lett.*, 2018, **3**, 1183.
89. S. Liu, Z. Wang, S. Zhou, F. Yu, M. Yu, C. Y. Chiang, W. Zhou, J. Zhao and J. Qiu, *Adv. Mater.*, 2017, **29**, 1700874.
90. S. Li, C. Cheng, X. Zhao, J. Schmidt and A. Thomas, *Angew. Chem. Int. Ed.*, 2018, **57**, 1856.
91. C. Li, M. Wu and R. Liu, *Appl. Catal. B: Environ.*, 2019, **244**, 150.
92. Z. Zhao, X. Fan, J. Ding, W. Hu, C. Zhong and J. Lu, *ACS Energy Lett.*, 2019, **4**, 2259.
93. Y. Li, C. Zhong, J. Liu, X. Zeng, S. Qu, X. Han, Y. Deng, W. Hu and J. Lu, *Adv. Mater.*, 2018, **30**, 1703657.
94. F. Meng, H. Zhong, D. Bao, J. Yan and X. Zhang, *J. Am. Chem. Soc.*, 2016, **138**, 10226.
95. Z. Yang, J. Ren, Z. Zhang, X. Chen, G. Guan, L. Qiu, Y. Zhang and H. Peng, *Chem. Rev.*, 2015, **115**, 5159.
96. S. Pan, H. Lin, J. Deng, P. Chen, X. Chen, Z. Yang and H. Peng, *Adv. Energy Mater.*, 2015, **5**, 1401438.
97. J. Fu, F. M. Hassan, C. Zhong, J. Lu, H. Liu, A. Yu and Z. Chen, *Adv. Mater.*, 2017, **29**, 1702526.
98. T. Zhou, W. Xu, N. Zhang, Z. Du, C. Zhong, W. Yan, H. Ju, W. Chu, H. Jiang, C. Wu and Y. Xie, *Adv. Mater.*, 2019, **31**, 1807468.
99. K. Kordek, L. Jiang, K. Fan, Z. Zhu, L. Xu, M. Al-Mamun, Y. Dou, S. Chen, P. Liu, H. Yin, P. Rutkowski and H. Zhao, *Adv. Energy Mater.*, 2019, **9**, 1802936.
100. L. Ma, S. Chen, D. Wang, Q. Yang, F. Mo, G. Liang, N. Li, H. Zhang, J. A. Zapien and C. Zhi, *Adv. Energy Mater.*, 2019, **9**, 1803046.
101. Y. Qiao, P. Yuan, Y. Hu, J. Zhang, S. Mu, J. Zhou, H. Li, H. Xia, J. He and Q. Xu, *Adv. Mater.*, 2018, **30**, 1804504.
102. X. Han, W. Zhang, X. Ma, C. Zhong, N. Zhao, W. Hu and Y. Deng, *Adv. Mater.*, 2019, **31**, 1808281.
103. Y. Xu, Y. Zhang, Z. Guo, J. Ren, Y. Wang and H. Peng, *Angew. Chem. Int. Ed.*, 2015, **54**, 15390.
104. Z. Pan, H. Chen, J. Yang, Y. Ma, Q. Zhang, Z. Kou, X. Ding, Y. Pang, L. Zhang, Q. Gu, C. Yan and J. Wang, *Adv. Sci.*, 2019, **6**, 1900628.
105. L. Zhu, D. Zheng, Z. Wang, X. Zheng, P. Fang, J. Zhu, M. Yu, Y. Tong and X. Lu, *Adv. Mater.*, 2018, **30**, 1805268.
106. P. Yu, L. Wang, F. Sun, Y. Xie, X. Liu, J. Ma, X. Wang, C. Tian, J. Li and H. Fu, *Adv. Mater.*, 2019, **31**, 1901666.
107. C. Su, H. Cheng, W. Li, Z. Liu, N. Li, Z. Hou, F. Bai, H. Zhang and T. Ma, *Adv. Energy Mater.*, 2017, **7**, 1602420.
108. S. Zeng, X. Tong, S. Zhou, B. Lv, J. Qiao, Y. Song, M. Chen, J. Di and Q. Li, *Small*, 2018, **14**, 1803409.
109. Y. Xu, P. Deng, G. Chen, J. Chen, Y. Yan, K. Qi, H. Liu and B. Y. Xia, *Adv. Funct. Mater.*, 2019, **29**, 1906081.
110. Y. Lian, W. Yang, C. Zhang, H. Sun, Z. Deng, W. Xu, L. Song, Z. Ouyang, Z. Wang, J. Guo and Y. Peng, *Angew. Chem. Int. Ed.*, 2019, **58**, 1.
111. W. Wang, M. Tang, Z. Zheng and S. Chen, *Adv. Energy Mater.*, 2019, **9**, 1803628.
112. W. Zang, A. Sumboja, Y. Ma, H. Zhang, Y. Wu, S. Wu, H. Wu, Z. Liu, C. Guan, J. Wang and S. J. Pennycook, *ACS Catal.*, 2018, **8**, 8961.
113. Y. Jiang, Y. P. Deng, R. Liang, J. Fu, D. Luo, G. Liu, J. Li, Z. Zhang, Y. Hu and Z. Chen, *Adv. Energy Mater.*, 2019, **9**, 1900911.
114. T. V. Tam, S. G. Kang, M. H. Kim, S. G. Lee, S. H. Hur, J. S. Chung and W. M. Choi, *Adv. Energy Mater.*, 2019, **9**, 1900945.
115. W. Liu, B. Ren, W. Zhang, M. Zhang, G. Li, M. Xiao, J. Zhu, A. Yu, L. Ricardez-Sandoval and Z. Chen, *Small*, 2019, **15**, 1903610.
116. Y. Zhong, Z. Pan, X. Wang, J. Yang, Y. Qiu, S. Xu, Y. Lu, Q. Huang and W. Li, *Adv. Sci.*, 2019, **6**, 1802243.
117. Q. Jin, B. Ren, J. Chen, H. Cui and C. Wang, *Appl. Catal. B: Environ.*, 2019, **256**, 117887.
118. H. Qiu, X. Du, J. Zhao, Y. Wang, J. Ju, Z. Chen, Z. Hu, D. Yan, X. Zhou and G. Cui, *Nat. Commun.*, 2019, **10**, 5374.
119. J. Zheng, Q. Zhao, T. Tang, J. Yin, C. Quilty, G. Renderos, X. Liu, Y. Deng, L. Wang, D. Bock, C. Jaye, D. Zhang, E. Takeuchi, K. Takeuchi, A. Marschilok and L. Archer, *Science*, 2019, **366**, 645.
120. X. Zhang, X. Chen, L. Hou, B. Li, X. Cheng, J. Huang and Q. Zhang, *ACS Energy Lett.*, 2019, **4**, 411.
121. L. Kang, M. Cui, F. Jiang, Y. Gao, H. Luo, J. Liu, W. Liang and C. Zhi, *Adv. Energy Mater.*, 2018, **8**, 1801090.
122. Y. Zeng, X. Zhang, R. Qin, X. Liu, P. Fang, D. Zheng, Y. Tong and X. Lu, *Adv. Mater.*, 2019, **31**, 1903675.
123. Q. Guan, Y. Li, X. Bi, J. Yang, J. Zhou, X. Li, J. Cheng, Z. Wang, B. Wang and J. Lu, *Adv. Energy Mater.*, 2019, **9**, 1901434.
124. L. Wang, N. Li, T. Wang, Y. Yin, Y. Guo and C. Wang, *Electrochim. Acta*, 2017, **244**, 172.
125. F. Wan, L. Zhang, X. Dai, X. Wang, Z. Niu and J. Chen, *Nat. Commun.*, 2018, **9**, 1656.
126. Y. Zeng, X. Zhang, Y. Meng, M. Yu, J. Yi, Y. Wu, X. Lu and Y. Tong, *Adv. Mater.*, 2017, **29**, 1700274.

127. C. Wang, K. Xia, H. Wang, X. Liang, Z. Yin and Y. Zhang, *Adv. Mater.*, 2019, **31**, 1801072.
128. M. Liao, L. Ye, Y. Zhang, T. Chen and H. Peng, *Adv. Electron. Mater.*, 2019, **5**, 1800456.
129. X. Fan, J. Liu, Z. Song, X. Han, Y. Deng, C. Zhong and W. Hu, *Nano Energy*, 2019, **56**, 454.
130. M. Wang, N. Xu, J. Fu, Y. Liu and J. Qiao, *J. Mater. Chem. A*, 2019, **7**, 11257.
131. J. Fu, J. Zhang, X. Song, H. Zarrin, X. Tian, J. Qiao, L. Rasen, K. Li and Z. Chen, *Energy Environ. Sci.*, 2016, **9**, 663.
132. N. Zhao, F. Wu, Y. Xing, W. Qu, N. Chen, Y. Shang, M. Yan, Y. Li, L. Li and R. Chen, *ACS Appl. Mater. Inter.*, 2019, **11**, 15537.
133. J. Fu, D. U. Lee, F. M. Hassan, L. Yang, Z. Bai, M. G. Park and Z. Chen, *Adv. Mater.*, 2015, **27**, 5617.
134. A. Poosapati, K. Negrete, N. Jang, L. Hu, Y. Lan and D. Madan, *MRS Commun.*, 2019, **9**, 1015.
135. Y. Li, X. Fan, X. Liu, S. Qu, J. Liu, J. Ding, X. Han, Y. Deng, W. Hu and C. Zhong, *J. Mater. Chem. A*, 2019, **7**, 25449.
136. H.-W. Kim, J.-M. Lim, H.-J. Lee, S.-W. Eom, Y. T. Hong and S.-Y. Lee, *J. Mater. Chem. A*, 2016, **4**, 3711.
137. A. Poosapati, E. Jang, D. Madan, N. Jang, L. Hu and L. Y., *MRS Commun.*, 2019, **9**, 122.
138. M. Li, B. Liu, X. Fan, X. Liu, J. Liu, J. Ding, X. Han, Y. Deng, W. Hu and C. Zhong, *ACS Appl. Mater. Inter.*, 2019, **11**, 28909.
139. Z. Cao, H. Hu, M. Wu, K. Tang and T. Jiang, *J. Mater. Chem. A*, 2019, **7**, 17581.
140. X. Cheng, J. Zhang, J. Ren, N. Liu, P. Chen, Y. Zhang, J. Deng, Y. Wang and H. Peng, *J. Phys. Chem. C*, 2016, **120**, 9685.
141. X. Xu, J. Chen, S. Cai, Z. Long, Y. Zhang, L. Su, S. He, C. Tang, P. Liu, H. Peng and X. Fang, *Adv. Mater.*, 2018, **30**, 1803165.
142. J. Lu, L. Cheng, K. C. Lau, E. Tyo, X. Luo, J. Wen, D. Miller, R. S. Assary, H. H. Wang, P. Redfern, H. Wu, J. B. Park, Y. K. Sun, S. Vajda, K. Amine and L. A. Curtiss, *Nat. Commun.*, 2014, **5**, 4895.
143. D. Aurbach, B. D. McCloskey, L. F. Nazar and P. G. Bruce, *Nat. Energy*, 2016, **1**, 16128.
144. D. Zhai, K. C. Lau, H. H. Wang, J. Wen, D. J. Miller, J. Lu, F. Kang, B. Li, W. Yang, J. Gao, E. Indacochea, L. A. Curtiss and K. Amine, *Nano Lett.*, 2015, **15**, 1041.
145. A. Dai, Q. Li, T. Liu, K. Amine and J. Lu, *Adv. Mater.*, 2019, **31**, 1805602.
146. G. Tan, L. Chong, R. Amine, J. Lu, C. Liu, Y. Yuan, J. Wen, K. He, X. Bi, Y. Guo, H. H. Wang, R. Shahbazian-Yassar, S. Al Hallaj, D. J. Miller, D. Liu and K. Amine, *Nano Lett.*, 2017, **17**, 2959.
147. Y. Qin, J. Lu, P. Du, Z. Chen, Y. Ren, T. Wu, J. T. Miller, J. Wen, D. J. Miller, Z. Zhang and K. Amine, *Energy Environ. Sci.*, 2013, **6**, 519.
148. Y. B. Yin, X. Y. Yang, Z. W. Chang, Y. H. Zhu, T. Liu, J. M. Yan and Q. Jiang, *Adv. Mater.*, 2018, **30**, 1703791.
149. S. Xu, Y. Yao, Y. Guo, X. Zeng, S. D. Lacey, H. Song, C. Chen, Y. Li, J. Dai, Y. Wang, Y. Chen, B. Liu, K. Fu, K. Amine, J. Lu and L. Hu, *Adv. Mater.*, 2018, **30**, 1704907.
150. C. Chen, S. Xu, Y. Kuang, W. Gan, J. Song, G. Chen, G. Pastel, B. Liu, Y. Li, H. Huang and L. Hu, *Adv. Energy Mater.*, 2019, **9**, 1802964.
151. W. J. Kwak, K. C. Lau, C. Shin, K. Amine, L. A. Curtiss and Y. Sun, *ACS Nano*, 2015, **9**, 4129.
152. Y. Hou, Y. Liu, Z. Zhou, L. Liu, H. Guo, H. Liu, J. Wang and J. Chen, *Electrochim. Acta*, 2018, **259**, 313.
153. Y. B. Yin, J. J. Xu, Q. C. Liu and X. B. Zhang, *Adv. Mater.*, 2016, **28**, 7494.
154. L. Wang, J. Pan, Y. Zhang, X. Cheng, L. Liu and H. Peng, *Adv. Mater.*, 2018, **30**, 1704378.
155. H. Xue, S. Wu, J. Tang, H. Gong, P. He, J. He and H. Zhou, *ACS Appl. Mater. Inter.*, 2016, **8**, 8427.
156. X. Zou, Q. Lu, Y. Zhong, K. Liao, W. Zhou and Z. Shao, *Small*, 2018, **14**, 1801798.
157. Q. C. Liu, T. Liu, D. P. Liu, Z. J. Li, X. B. Zhang and Y. Zhang, *Adv. Mater.*, 2016, **28**, 8413.
158. T. Liu, Q. C. Liu, J. J. Xu and X. B. Zhang, *Small*, 2016, **12**, 3101.
159. J. Kang, J. Kim, S. Lee, S. Wi, C. Kim, S. Hyun, S. Nam, Y. Park and B. Park, *Adv. Energy Mater.*, 2017, **7**, 1700814.
160. X. Yang, J. Xu, Z. Chang, D. Bao, Y. Yin, T. Liu, J. Yan, D. Liu, Y. Zhang and X. Zhang, *Adv. Energy Mater.*, 2018, **8**, 1702242.
161. X. Y. Yang, J. J. Xu, D. Bao, Z. W. Chang, D. P. Liu, Y. Zhang and X. B. Zhang, *Adv. Mater.*, 2017, **29**, 1700378.
162. K. Yoon, K. Shin, J. Park, S. Cho, C. Kim, J. Jung, J. Cheong, H. Byon, H. Lee and I. Kim, *ACS Nano*, 2018, **12**, 128.
163. J. Long, Z. Hou, C. Shu, C. Han, W. Li, R. Huang and J. Wang, *ACS Appl. Mater. Inter.*, 2019, **11**, 3834.
164. X. Yang, X. Feng, X. Jin, M. Shao, B. Yan, J. Yan, Y. Zhang and X. Zhang, *Angew. Chem. Int. Ed.*, 2019, **58**, 16411.
165. Z. Sun, S. Jin, H. Jin, Z. Du, Y. Zhu, A. Cao, H. Ji and L. Wan, *Adv. Mater.*, 2018, **30**, 1800884.
166. S. Chi, Y. Liu, W. Song, L. Fan, Q. Zhang, *Adv. Funct. Mater.*, 2017, **27**, 1700348.
167. A. Raji, R. Villegas Salvatierra, N. Kim, X. Fan, Y. Li, G.A.L. Silva, J. Sha, J.M. Tour, *ACS Nano*, 2017, **11**, 6362.
168. D. Lin, Y. Liu, Z. Liang, H.W. Lee, J. Sun, H. Wang, K. Yan, J. Xie and Y. Cui, *Nat. Nanotech.*, 2016, **11**, 626.
169. Y. Yin, Z. Yu, Z. Ma, T. Zhang, Y. Lu, T. Ma, F. Zhou, H. Yao and S. Yu, *Natl. Sci. Rev.*, 2019, **6**, 247.
170. X. Wang, Z. Pan, J. Yang, Z. Lyu, Y. Zhong, G. Zhou, Y. Qiu, Y. Zhang, J. Wang and W. Li, *Energy Storage Mater.*, 2019, **22**, 179.
171. Q. Liu, J. Xu, S. Yuan, Z. Chang, D. Xu, Y. Yin, L. Li, H. Zhong, Y. Jiang, J. Yan and X. Zhang, *Adv. Mater.*, 2015, **27**, 5241.
172. T. Liu, X. Feng, X. Jin, M. Shao, Y. Su, Y. Zhang and X. Zhang, *Angew. Chem. Int. Ed.*, 2019, **131**, 18408.
173. B. Liu, W. Xu, J. Tao, P. Yan, J. Zheng, M. Engelhard, D. Lu, C. Wang and J. Zhang, *Adv. Energy Mater.*, 2018, **8**, 1702340.
174. C. Yan, X. Cheng, Y. Yao, X. Shen, B. Li, W. Li, R. Zhang, J. Huang, H. Li and Q. Zhang, *Adv. Mater.*, 2018, **30**, 1804461.
175. C. Zhao, J. Liang, Y. Zhao, J. Luo, Q. Sun, Y. Liu, X. Lin, X. Yang, H. Huang, L. Zhang, S. Zhao, S. Lu and X. Sun, *J. Mater. Chem. A*, 2019, **7**, 24947.
176. G. Huang, J. Han, C. Yang, Z. Wang, T. Fujita, A. Hirata and M. Chen, *NPG Asia Mater.*, 2018, **10**, 1037.
177. Z. Guo, J. Li, Y. Xia, C. Chen, F. Wang, A. Tamirat, Y. Wang, Y. Xia, L. Wang and S. Feng, *J. Mater. Chem. A*, 2018, **6**, 6022.
178. D. Safanama and S. Adams, *ACS Energy Lett.*, 2017, **2**, 1130.
179. J. Yi, Y. Liu, Y. Qiao, P. He and H. Zhou, *ACS Energy Lett.*, 2017, **2**, 1378.
180. X. Lei, X. Liu, W. Ma, Z. Cao, Y. Wang and Y. Ding, *Angew. Chem. Int. Ed.*, 2018, **57**, 16131.
181. H. Kim, T. Y. Kim, V. Roev, H. C. Lee, H. J. Kwon, H. Lee, S. Kwon and D. Im, *ACS Appl. Mater. Inter.*, 2016, **8**, 1344.
182. Y. Liu, P. He and H. Zhou, *Adv. Energy Mater.*, 2018, **8**, 1701602.
183. N. Feng, P. He and H. Zhou, *Adv. Energy Mater.*, 2016, **6**, 1502303.
184. W. Xu, J. Wang, F. Ding, X. Chen, E. Nasybulin, Y. Zhang and J.-G. Zhang, *Energy Environ. Sci.*, 2014, **7**, 513.
185. Z. Jian, Y. Chen, F. Li, T. Zhang, C. Liu and H. Zhou, *J. Power Sources*, 2014, **251**, 466.
186. P. Hartmann, C. L. Bender, M. Vracar, A. K. Durr, A. Garsuch, J. Janek and P. Adelhelm, *Nat. Mater.*, 2013, **12**, 228.
187. J. L. Ma, F. L. Meng, Y. Yu, D. P. Liu, J. M. Yan, Y. Zhang, X. B. Zhang and Q. Jiang, *Nat. Chem.*, 2019, **11**, 64.
188. J. L. Ma, F. L. Meng, D. Xu and X. B. Zhang, *Energy Storage Mater.*, 2017, **6**, 1.
189. S. Xu, S. K. Das and L. A. Archer, *RSC Adv.*, 2013, **3**, 6656.
190. W. Zhang, C. Hu, Z. Guo and L. Dai, *Angew. Chem. Int. Ed.*, 2020, **59**, 3470.
191. X. Wang, X. Zhang, Y. Lu, Z. Yan, Z. Tao, D. Jia and J. Chen, *ChemElectroChem*, 2018, **5**, 3628.
192. B. Huang and G. Frapper, *J. Am. Chem. Soc.*, 2018, **140**, 413.
193. H. Lim, H. Lim, K. Park, D. Seo, H. Gwon, J. Hong, W. Goddard, H. Kim and K. Kang, *J. Am. Chem. Soc.*, 2013, **135**, 9733.
194. Y. Hou, J. Wang, L. Liu, Y. Liu, S. Chou, D. Shi, H. Liu, Y. Wu, W.

Zhang and J. Chen, *Adv. Funct. Mater.*, 2017, **27**, 1700564.
195. W. Yin, A. Grimaud, I. Azcarate, C. Yang and J.-M. Tarascon, *J. Phys. Chem. C*, 2018, **122**, 6546.
196. A. Khurram, M. He and B. M. Gallant, *Joule*, 2018, **2**, 1.
197. K. Takechi, T. Shiga and T. Asaoka, *Chem. Commun.*, 2011, **47**, 3463.
198. Y. Liu, R. Wang, Y. Lyu, H. Li and L. Chen, *Energy Environ. Sci.*, 2014, **7**, 677.
199. S. R. Gowda, A. Brunet, G. M. Wallraff and B. D. McCloskey, *J. Phys. Chem. Lett.*, 2013, **4**, 276.
200. Z. Zhang, Q. Zhang, Y. Chen, J. Bao, X. Zhou, Z. Xie, J. Wei and Z. Zhou, *Angew. Chem. Int. Ed.*, 2015, **127**, 6550.
201. L. Qie, Y. Lin, J. W. Connell, J. Xu and L. Dai, *Angew. Chem. Int. Ed.*, 2017, **56**, 6970.
202. C. Lv, C. Yan, G. Chen, Y. Ding, J. Sun, Y. Zhou and G. Yu, *Angew. Chem. Int. Ed.*, 2018, **57**, 6073.
203. X. Zhang, C. Wang, H. Li, X.-G. Wang, Y.-N. Chen, Z. Xie and Z. Zhou, *J. Mater. Chem. A*, 2018, **6**, 2792.
204. Z. Zhang, X. G. Wang, X. Zhang, Z. Xie, Y. N. Chen, L. Ma, Z. Peng and Z. Zhou, *Adv. Sci.*, 2018, **5**, 1700567.
205. S.-M. Xu, Z.-C. Ren, X. Liu, X. Liang, K.-X. Wang and J.-S. Chen, *Energy Storage Mater.*, 2018, **15**, 291.
206. Z. Zhang, Z. Zhang, P. Liu, Y. Xie, K. Cao and Z. Zhou, *J. Mater. Chem. A*, 2018, **6**, 3218.
207. Y. Mao, C. Tang, Z. Tang, J. Xie, Z. Chen, J. Tu, G. Cao and X. Zhao, *Energy Storage Mater.*, 2018, **18**, 405.
208. Y. Qiao, J. Yi, S. Wu, Y. Liu, S. Yang, P. He and H. Zhou, *Joule*, 2017, **1**, 359.
209. B. Ge, Y. Sun, J. Guo, X. Yan, C. Fernandez and Q. Peng, *Small*, 2019, **15**, 1902220.
210. H. Liang, Y. Zhang, F. Chen, S. Jing, S. Yin and P. Tsiakaras, *Appl. Catal. B: Environ.*, 2019, **244**, 559.
211. H. Wang, K. Xie, Y. You, Q. Hou, K. Zhang, N. Li, W. Yu, K. Loh, C. Shen and B. Wei, *Adv. Energy Mater.*, 2019, **9**, 1901806.
212. Z. Guo, J. Li, H. Qi, X. Sun, H. Li, A. G. Tamirat, J. Liu, Y. Wang and L. Wang, *Small*, 2019, **15**, 1803246.
213. S. Li, Y. Dong, J. Zhou, Y. Liu, J. Wang, X. Gao, Y. Han, P. Qi and B. Wang, *Energy Environ. Sci.*, 2018, **11**, 1318.
214. Y. Xing, Y. Yang, D. Li, M. Luo, N. Chen, Y. Ye, J. Qian, L. Li, D. Yang, F. Wu, R. Chen and S. Guo, *Adv. Mater.*, 2018, **30**, 1803124.
215. J. Chen, K. Zou, P. Ding, J. Deng, C. Zha, Y. Hu, X. Zhao, J. Wu, J. Fan and Y. Li, *Adv. Mater.*, 2018, **31**, 1805484.
216. Q.-C. Zhu, S.-M. Xu, Z.-P. Cai, M. M. Harris, K.-X. Wang and J.-S. Chen, *Energy Storage Mater.*, 2017, **7**, 209.
217. S. Xu, C. Chen, Y. Kuang, J. Song, W. Gan, B. Liu, E. Hitz, J. Connell, Y. Lin and L. Hu, *Energy Environ. Sci.*, 2018, **11**, 3231.
218. C. Wang, Q. Zhang, X. Zhang, X. G. Wang, Z. Xie and Z. Zhou, *Small*, 2018, **14**, 1800641.
219. Y. Li, J. Zhou, T. Zhang, T. Wang, X. Li, Y. Jia, J. Cheng, Q. Guan, E. Liu, H. Peng and B. Wang, *Adv. Funct. Mater.*, 2019, **29**, 1808117.
220. X. Li, J. Zhou, J. Zhang, M. Li, X. Bi, T. Liu, T. He, J. Cheng, F. Zhang, Y. Li, X. Mu, J. Lu and B. Wang, *Adv. Mater.*, 2019, **31**, 1903852.
221. L. Guo, B. Li, V. Thirumal and J. Song, *Chem. Commun.*, 2019, **55**, 7946.
222. T. Shiga, Y. Kato, M. Inoue and Y. Hase, *ACS Sustain. Chem. Eng.*, 2019, **7**, 14280.
223. R. Pipes, A. Bhargav and A. Manthiram, *Adv. Energy Mater.*, 2019, **9**, 1900453.
224. J. Li, H. Zhao, H. Qi, X. Sun, X. Song, Z. Guo, A. G. Tamirat, J. Liu, L. Wang and S. Feng, *Adv. Funct. Mater.*, 2019, **29**, 1806863.
225. C. Li, Z. Guo, B. Yang, Y. Liu, Y. Wang and Y. Xia, *Angew. Chem. Int. Ed.*, 2017, **129**, 9254.
226. J. Ma, D. Bao, M. Shi, J. Yan and X. Zhang, *Chem*, 2017, **2**, 525.
227. P. Andrei, J. P. Zheng, M. Hendrickson and E. J. Plichta, *J. Electrochem. Soc.*, 2012, **159**, A770.
228. K. G. Gallagher, S. Goebel, T. Greszler, M. Mathias, W. Oelerich, D. Eroglu and V. Srinivasan, *Energy Environ. Sci.*, 2014, **7**, 1555.

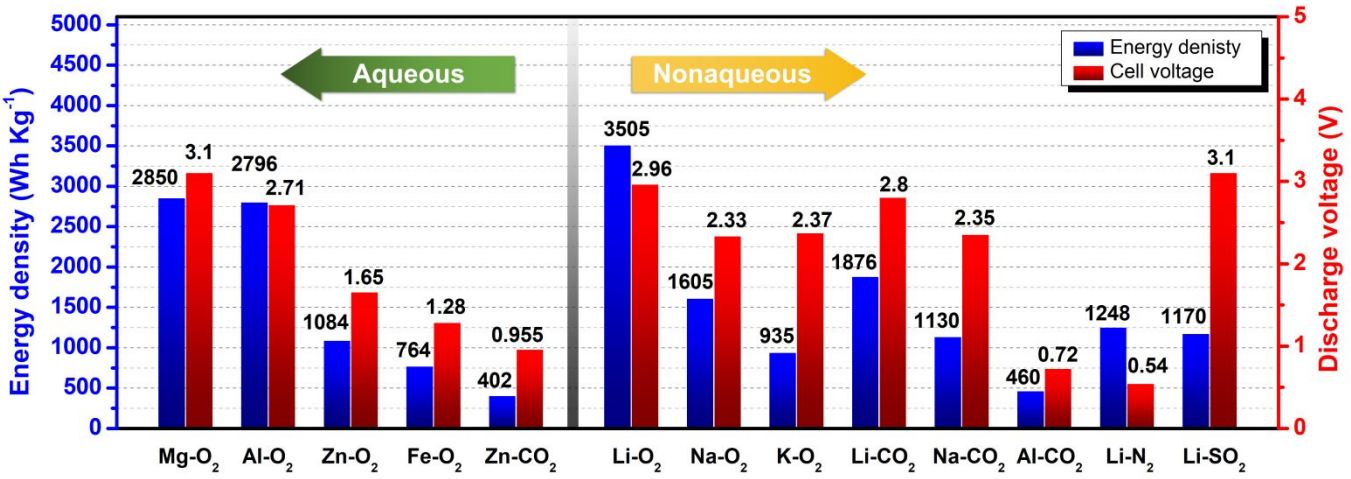

Fig. 1 Theoretical energy densities and cell working voltages for various metal-gas batteries. The data was directly obtained or calculated from previously reported literatures.[20-32] All the theoretical energy densities are given based on the total weight of discharge products unless specified.

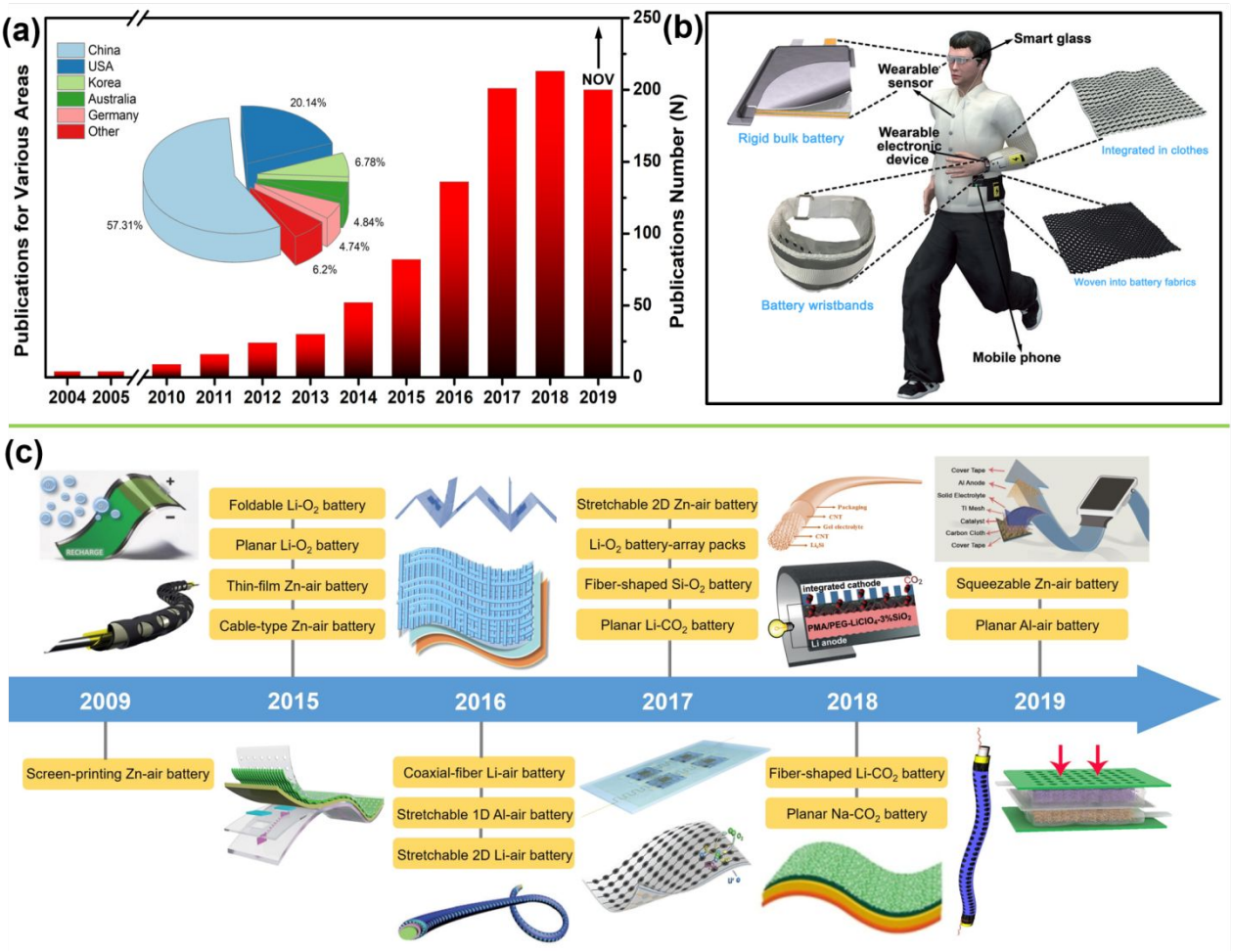

Fig. 2 (a) Number of publications about "flexible metal-gas batteries" according to Web of Science (as of November 2019). (b) Potential applications of flexible metal-gas batteries on wearable electronics. (c) Timeline of developments on flexible metal-gas batteries. The metal-gas batteries which have achieved flexibility so forth mainly includes Zn-air, Li-O_2/air, Al-air, Si-O_2, Li-CO_2, Na-CO_2 batteries.[21, 29, 55, 59-70]

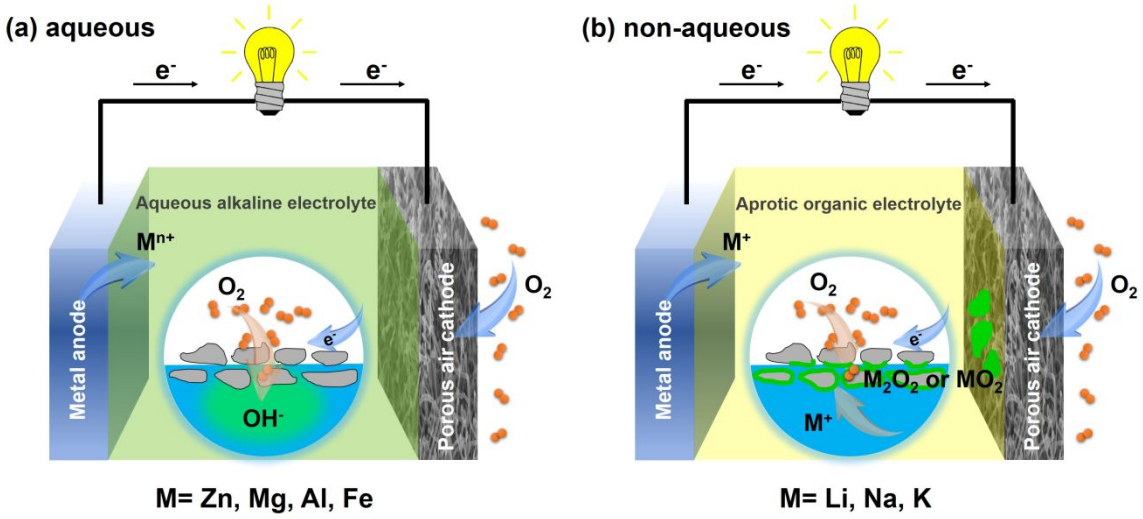

Fig. 3 Schematic configurations and working principles of (a) aqueous and (b) nonaqueous metal-O_2/air batteries. The inset pictures demonstrate the different oxygen reduction reactions happening on the porous air cathodes.

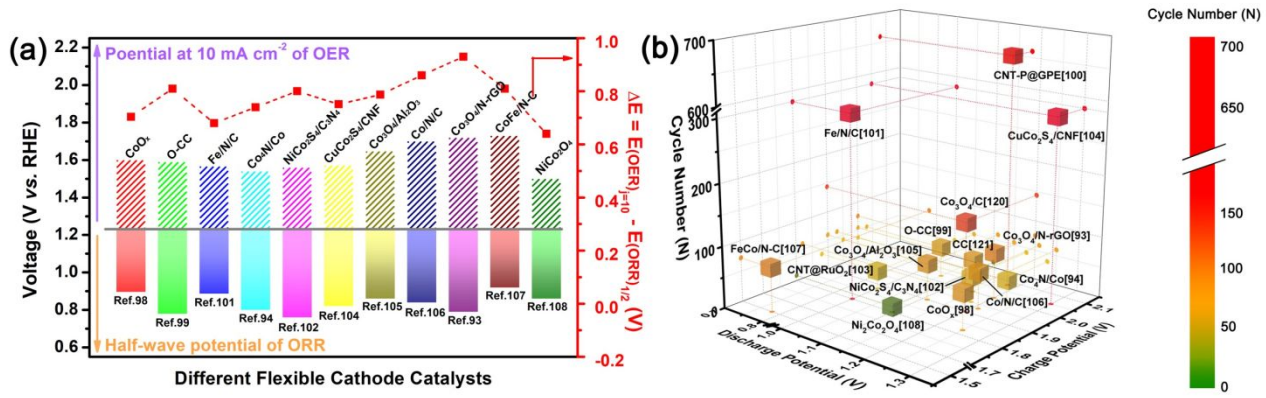

Fig. 4 Comparisons on (a) potential difference between the half-wave potential of ORR and overpotential at 10 mA cm^{-2} of OER for typical previously reported bifunctional flexible air cathodes, and (b) discharge voltage, charge voltage and cycling performance of those flexible ZABs using different kinds of flexible air cathodes.[22, 59, 93, 94, 98-108]

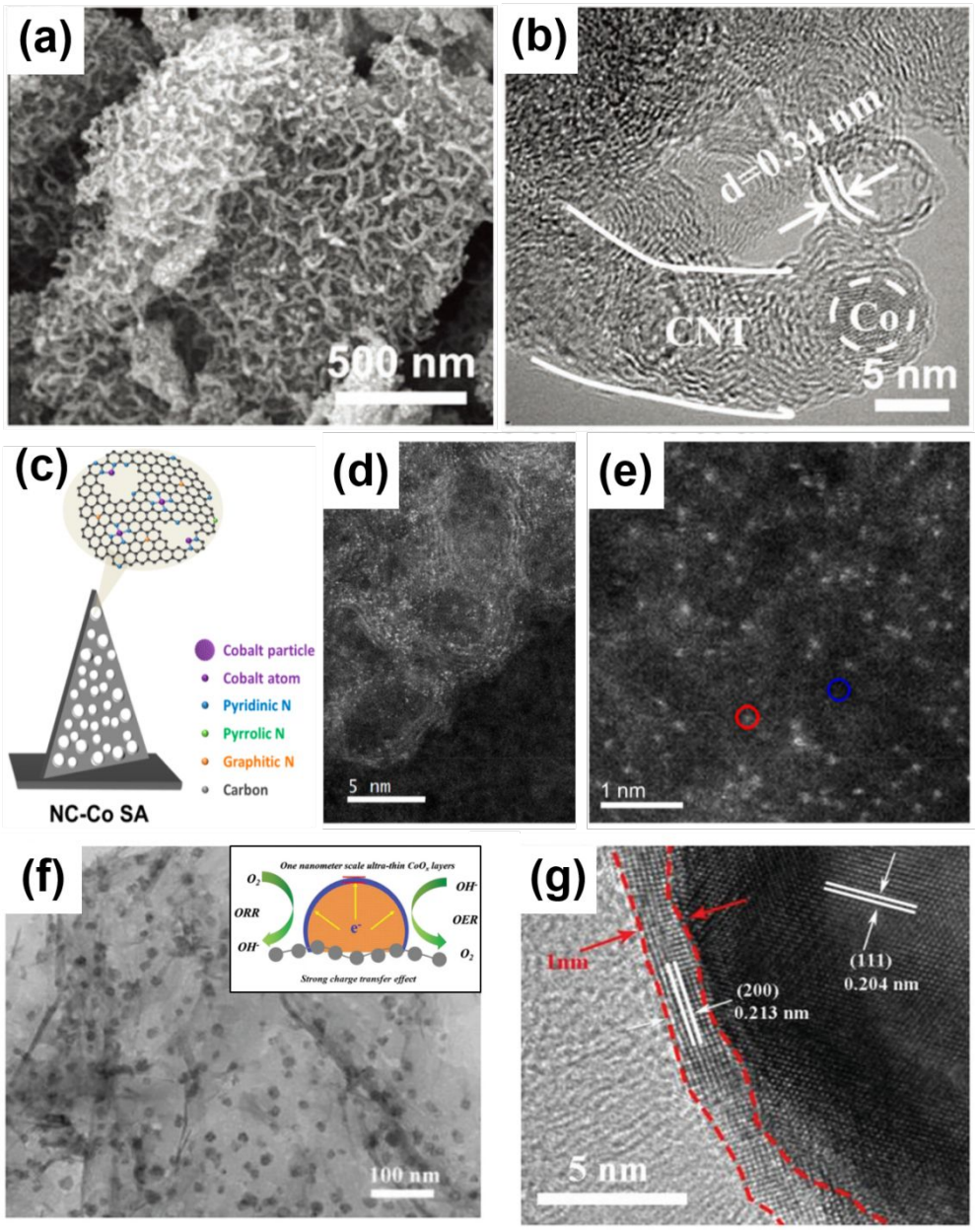

Fig. 5 (a) SEM and (b) TEM images of 2D N-doped CNTs/G hybrid. Reproduced with permission. Copyright 2019, Wiley-VCH.[109] (c) Schematic illustration for the microstructure, (d) STEM and (e) HAADF STEM images of Co atoms distributed across the N-doped carbonaceous support. Reproduced with permission. Copyright 2018, American Chemical Society.[112] (f,g) TEM and HRTEM images of 1 nm-CoO_x layer on metallic substrate of Co/N-RGO. Reproduced with permission. Copyright 2019, Wiley-VCH.[98]

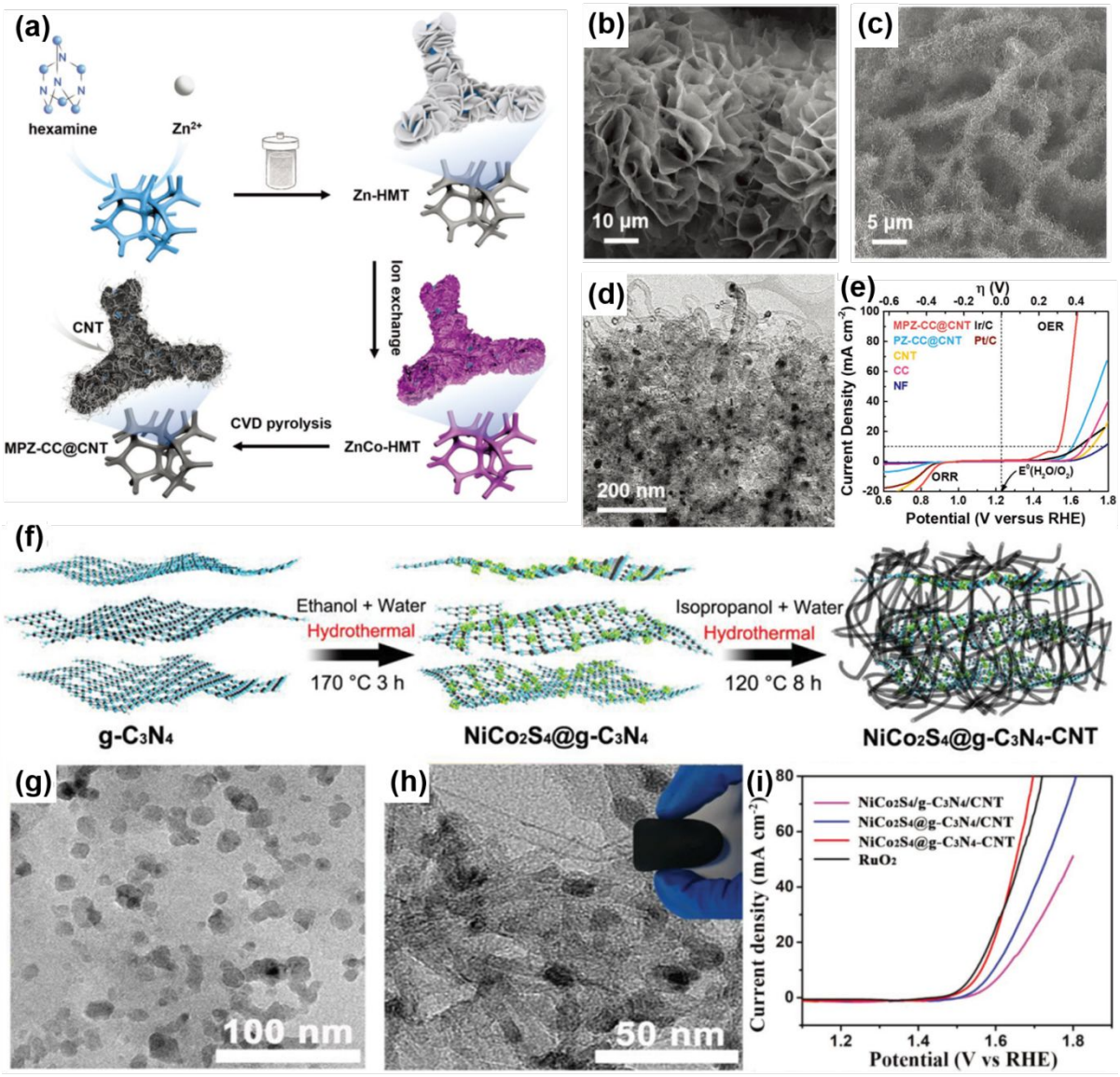

Fig. 6 (a) Scheme of the synthesis for MPZ-CC@CNT on nickel foam. SEM images of (b) ZnCo-hexamine and (c) MPZ-CC@CNT. (d) TEM image and (e) ORR/OER polarization curves of MPZ-CC@CNT. Reproduced with permission. Copyright 2019, Wiley-VCH.[113] (f) Fabrication procedures of $NiCo_2S_4$@g-C_3N_4-CNT. TEM images of (g) $NiCo_2S_4$@g-C_3N_4 and (h) $NiCo_2S_4$@g-C_3N_4-CNT. (i) OER activities of different $NiCo_2S_4$/g-C_3N_4/CNT samples. Reproduced with permission. Copyright 2019, Wiley-VCH.[102]

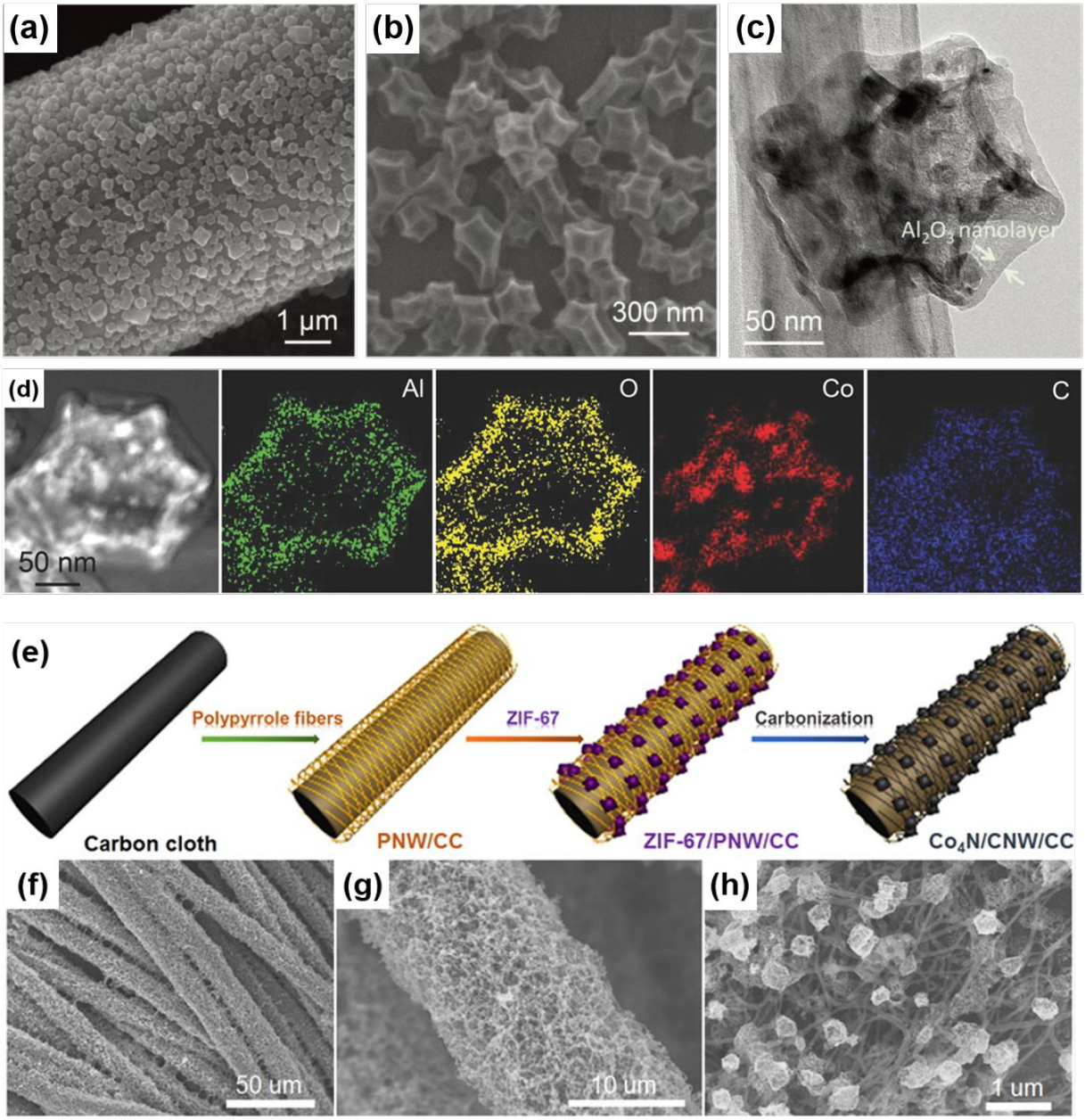

Fig. 7 SEM images of (a) the Zn/Co-ZIFs and (b) the Co-NC@Al_2O_3 grown on carbon cloth. (c) TEM image and (d) elemental mappings of the Co-NC@Al_2O_3 particle. Reproduced with permission. Copyright 2018, Wiley-VCH.[105] (e) Schematic illustrating the synthesis procedure and (f-h) SEM images of Co_4N/CNW/CC. Reproduced with permission. Copyright 2016, American Chemical Society.[94]

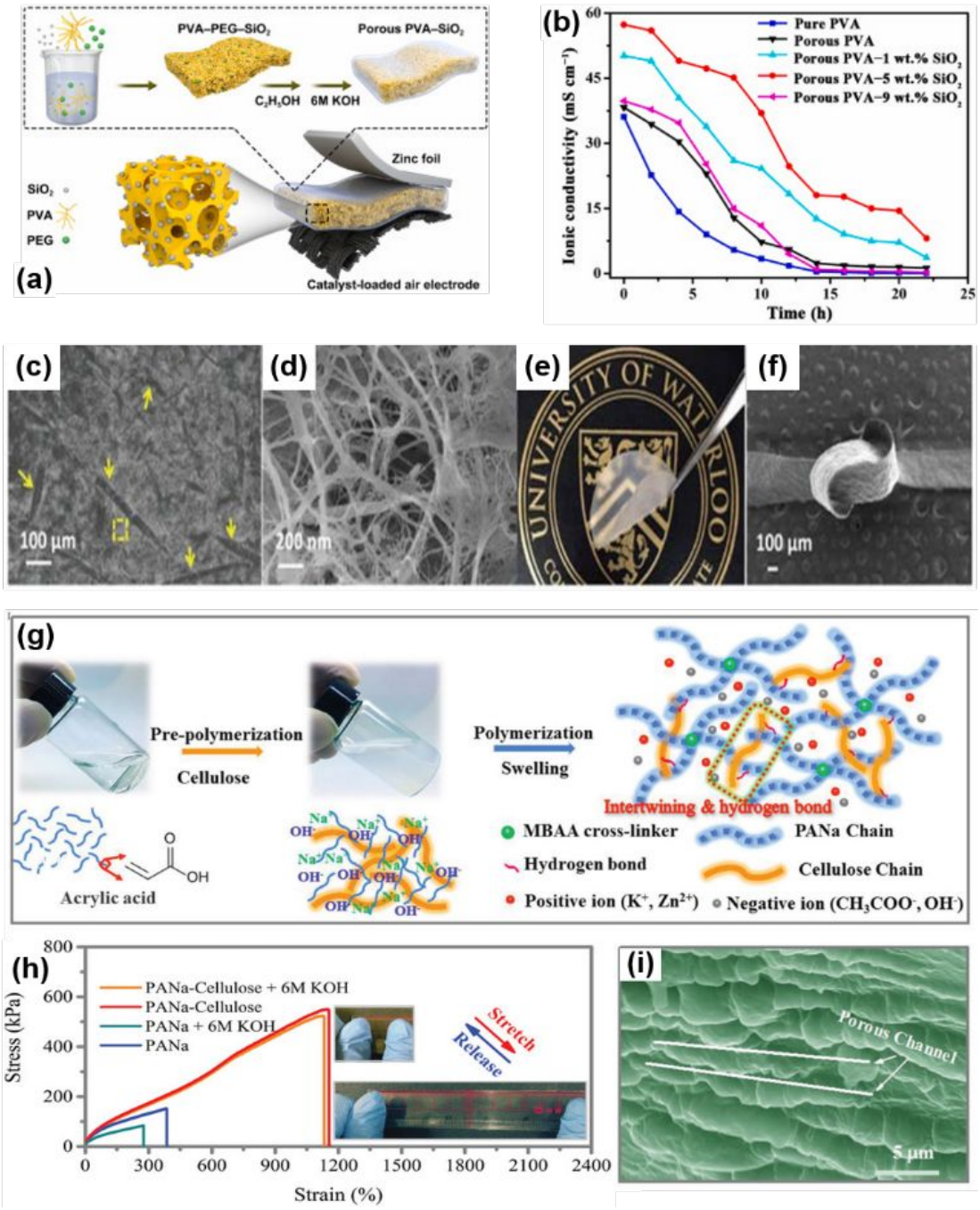

Fig. 8 (a) Schematic diagram of PVA-based GPE. (b) Ionic conductivity of porous PVA–1, 5, 9 wt% SiO_2 nanocomposite GPEs at 25 °C, 50% RH. Reproduced with permission. Copyright 2018, Elsevier.[129] (c,d,f) SEM images (surface view) and (e) photograph of the 2-QAFC membrane. Reproduced with permission. Copyright 2016, The Royal Society of Chemistry.[131] (g) Synthetic procedure, (h) stress-strain curves, and (i) SEM image (cross-section view) of the PANa-cellulose hydrogel electrolyte. Reproduced with permission. Copyright 2019, Wiley-VCH.[100]

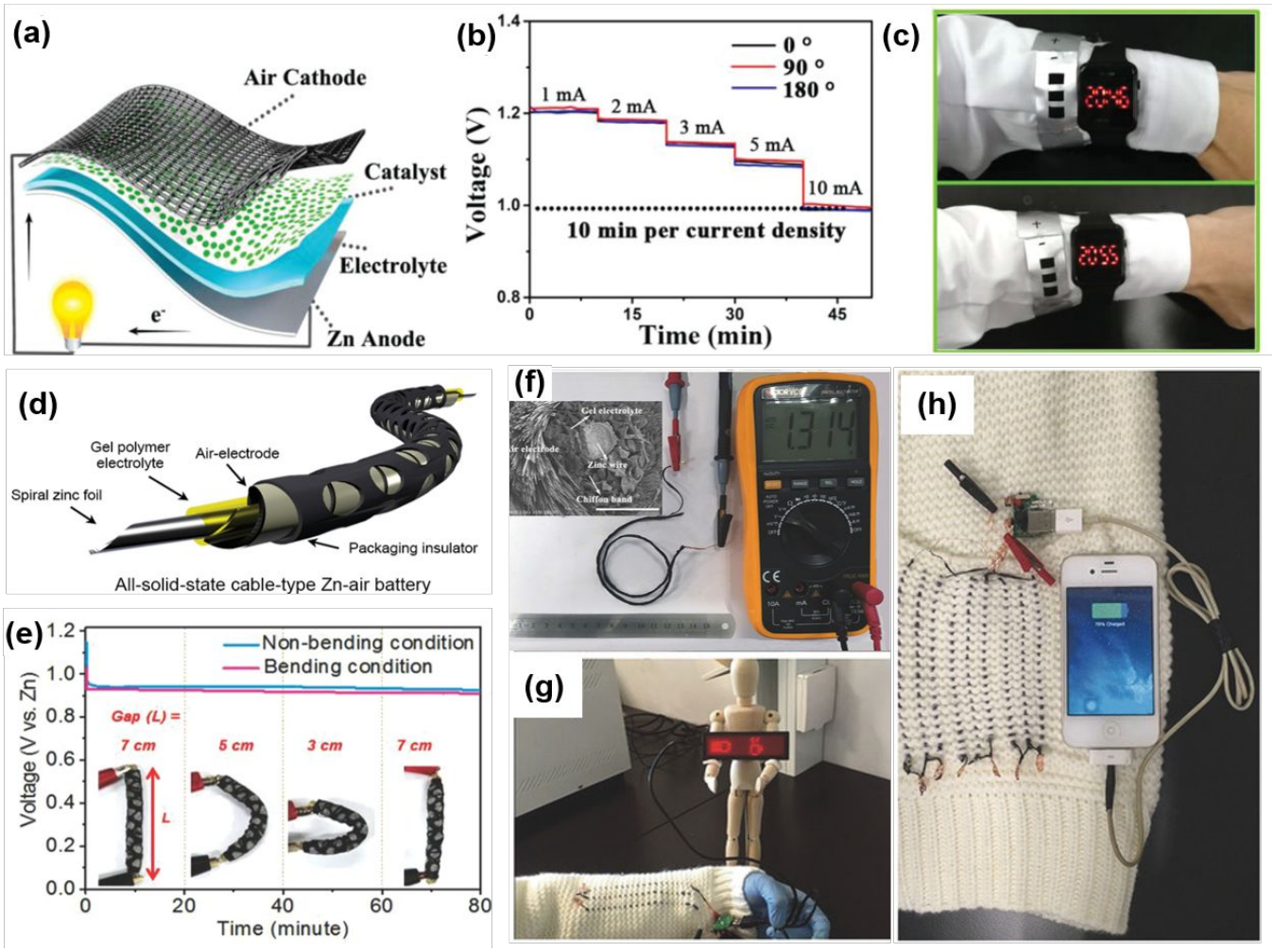

Fig. 9 (a) Schematic illustration of a typical planar flexible ZAB. (b) Rate performance of planar flexible solid-state ZABs based on $NiCo_2S_4$@g-C_3N_4-CNT electrodes. (c) Two solid-state ZABs in series powering a LED watch. Reproduced with permission. Copyright 2019, Wiley-VCH.[102] (d) Schematic diagram of the all-solid-state cable-type flexible ZAB. (e) Discharge curves of cable-type ZAB under different bending angles. Reproduced with permission. Copyright 2014, Wiley-VCH.[59] (f) Cross-sectional SEM image and OCP demonstration of a fiber-shaped ZAB using catalysts-loading carbon fiber bundles as wrapping cathode. (g,h) Potential applications of self-powered textile knitted with three ZABs in series. Reproduced with permission. Copyright 2017, Wiley-VCH.[93]

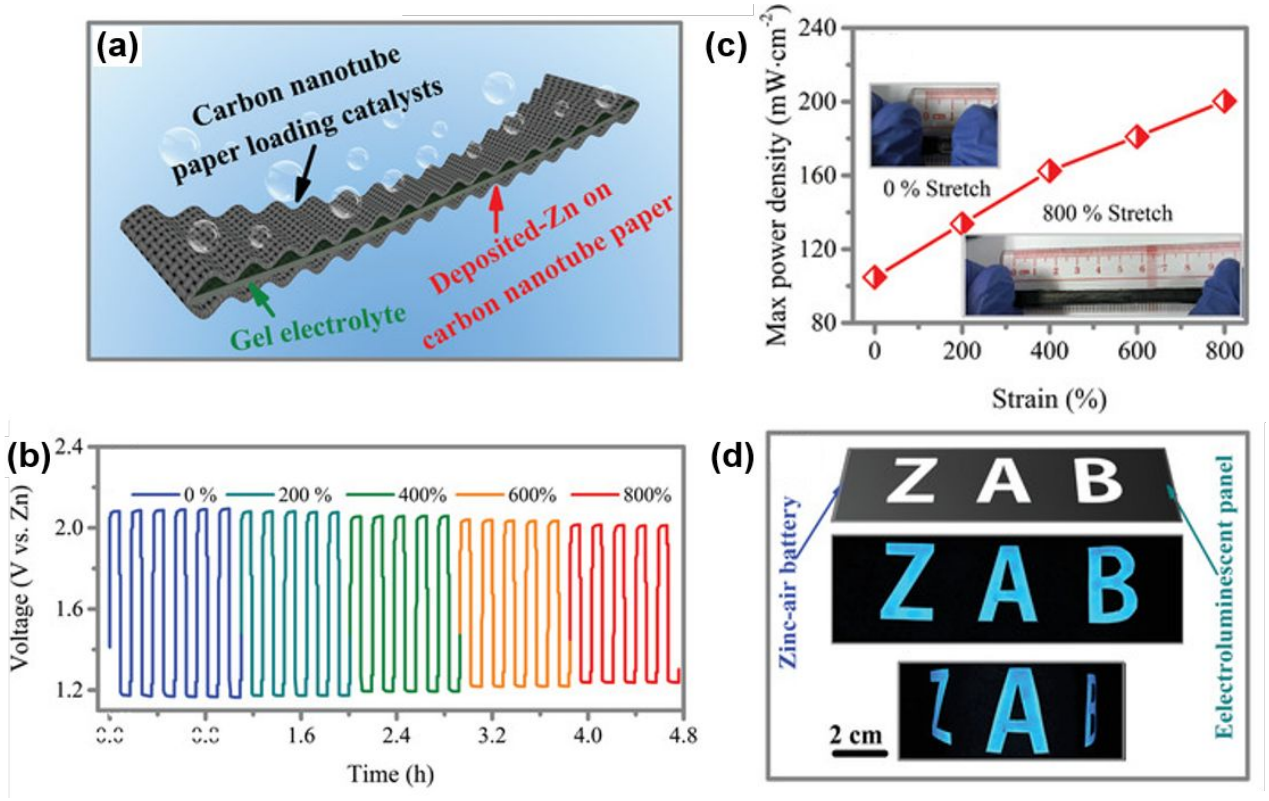

Fig. 10 (a) Schematic illustration of the 800% stretchable flat-shape zinc–air battery. (b) Galvanostatic discharge/charge cycling curves, (c) max power density as a function of the tensile strain and (d) application demonstration of the stretchable flat ZABs. Reproduced with permission. Copyright 2019, Wiley-VCH.[100]

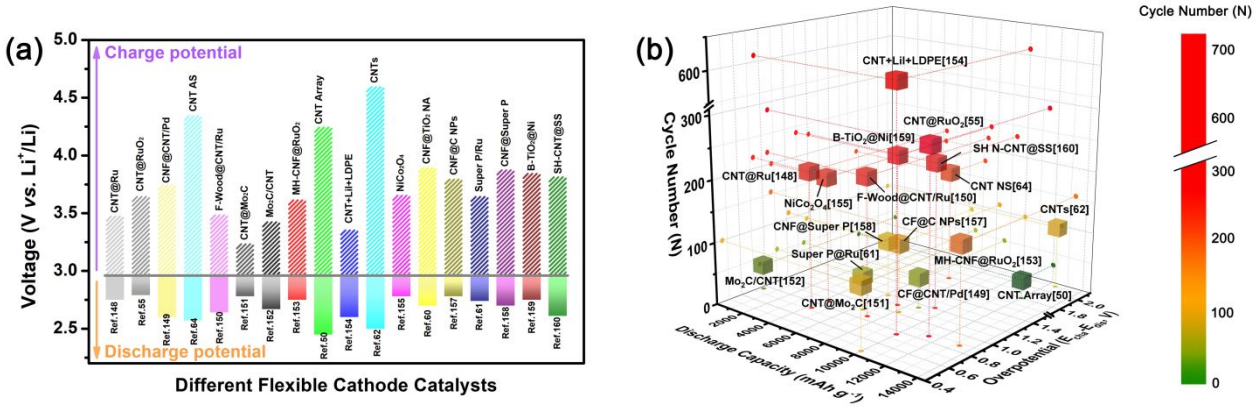

Fig. 11 Comparisons on (a) potential difference between the charge voltage and discharge voltage of typical previously reported bifunctional flexible Li-O_2 battery air cathodes, and (b) discharge capacity, overpotential and cycling performance of those flexible Li-O_2 batteries using different kinds of flexible air cathodes.[50, 53, 55, 60-62, 64, 148-160]

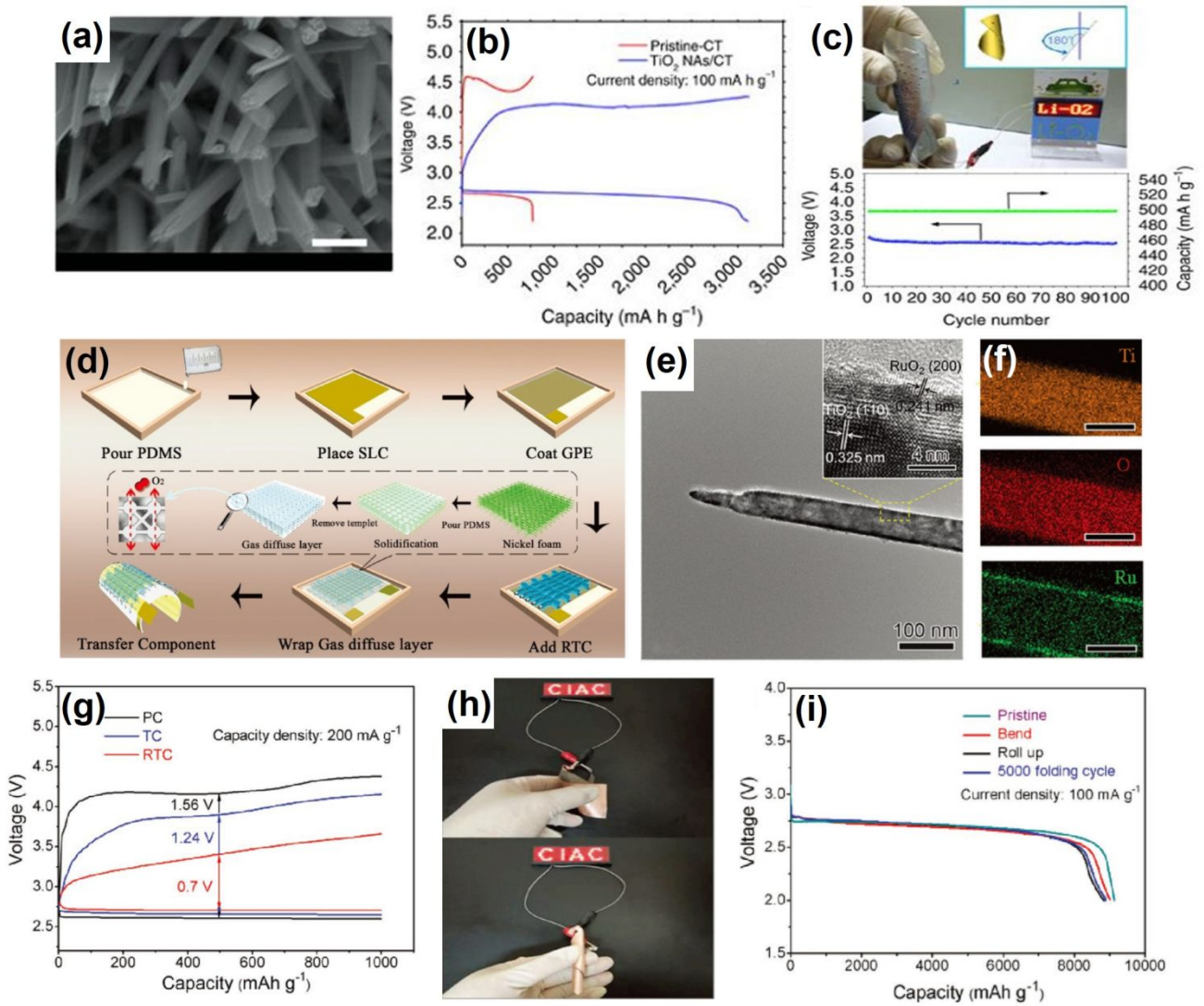

Fig. 12 (a) SEM image of the TiO_2 NAs/CT cathode. (b) Full discharge/charge profiles and (c) bending property at 180° of the planar flexible Li-O_2 cell. Reproduced with permission. Copyright 2015, Nature Publishing Group.[60] (d) Scheme depicting the fabrication of the integrated, flexible Li–O_2 battery. (e) TEM and HRTEM (inset) images, (f) elemental mappings and (g) first discharge-charge curves of RuO_2/TiO_2 NWs. (h) The integrated flexible Li–O_2 battery powering a LED screen at various bended and twisted conditions and (i) their corresponding discharge profiles. Reproduced with permission. Copyright 2017, Wiley-VCH.[161]

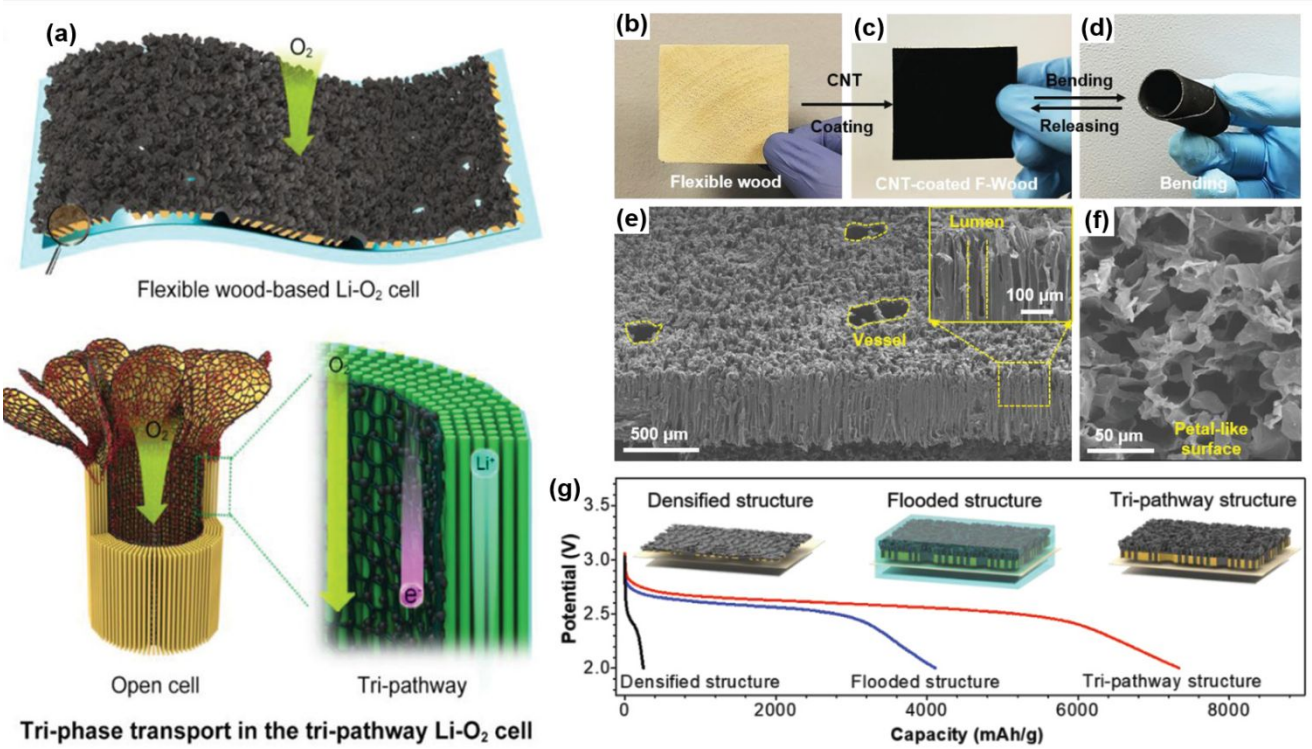

Fig. 13 (a) Schematic elucidating the tree-inspired tri-pathway design for flexible Li–O_2 cells. (b-f) Morphology of the flexible CNT-coated F-Wood membrane. (g) Discharge curves for the CNT/Ru-coated F-Wood electrodes with moderate amount (tri-pathway structure) or excess amount of electrolyte (flooded structure), and the densified electrode (densified structure). Reproduced with permission. Copyright 2019, Wiley-VCH.[150]

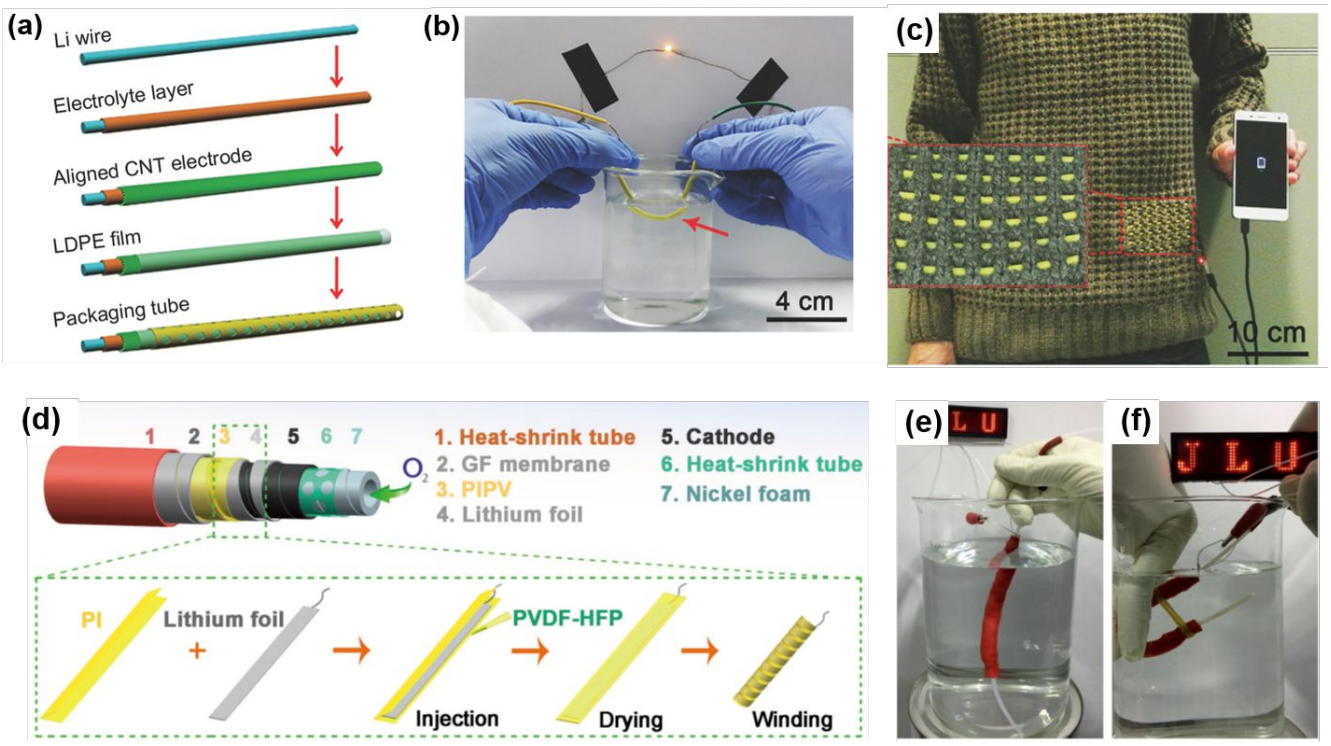

Fig. 14 (a) Scheme of the fabrication process. (b) The water-proof property of the flexible fiber-shaped Li–air battery with LDPE layer. (c) Potential applications of the Li–air battery woven into fabric to charge portable phone. Reproduced with permission. Copyright 2017, Wiley-VCH.[154] (d) Schematic depicting the architecture and (e,f) water-proof property of the trans-structured SFLO battery. Reproduced with permission. Copyright 2017, Wiley-VCH.[148]

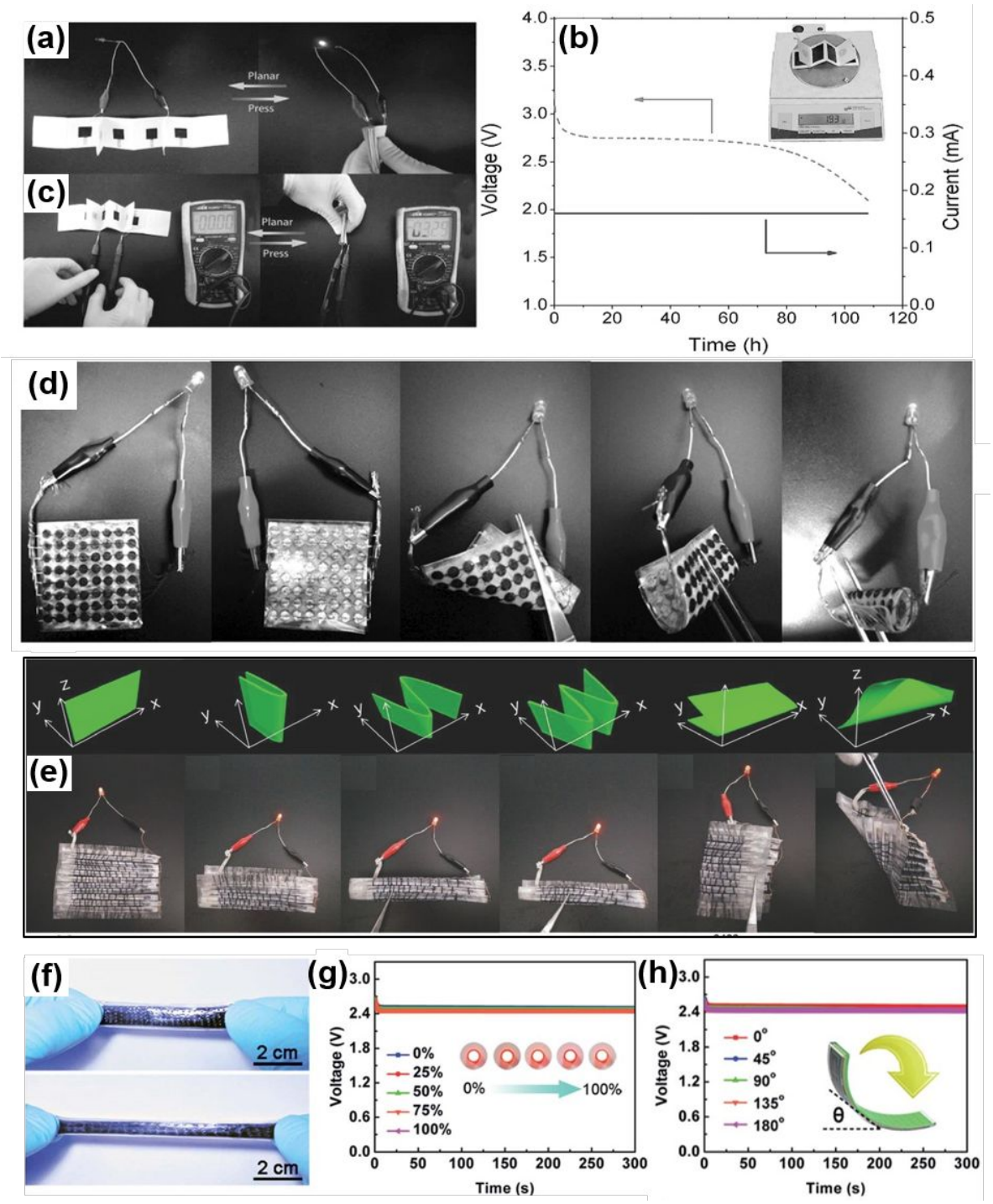

Fig. 15 (a-c) The working mechanism of a foldable Li–O_2 battery pack and its corresponding electrochemical performance. Reproduced with permission. Copyright 2015, Wiley-VCH.[61] (d) An ultrathin, lightweight, and wearable segmented Li-O_2 prototype powering a LED at bended conditions. Reproduced with permission. Copyright 2016, Wiley-VCH.[55] (e) The bamboo-slips-like structured Li–O_2 battery powering a LED under various deformation conditions. Reproduced with permission. Copyright 2016, Wiley-VCH.[157] (f) The stretchable Li-air battery before and after stretching. Discharge curves of the stretchable Li-air battery under increasing strains (g) and different bending angles (h). Reproduced with permission. Copyright 2016, The Royal Society of Chemistry.[64]

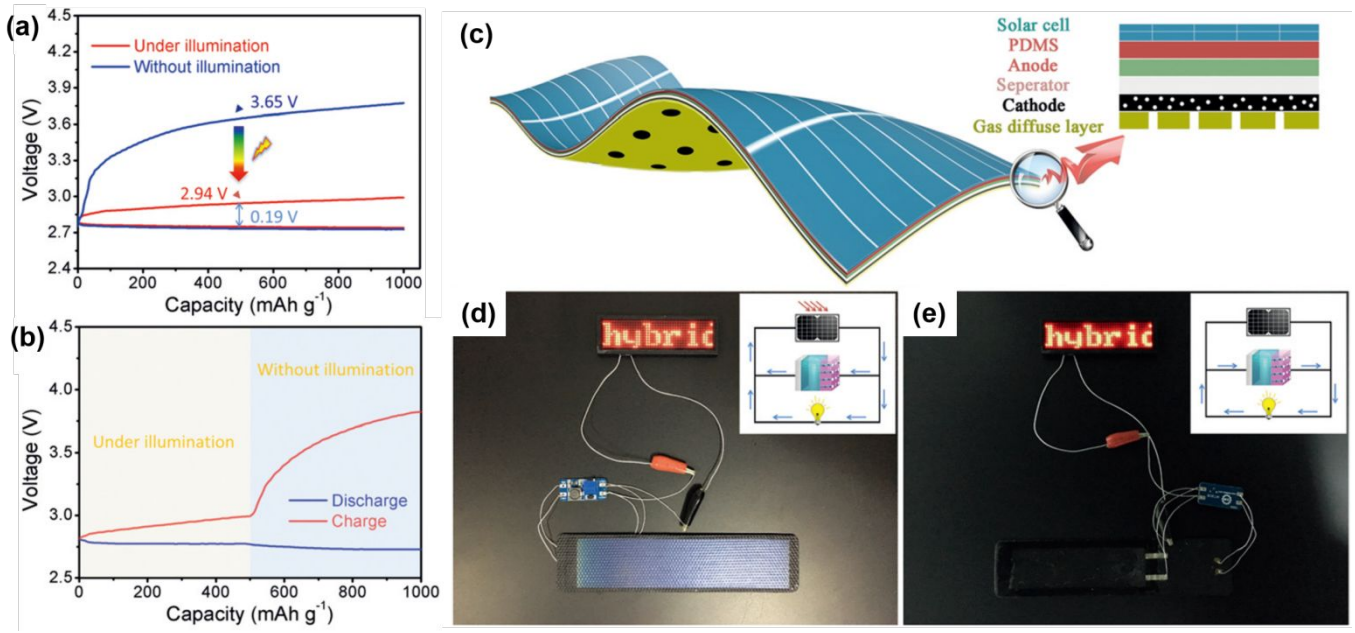

Fig. 16 (a) The discharge-charge profiles and (b) dynamic light-response discharge-charge voltage of the CC@TiN/TiO_2 NW cathodes with or without illumination. (c) Illustration of the structure of the self-powered energy system. (d,e) Digital photographs of the assembled self-powered energy system working with or without the light. Reproduced with permission. Copyright 2019, Wiley-VCH.[164]

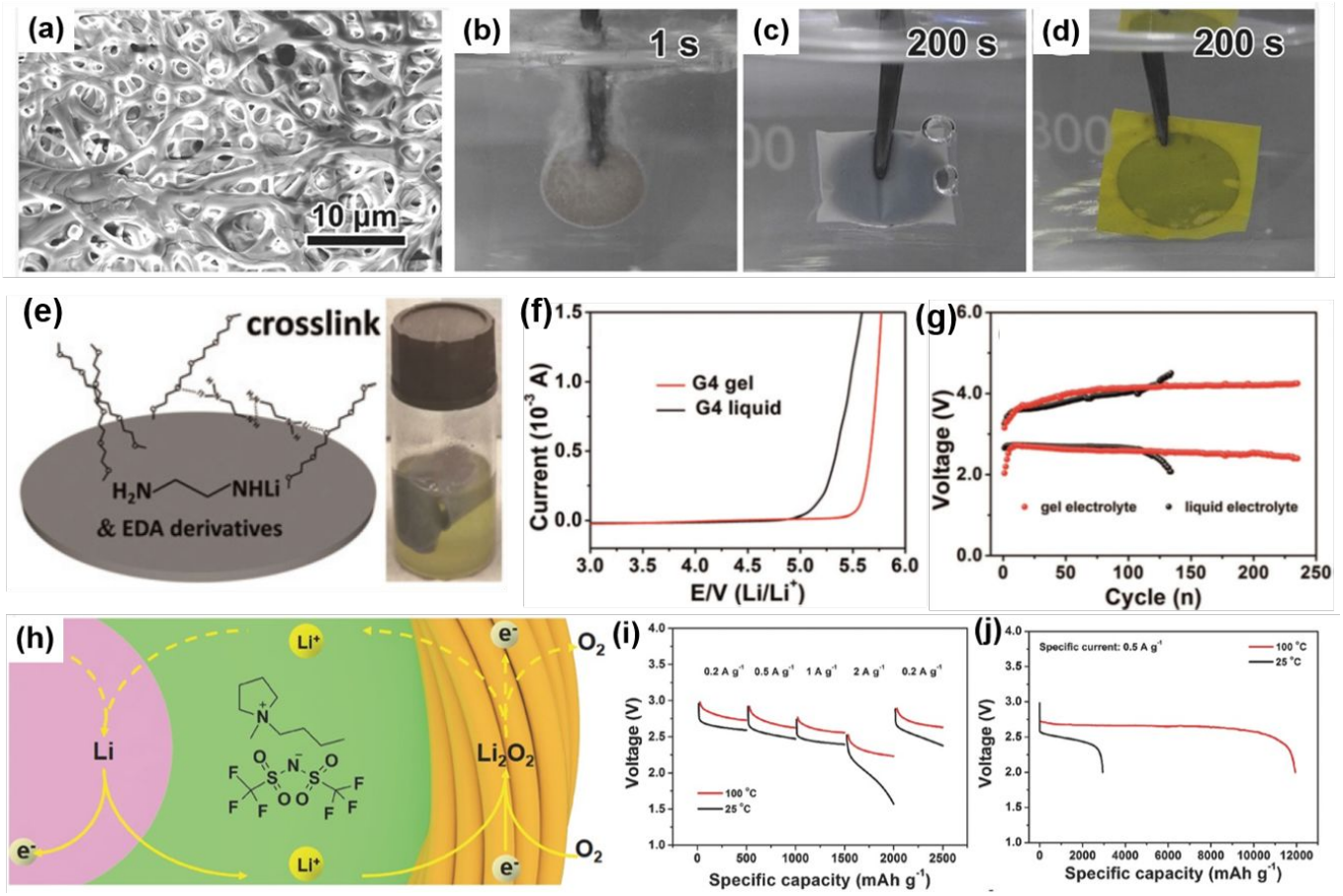

Fig. 17 (a) SEM image of PI. The photographs of (b) pristine lithium sheet, lithium coated by (c) PP and (d) PIPV immersed in water. Reproduced with permission. Copyright 2017, Wiley-VCH.[148] (e) Schematic and photographic illustration of the G4 GPE formation process on Li foil. (f) LSV of G4 gel and liquid with 0.5 M $LiClO_4$. (d) Cycling performances of the flexible Li-air batteries using G4 GPE and liquid electrolyte. Reproduced with permission. Copyright 2018, Wiley-VCH.[180] (h) The working mechanism and (i,j) electrochemical performances of the ionic liquid based GPE in ambient and high-temperature environment. Reproduced with permission. Copyright 2017, Wiley-VCH.[50]

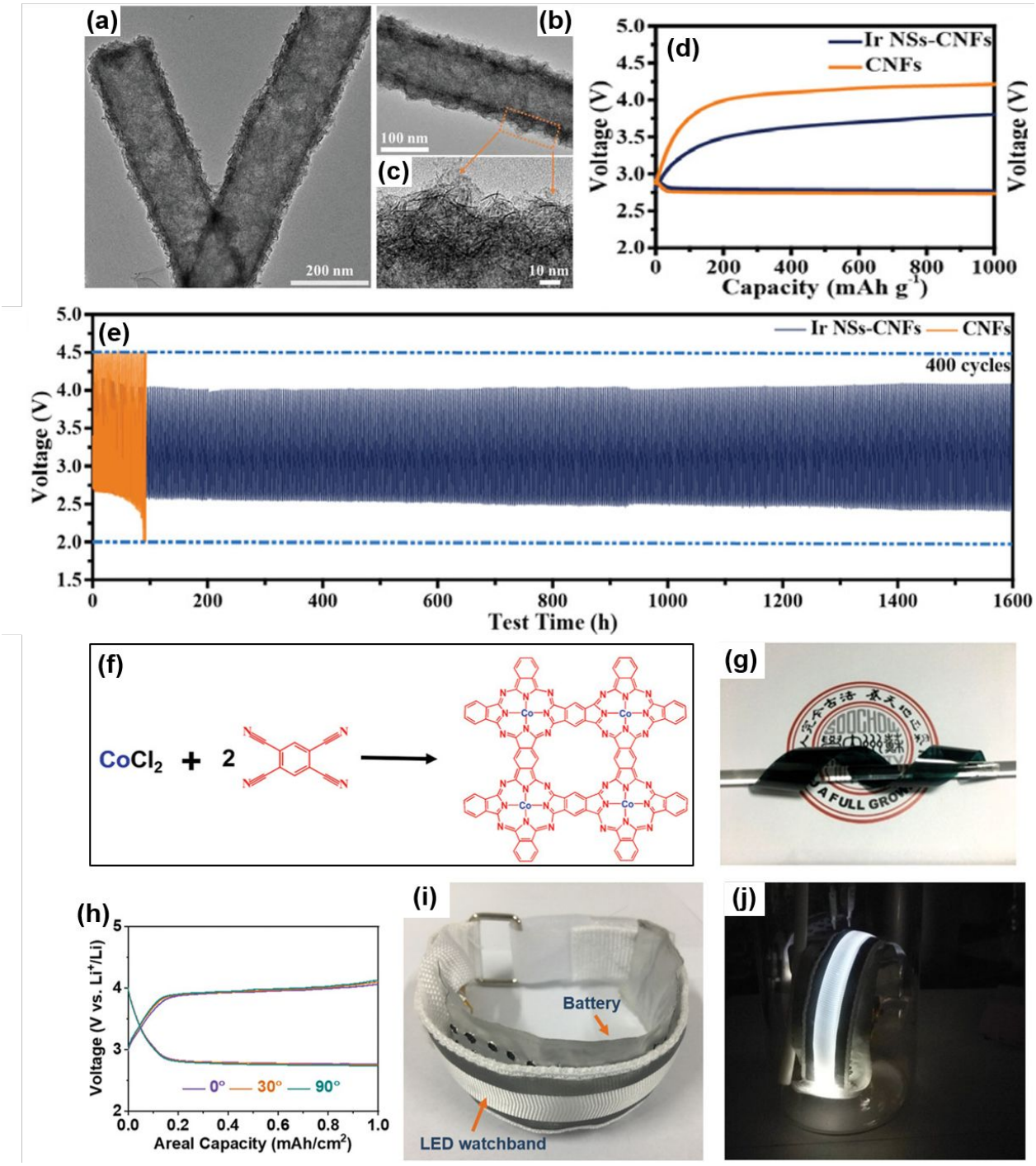

Fig. 18 (a-c) SEM images, (d) The first discharge/charge profiles and (e) cycling performance of the Li–CO_2 batteries with Ir NSs-CNFs and CNFs as cathodes. Reproduced with permission. Copyright 2018, Wiley-VCH.[214] (f) Preparation and structural characterizations of CoPPc. (g) CoPPc film cast on a twisted PET substrate. (h) Discharge/charge curves under various bending states and (i,j) potential applications of the flexible Li–CO_2 pouch cell. Reproduced with permission. Copyright 2018, Wiley-VCH.[215]

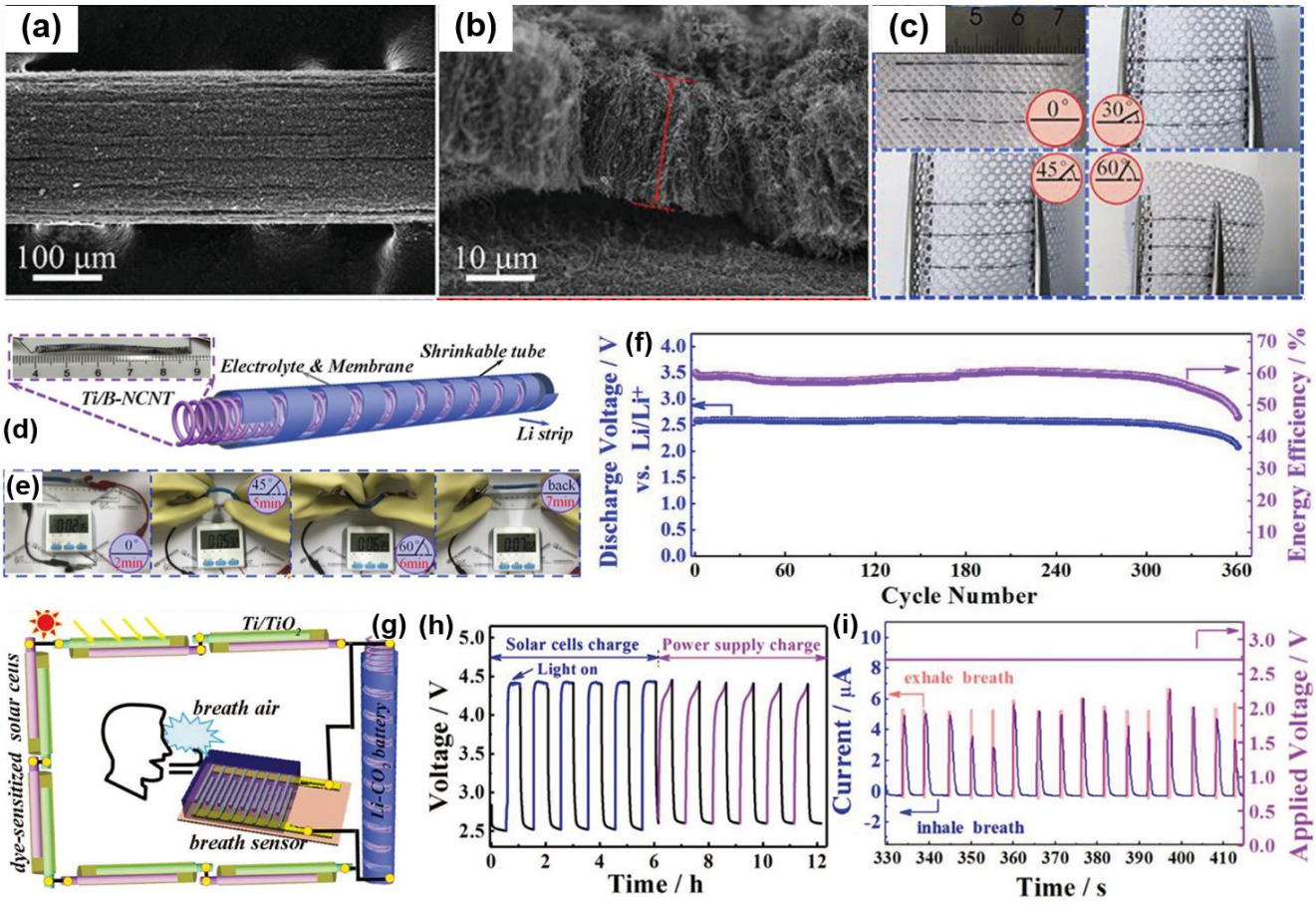

Fig. 19 (a,b) SEM images of B-NCNT grown on Ti wire. (c) Ti/B-NCNT electrodes woven into a fabric at different bending angles. (d) Schematic diagram of FLCBs. e) The photographs of a digital timer powered by the FLCBs at different bending angles. (f) The cycling performance of FLCBs. (g) Schematic illustration of a self-powered breath monitor consisting of energy harvester (FDSSCs), energy storage (FLCBs), and response device. Electrochemical responses of (h) self-powered FLCBs photocharging by FDSSCs or galvanostatic power supply and (i) breath monitor. Reproduced with permission. Copyright 2019, Wiley-VCH.[220]

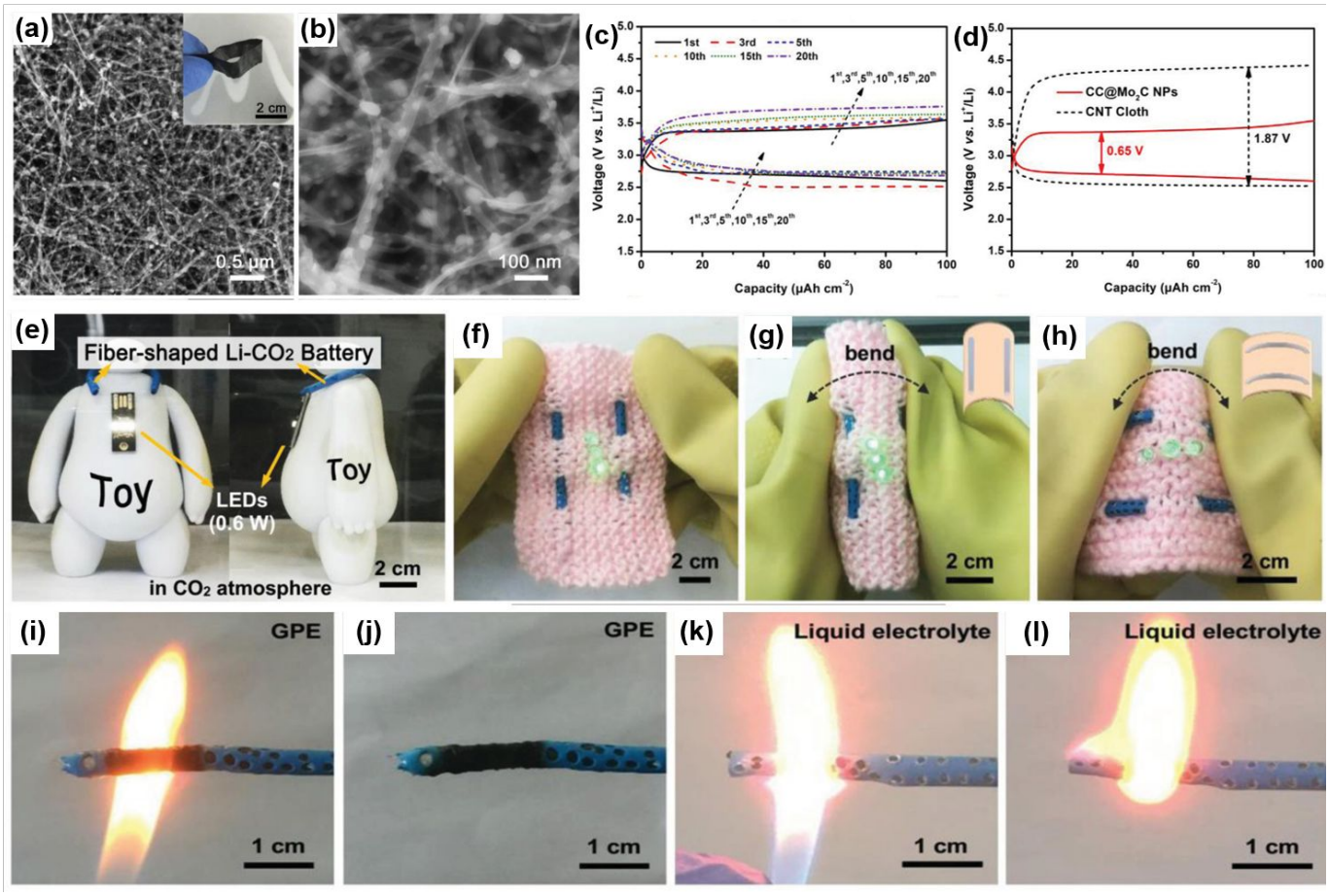

Fig. 20 (a,b) SEM images and (c,d) electrochemical performances of CC@Mo_2C NPs film. (e) Flexibility and potential application demonstration of this quasi-solid-state fiber-shaped Li-CO_2 battery using CC@Mo_2C NPs cathode. (i-l) Comparison on fire-resistance of Li-CO_2 batteries with GPE and traditional liquid electrolyte. Reproduced with permission. Copyright 2018, Wiley-VCH.[67]

Tab. 1 Comparison on different kinds of GPE for solid-state flexible ZABs.

Polymer matrix	Solutes	Additives	Ionic conductivity (mS cm^{-1})	Advantages	Limitations
PVA	KOH	/[116]	/	General compatibility/ Moderate ionic conductivity	Viscous fluid/ Poor processability
	KOH	SiO_2[129]	57.3		
	KOH	GA/HCl[133]	15		
	KOH	Cellulose (NFC) hydrogel[134]	75		
	OH^-	GG/GA/PCL[130]	123		
	$KOH/Zn(Ac)_2$	/[113]	/		
	$KOH/Zn(Ac)_2$	Bacterial cellulose[132]	80.8		
	$KOH/NH_4Cl/ ZnCl_2$ (neutral)	/[135]	71.4		
PVA-PEO	KOH	Glass fibers[12]	10	Good mechanical strength	Low ionic conductivity
PVA-PAA	Nafion/OH^-	/[136]	6.6	Thin film/ Low crossover of $Zn(OH)_4^{2-}$	Low ionic conductivity
PAA	KOH	NFC hydrogel/ APS/Gelatin[137]	96.9	Moderate ionic conductivity	Low mechanical strength
	$KOH/ZnO/ (NH_4)_2S_2O_8$	N,N'-MBA[117]	/		
PAM	KOH	MBAa/APS[54]	330	High ionic conductivity/UV-induced fast polymerization	Low mechanical resistance to alkaline solution
DMOAP	OH^-	Cellulose nanofibers[131]	21.2	Thin film	Low ionic conductivity
PANa	KOH	Cellulose/ MBAA[100]	280	High ionic conductivity/ Super stretchability	Tedious preparation

Tab. 2 Comparison on typical kinds of aprotic GPE reported previously for flexible Li-O_2/air batteries.

Polymer matrix	Electrolyte	Additives	Ionic conductivity (mS cm^{-1})	Voltage window (V)	Advantages	Limitations
PVDF-HFP	LiTFSI-TEGDME	SH-SiO_2/ Cellulose fiber[53]	0.93	4.75	water-resistance	
	$LiClO_4$/$LiNO_3$-TEGDME	MnOOH@ Al_2O_3 film[175]	1.04	4.5	Moderate mechanical strength	Complex components
	$LiCF_3SO_3$-TEGDME	HMPP/TMPET /LiI[154]	2.52	<3.75	High ionic conductivity/ UV-induced fast polymerization	Weak mechanical strength
	BMPy-TFSI/ LiTFSI	/[50]	0.335 (25°C) 1.16 (100°C)	4.5	Work in high temperature	High cost
	$LiClO_4$-DMSO	SiO_2/TTF[176]	/	4.75	mediate Li_2O_2 oxidation reaction	Unhealthy/Volatilization
	LiTFSI-TEGDME	HMPP/TMPET /LiI/SiO_2[177]	1.01	4.5	mediate Li_2O_2 oxidation reaction/ UV-induced fast polymerization	Weak mechanical strength
PVDF-BBP-PVB	BF_4Li/ $Li_{1+x}A_xGe_{2-x}(PO_4)_3$	/[178]	0.003	/		Low ionic conductivity/ Unstable
PVDF-HFP/ PI	$LiCF_3SO_3$-TEGDME	/[148]	0.025	4.5	Fire-resistance	Low ionic conductivity
PMS	$Li_{1.6}Al_{0.5}Ge_{1.5}(PO_4)_3$/LiTSFI-TEGDME	PE separator/ SiO_2[179]	0.32	5.2	High voltage window	High cost/ Tedious preparation
EDA	Li^+-TEGDME	/[180]	/	5.5	High voltage window/Resistance to moisture	Poor processibility
PEGDME	LiTSFI	SiO_2[181]	/	4.6	Easy preparation	Weak mechanical strength
TPU	LiTFSI-TEGDME	SiO_2/Nonwoven fabric[156]	1.02	5.0	High mechanical strength/water-resistance	Limited flexibility

Tab. 3 Theoretical voltage, capacity, energy density, chemical reaction mechanism and progress on flexibility of other categories of metal-O_2/air batteries.

Battery Type	Chemical Reaction Mechanism (electrolyte categories)	Theoretical Voltage (V)	Theoretical Capacity (mAh g^{-1})	Theoretical Energy Density (Wh kg^{-1})	Progress on Flexibility
Fe-O_2[23]	$3Fe+2O_2 \rightleftharpoons Fe_3O_4$ (alkaline aqueous electrolyte)	1.28	597	764	Catalyst Powder
Mg-O_2[20]	$2Mg+O_2+H_2O \rightleftharpoons 2Mg(OH)_2$ (alkaline aqueous electrolyte)	3.1	919	2850	Catalyst Powder
Na-O_2[26]	$2Na+O_2 \rightleftharpoons Na_2O_2$ $Na+O_2 \rightleftharpoons NaO_2$ (organic electrolyte)	2.33 2.27	688 487	1605 1105	Catalyst Powder
K-O_2[27]	$K+O_2 \rightleftharpoons KO_2$ (organic electrolyte)	2.37	394	935	Catalyst Powder
Si-O_2[65]	$2LixSi+xO_2 \rightleftharpoons xLi_2O_2+2Si$ (organic electrolyte)	~2.5	/	/	Flexible 1D device
Al-O_2[63]	$4Al+3O_2+6H_2O \Rightarrow 4Al(OH)_3$ (alkaline aqueous electrolyte)	2.71	1031	2796	Flexible 1D/2D devices

Tab. 4 Theoretical voltage, capacity, energy density and chemical reaction mechanism of other categories of metal-CO_2 batteries known to date.

Battery Type	Chemical Reaction Mechanism（electrolyte categories）	Cathode Catalyst	Theoretical Voltage (V)	Theoretical Capacity (mAh g^{-1})	Theoretical Energy Density (Wh kg^{-1})
Li-CO_2[189]	$4Li+3CO_2 \rightleftharpoons 2Li_2CO_3+C$ (organic LiTFSI/TEGDME)	CNT/ graphene	2.80	670	1876
Na-CO_2[191]	$4Na+3CO_2 \rightleftharpoons 2Na_2CO_3+C$ (organic $NaClO_4$/TEGDME)	activated MCNT	2.35	480	1130
K-CO_2[190]	$4K+3CO_2 \rightleftharpoons 2K_2CO_3+C$ (organic KTFSI/TEGDME)	N-CNT-rGO	2.48	372	922
Al-CO_2[30]	$4Al+9CO_2 \rightleftharpoons 2Al_2(CO_3)_3+3C$ (ionic liquid $AlCl_3$/[EMIm]Cl)	Au@Pd	~0.72	638	~460
Zn-CO_2 (1)[24]	$Zn+CO_2+H_2O \rightleftharpoons ZnO+HCOOH$ (aqueous KOH/NaCl)	3D Pd nano-sheets	0.955	825 420	788 (Zn) 402 (ZnO+HCOOH)
Zn-CO_2 (2)[44]	$Zn+CO_2+H_2O+2OH^- \Rightarrow Zn(OH)_4^{2-}+CO$ (Discharge) $Zn(OH)_4^{2-} \Rightarrow Zn+1/2O_2+2OH^-+H_2O$ (Charge) (aqueous KOH/$KHCO_3$)	Ir@Au	0.707	825 332	583 (Zn) 235 ($Zn(OH)_4^{2-}$+CO)

Tab. 5 Theoretical voltage, capacity, energy density and chemical reaction mechanism of other categories of metal-gas batteries known to date.

Battery Type	Chemical Reaction Mechanism（electrons transfer number）	Theoretical Voltage (V)	Theoretical Capacity (mAh g^{-1})	Theoretical Energy Density (Wh kg^{-1})	Progress on Flexibility
Li-N_2[226]	$6Li+N_2 \rightleftharpoons 2Li_3N$ ($6e^-$)	0.54	2311	1248	Flexible Cathode
Li-O_2/H_2O[227]	$4Li+O_2+2H_2O \rightleftharpoons 4LiOH$ ($4e^-$)	3.4	1119	3804	Catalyst Powder
Li-O_2/HCl[228]	$4Li+O_2+4HCl \rightleftharpoons 4LiOH+2H_2O$ ($4e^-$)	4.3	521.4	2242	Catalyst Powder
Li-SO_2[32]	$2Li+2SO_2 \rightleftharpoons Li_2S_2O_4$ ($2e^-$)	3.1	377	1170	Catalyst Powder

An overview on recent technical advances and major dilemmas facing current flexible metal-gas batteries for wearable electronics is presented.

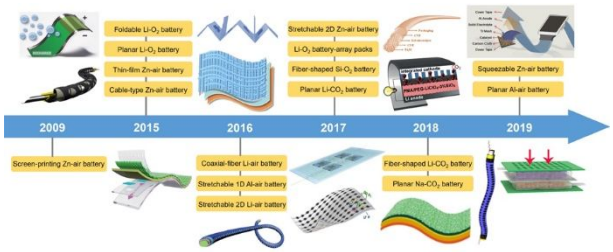

With the popularity of flexible electronics, it imposes higher requirements on energy supply and space adaptability of their power accessories. Due to the high energy densities, metal-gas batteries seem to be a potential option for next-generation energy storage systems of flexible consumer electronic products, especially proper for wearable electronics with the characteristics of long-term and low-power operation. Despite numerous efforts have been made to enhance the electrochemical performance of cathode catalysts, how to synchronously integrate high flexibility and superior performance into metal-gas batteries still remains unsolved. In fact, the properties of gas cathodes, metal anodes, electrolytes and battery configurations all make a significant effect on electrochemical performance and functionality of flexible metal-gas batteries, which should be carefully designed and optimized to accommodate various deformations. Besides flexibility, some other factors like fire/water-resistance, stretchability, safety and comfortability are also worth attention. This article reviews the development status and discusses the recent technical advances, unsolved challenges, expected functions and application opportunities of flexible metal-gas batteries for wearable electronics. It is hoped that some new insights and proposed methodology can drive the advance of flexible metal-gas batteries toward practical applications and provide design inspiration for other flexible energy storage devices.